AD-A191 697 RAPIDLY SOLIDIFIED LIGHTWEIGHT DURABLE DISK MATERIAL (U) PRATT AND WHITNEY WEST PALM BEACH FL GOVERNMENT PRODUCTS DIV C C LAW ET AL 15 DEC 87 1/2

UNCLASSIFIED PW/GPD-FR-19875 AFWAL-TR-87-4102 F/G 11/6.1 NL

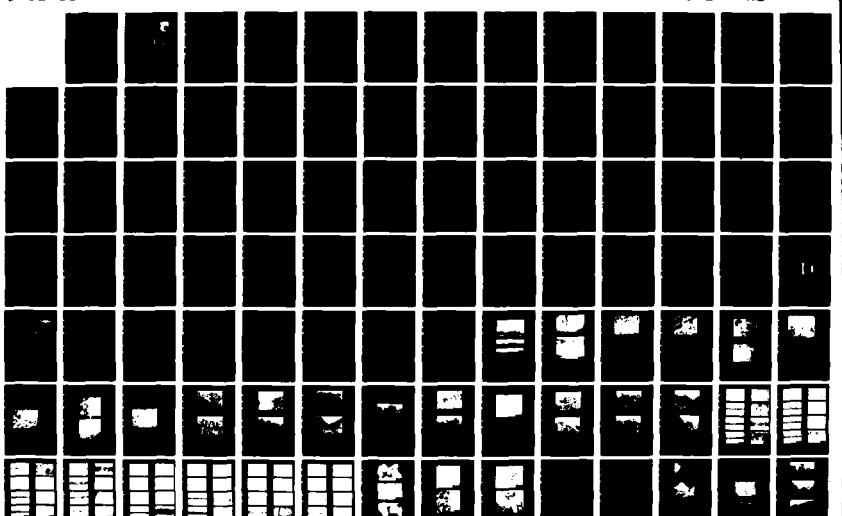

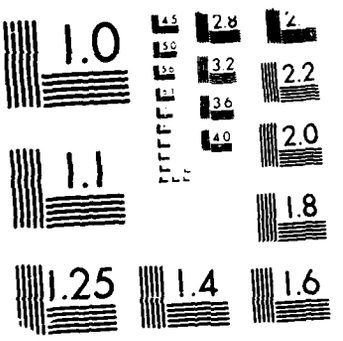

MICROCOPY RESOLUTION TEST CHART

AD-A191 697

(2)

AFWAL-TR-87-4102

RAPIDLY SOLIDIFIED LIGHTWEIGHT DURABLE DISK MATERIAL

C.C. Law, M.J. Blackburn
United Technologies Corporation
Pratt & Whitney Group
Government Engine Business
P.O. Box 2691
West Palm Beach, Florida 33402

December 1987

Final Report for Period June 1984 - March 1987

Approved for public release; distribution is unlimited

Materials Laboratory
Air Force Wright Aeronautical Laboratories
Air Force Systems Command
Wright-Patterson Air Force Base, Ohio 45433-6533

NOTICE

When Government drawings, specifications, or other data are used for any purpose other than in connection with a definitely Government-related procurement, the United States Government incurs no responsibility or any obligation whatsoever. The fact that the Government may have formulated or in any way supplied the said drawings, specifications, or other data, is not to be regarded by implication, or otherwise in any manner construed, as licensing the holder, or any other person or corporation; or as conveying any rights or permission to manufacture, use, or sell any patented invention that may in any way be related thereto.

This report has been reviewed by the Office of Public Affairs (ASD/PA) and is releasable to the National Technical Information Service (NTIS). At NTIS, it will be available to the general public, including foreign nations.

This technical report has been reviewed and is approved for publication.

DAVID B. MIRACLE
Project Engineer

ALLAN P. KATZ
Actg Ch, Processing & High Temperature Materials Br

FOR THE COMMANDER

NORMAL M. TALLAN
Ch, Metals & Ceramics Div

If your address has changed, if you wish to be removed from our mailing list, or if the addressee is no longer employed by your organization please notify AFWAL/MLLM, Wright-Patterson AFB, OH 45433-6563 to help us maintain a current mailing list.

Copies of this report should not be returned unless return is required by security considerations, contractual obligations, or notice on a specific document.

REPORT DOCUMENTATION PAGE

1a. REPORT SECURITY CLASSIFICATION: Unclassified	1b. RESTRICTIVE MARKINGS
2a. SECURITY CLASSIFICATION AUTHORITY	3. DISTRIBUTION/AVAILABILITY OF REPORT: Approved for Public Release: Distribution is Unlimited.
2b. DECLASSIFICATION/DOWNGRADING SCHEDULE	
4. PERFORMING ORGANIZATION REPORT NUMBER(S): PR-19877	5. MONITORING ORGANIZATION REPORT NUMBER(S): AFWAL-TR-87-4102
6a. NAME OF PERFORMING ORGANIZATION: Pratt & Whitney (6b. OFFICE SYMBOL (If applicable): MLEL)	7a. NAME OF MONITORING ORGANIZATION: AF Materials Laboratory (AFWAL/MLLM) Wright Aeronautical Laboratories
6c. ADDRESS (City, State and ZIP Code): United Technologies Corporation, Pratt & Whitney Group/Gov. Prod. Div., P.O. Box 2691, W. Palm Beach, FL 33402	7b. ADDRESS (City, State and ZIP Code): Wright-Patterson AFB, Dayton, OH 45433-6533
8a. NAME OF FUNDING/SPONSORING ORGANIZATION: AF Wright Aeronautical Lab. (8b. OFFICE SYMBOL (If applicable): AFWAL/MLLM)	9. PROCUREMENT INSTRUMENT IDENTIFICATION NUMBER: F33615-84-C-5067
8c. ADDRESS (City, State and ZIP Code): AF Wright Aeronautical Laboratories, Materials Laboratory (AFWAL/MLLM), Wright-Patterson AFB, Ohio 45433-6533	10. SOURCE OF FUNDING NOS.

PROGRAM ELEMENT NO.	PROJECT NO.	TASK NO.	WORK UNIT NO.
62102F	ILIR	01	73

11. TITLE (Include Security Classification): Rapidly Solidified Lightweight Durable Disk Material

12. PERSONAL AUTHOR(S): C. C. Law and M. J. Blackburn

13a. TYPE OF REPORT	13b. TIME COVERED	14. DATE OF REPORT (Yr., Mo., Day)	15. PAGE COUNT
Final	FROM 6/84 TO 3/87	1987 December 15	127

16. SUPPLEMENTARY NOTATION: This research was partially funded by the in-house independent research fund.

17. COSATI CODES		
FIELD	GROUP	SUB. GR.
11	06	

18. SUBJECT TERMS (Continue on reverse if necessary and identify by block number): Nickel Aluminide, Ordered Alloys, Intermetallic, Ductility, Disk Alloys

19. ABSTRACT (Continue on reverse if necessary and identify by block number)

A 2-year program was conducted to explore the potential of NiAl as a high temperature structural material with emphasis on overcoming the low temperature brittleness problem. The inherent ductility characteristics of binary alloys containing 29 a/o Al to 54 a/o Al were studied and it was observed that room temperature ductility was achieved only in alloys with lower amounts of Al. The highest Al level in which room temperature ductility was observed is process dependent, being 35 a/o in the case of the melt spun alloys and 29 a/o for the cast alloys. The brittle to ductile transition temperatures, T_{BD}, for the higher Al alloys (43 a/o -52 a/o) were found to be in the range 375°C to 625°C, showing no clear trends in terms of the Al content and starting material form (castings versus powder). Minor additions of boron significantly raised strength and the brittle to ductile transition temperature. An attempt to improve the ductility of NiAl through modification of the basic deformation behavior was made. It was observed that additions of Cr and Mn resulted in <111> slip in room temperature

20. DISTRIBUTION/AVAILABILITY OF ABSTRACT	21. ABSTRACT SECURITY CLASSIFICATION
UNCLASSIFIED/UNLIMITED ☒ SAME AS RPT. ☐ DTIC USERS ☐	Unclassified

22a. NAME OF RESPONSIBLE INDIVIDUAL	22b. TELEPHONE NUMBER (Include Area Code)	22c. OFFICE SYMBOL
Daniel B. Miracle	(513)-255-9833	AFWAL/MLLM

DD FORM 1473, 83 APR — EDITION OF 1 JAN 73 IS OBSOLETE

19. Abstract (Cont.)

compressive deformation in contrast to the <100> slip observed in binary alloys. However, the T_{so} temperature was not reduced by the <111> slip mode possibly due to the low mobility of the <111> dislocations. The strength characteristics of NiAl alloyed with Ti and Cr were also studied. It was found that strength levels approaching those of superalloys could be achieved, but the creep and ductility properties tended to be poor. The best property combination was found in two alloys, Ni-22 a/o Al-27 a/o Fe and Ni-25 a/o Al-25 a/o Co, which showed a good balance of strength and ductility. These materials were selected for study in more detail. The tensile yield strengths were found to be 550 MPa to 830 MPa (80 ksi to 120 ksi), fatigue crack growth rates were about equal to current advanced turbine disk alloys, but creep resistance was still rather poor.

TABLE OF CONTENTS

TABLE OF CONTENTS (Concluded)

LIST OF ILLUSTRATIONS

LIST OF ILLUSTRATIONS (Continues)

LIST OF ILLUSTRATIONS (Continues)

LIST OF ILLUSTRATIONS (Continues)

LIST OF ILLUSTRATIONS (Continues)

LIST OF ILLUSTRATIONS (Continued)

LIST OF ILLUSTRATIONS (Concluded)

LIST OF TABLES

LIST OF TABLES (Concluded)

1.0 INTRODUCTION

Future power plants will have to operate with higher shaft speeds to increase the thrust-to-weight ratio and preserve tactical superiority of our defense systems. Materials with improved specific strength properties will be needed to sustain the increased forces of higher speeds. Other material characteristics will also have to be maintained or improved to withstand the complex thermal and stress conditions experienced by these gas turbine components. Only two candidate systems show specific strengths well beyond current levels: fibrous composites and ordered or intermetallic alloys containing high concentrations of aluminum. The fibrous composites show no ductility at low temperatures and are difficult to fabricate. The ordered alloys also exhibit poor ductility at low temperatures, but have adequate hot formability.

Recent programs, many under Air Force sponsorship, have demonstrated that poor ductility at ambient temperatures can be overcome in some aluminide systems. Alloys based on Ti_3Al, Fe_3Al, and Ni_3Al with adequate plasticity for engineering applications have been identified. Technological payoffs would be greater for the equiatomic alloys TiAl, FeAl, and NiAl, but less progress has been made in this area. The metallurgical and processing research and development that has accumulated over the past decade for the A_3B type alloys points the way for a comprehensive program to define useful alloys based on NiAl. If such a program is successful, exploitation of the basic high temperature characteristics and low density of the nickel aluminide could lead to major benefits in the turbine section of jet engines. The weight of disks and some low turbine blades could be reduced by 20 percent or more.

This 2-year program explored the potential of alloys based on the intermetallic compound NiAl. Specifically, it attempted to determine if its properties could be altered by alloying/processing modifications such that it could be considered as a candidate material for aircraft turbine engine (disk) applications.

A brief review of the mechanical properties of NiAl will be given first and the approaches selected to modify behavior will then be described.

1.1 STRENGTH AND DUCTILITY CHARACTERISTICS OF BINARY NiAl ALLOYS

Strength characteristics of NiAl type alloys are well established as quite extensive studies have been performed since the early sixties. The effect of stoichiometry on the strength of NiAl alloys in terms of the proportional limits determined in compressive tests by Lautenschlager (Reference 1) is presented in Figure 1. At temperatures of 700°C and below, the minimum strengths were observed near the stoichiometric composition, while a significant increase in strength occurred in both the low nickel and high nickel regions. At 900°C, the minimum strength at stoichiometry begins to disappear; and at 1100°C, all alloys have approximately the same strengths. The strengthening in off-stoichiometric have compositions at temperatures

below about 700°C has been rationalized in terms of interactions of dislocations with defect clusters, vacancies in the nickel sublattice in aluminum-rich alloys and substitutional defects in nickel-rich alloys. Formation of such defect clusters has been deduced from both X-ray diffraction studies (Reference 2) and transmission electron microscopy observations (Reference 2). The increase in strength of the off-stoichiometric alloys at high temperatures was attributed to breaking up of defect clusters due to thermal motion and diffusion, thus destroying a rather effective barrier to dislocation motion (Reference 3).

In spite of the technological importance of NiAl as a high temperature turbine blade coating, very little information on creep behavior has been generated. Results from studies by Yang and Dodd (Reference 4), summarized in Figure 2 appear to indicate that the nickel-rich alloys exhibit better creep resistance than the Al-rich alloys. Another interesting feature of the creep data is that the steady state creep rate is more sensitive to stress in the stoichiometric and near-stoichiometric compositions than in the off-stoichiometric compositions. A stress exponent of about 4.6 was obtained for alloys containing 49 and 50 a/o Al versus 3.6 for alloys with larger deviations from the stoichiometry. The lower creep resistance of the Al-rich alloys may be associated with the presence of vacancies at nickel sites which increase the diffusivities.

In contrast to numerous studies on strength and deformation mechanisms of NiAl alloys, (References 1 through 10), few studies have been conducted to investigate the brittleness problem of NiAl alloys. It is generally known that the ductility of NiAl alloys is very poor at ambient temperatures, approaching zero at room temperature. Recently, Schulson (Reference 11) studied the tensile ductility of Ni-49 a/o Al as a function of grain size. He observed that the NiAl alloy fractured at room temperature without tensile elongation irrespective of grain size in the alloy which was studied in the range of 5 to 140 m. Ductility improvement by grain refinement was not observed until the temperature exceeded about 300°C (Figure 3). A mixed mode of fracture, consisting of cleavage and intergranular separation, was observed up to about 300°C irrespective of grain size. At higher temperatures, ductile tearing becomes an increasingly important mode of fracture. The poor ductility of NiAl at low temperature is usually attributed to its lack of sufficient independent slip systems, because of the predominantly <001> slip, and/or the poor grain boundary cohesion. Over the years there have been various attempts to improve the ductility and strength characteristics of NiAl alloys with the objective of developing them as high temperature structural materials. Most of these efforts focused on increasing the strength capability of NiAl alloys, as in References 12 through 14, which were rather successful. By strengthening NiAl with Ni_2AlTi particles which precipitated coherently in NiAl, Polvani et al (Reference 14) observed a creep strength comparable to the nickel-base superalloy MAR-M200. In contrast, no progress has been made to overcome the brittleness problem in NiAl which is a major obstacle to its consideration as a candidate for a high temperature structural alloy. The above review indicates that grain refinement by thermomechanical working or even rapid solidification as a means for overcoming the brittleness problem in NiAl is of limited scope. Alloy stoichiometry was shown to play an important role in NiAl strength and perhaps could influence ductility as well and therefore, was studied in this program. The approaches pursued in this program are presented in the following section.

1.2 ALLOYING STRATEGIES FOR DUCTILITY IMPROVEMENTS IN NiAl

1.2.1 Substitutional Alloying

The brittleness problem in NiAl at ambient temperatures is usually considered basically related to its ‹100› slip mode which provides only three of the five independent slip systems needed in order to accommodate an arbitrary shape change (Von Mises criterion). Thus, a major thrust in this program was to attempt to alter the slip behavior of NiAl through alloying additions. In particular, the ‹111›-type of slip mode was sought, which at least satisfies the geometrical requirement for general plasticity. Rachinger and Cottrell (Reference 15) surveyed the slip systems of compounds in the B2 family and made two interesting observations which pointed to potential directions for modification. They observed a relationship between atomic bonding in B2 compounds and the selection of slip systems: ionic bonding (such as that in thallium halides) promotes slip along ‹100›, while bonding of a metallic nature (such as that in CuZn and AgMg) favors slip along ‹111›. However, this guideline is difficult to exploit, as at present, the nature of atomic bonding in transition metal B2 aluminides and the way it is perturbed by alloying additions are not understood. Another interesting observation was derived from their analysis of a ‹111› dislocation dissociation behavior in B2 compounds. Two types of dissociation were proposed, either:

$$a[111] \rightarrow a[100] + a[010] + a[001] \qquad (1)$$

or

$$a[111] \rightarrow 1/2a[111] + 1/2a[111] \qquad (2)$$

Reaction (1) results in no change in dislocation elastic energy but the partials are all glissile in the B2 structure so that a stress that acts more strongly on one component can move this component independent of the others. Reaction (2) is encouraged by a reduction in elastic energy and, therefore, would prevail to produce ‹111› slip if the separation of the 1/2a[111] partials are sufficiently large. Otherwise, constriction of the 1/2a[111] partials occurs readily under stress and results in dissociation of the first type. The separation of the 1/2a[111] partials is determined by the Antiphase Boundary (APB) energy, and a large separation is promoted by small APB energy. For the completely ordered B2 structure, it is shown by Flinn (Reference 16) for an 1/2a‹111› 110 type APB that:

$$APB = \frac{4V}{\sqrt{2}\, a^2} \qquad (3)$$

where V is the bond energy which is proportional to the ordering energy of the compound. Thus, reduction of the ordering energy promotes ‹111› slip in B2 compounds, again pointing in a direction for alloy modification if the degree of order can be manipulated.

A survey of the B2 aluminides would give insight for alloying changes which tend to reduce the degree of order in NiAl. Among the 213 known B2 compounds there are 15 aluminides. As indicated in Figure 4 the partner components of these B2 aluminides belong to Groups VIIB and VIII, the Lanthanum and Actinium Series. The B2 aluminides of obvious interest to this program are those which

lie in the first long period among which the NiAl is of primary interest. Elements which form B2 phases with nickel are also indicated in Figure 4. The heats of formation for some of the B2 compounds of interest are summarized in Table 1 which shows the relative stability of the B2 aluminides as

$$NiAl > CoAl > FeAl > MnAl > CrAl\ (?) \qquad (4)$$

The calculated ordering energies (Reference 17) follow the same order. Thus, it was proposed to study the slip behavior and ductility of NiAl alloyed with early transition elements like Cr and Mn.

Another potential way to improve the ductility of NiAl can be inferred from an analysis of dislocation energies and mobilities. If the dislocation self energies in several potential slip systems do not differ significantly, which is the case for $\langle 010 \rangle \{101\}$ screws and edges and $\langle 111 \rangle \{110\}$ screws in NiAl with values of 9.3, 8.3 and 12.5×10^{-4} erg/cm, respectively (Reference 18), then the dislocations with the highest mobility would dominate the deformation process. The current analysis of dislocation mobility takes into consideration both the dislocation core size and a stress required for rigid translation of two adjacent slip planes. For a given core size, the smaller this stress the higher the dislocation mobility. Obviously, the atomic radius ratio of the constituent atoms is a major consideration in determining the magnitude of the stress needed for rigid translation of two adjacent atomic planes. As a first approximation, the stress can be assumed to be proportional to the maximum vertical displacement of the atomic planes during rigid translation. The calculated vertical displacements, d_v, for rigid translation of 110 planes along $\langle 001 \rangle$ and $\langle 111 \rangle$ directions are plotted in Figure 5. This figure shows that the stress for rigid translation along $\langle 001 \rangle$ increases while that for $\langle 111 \rangle$ translation decreases with increasing atomic radius ratio. Thus, alloying additions to NiAl which tend to increase the atomic radius ratio may promote $\langle 111 \rangle$ slip. The atomic radius ratios for some B2 compounds are given in Table 1 from which it appears that substituting Be for Al is the most effective way of increasing the atomic radius ratio of NiAl. Therefore, beryllium was one of the alloying additions selected for study in this program.

1.2.2 Formation of Ductilizing Phases

In the preceding section, substitutional alloying was discussed as a means to ductilize NiAl through modification of the basic slip behavior. The possibility of achieving ductility through multiphase NiAl alloys is another potentially useful approach. In general, the toughness of a multiphase alloy can be improved by mechanisms such as slip dispersal, crack deflection and blunting, and stress induced phase transformations. The most obvious candidate for toughening NiAl was considered to be the Ni_3Al phase. In fact some toughening of NiAl alloys resulting from precipitation of Ni_3Al phase in binary alloys was reported by Russell and Edington (Reference 19) and in ternary NiAl alloys containing Fe and Co by Inoue and Masumoto (Reference 20). Another potential ductilizing phase in NiAl alloys was considered to be martensite which forms in low aluminum NiAl alloys as a result of cooling to low temperatures and/or applying stress (References 21, 22 and 23). In a fully

transformed martensitic alloy, plasticity can be accommodated by switching of martensite variants to those with more favorable orientations with respect to the imposed strain, for example in NiTi alloys at room temperature. Alternatively, plasticity can be accommodated by stress induced martensitic transformation, for example in TRIP steels. Thus, binary and ternary NiAl alloys were formulated (see the following section) to explore the effectiveness of some of these toughening mechanisms.

1.2.3 Grain Boundary Strengthening

Besides the slip system, the nature of grain boundaries in ordered compounds plays an important role in fracture behavior. In addition to the characteristics attributed to lattice distortion, grain boundaries in ordered alloys also contain bonding defects. For an AB compound the grain boundary energy associated with these bonding defects increases with increasing anisotropy among the A-A, B-B and A-B pairwise interaction energies. Therefore, grain boundaries of ordered compounds are inherently strong segregation sites. Such grain boundary characteristics in ordered compounds have led to severe grain boundary fragility and chemical reactivity, especially in compounds with high ordering energies. Micro-alloying techniques were selected as a means to overcome the grain boundary fragility problem in NiAl. Based on its success in the Ni_3Al alloys, boron was considered a primary candidate for ductility enhancement in NiAl.

1.3 ALLOYING STRATEGIES FOR STRENGTH IMPROVEMENTS

As noted above, the intrinsic tensile and creep strengths of NiAl are rather low. It is generally recognized that the most potent means of increasing strength, especially at high temperatures, is provided by precipitation of certain types of coherent particles. Consequently, precipitation of B2 structure related phases was investigated as a primary approach for strengthening NiAl alloys. Strengthening by substitutional solutes and particle dispersions were other approaches evaluated in this program.

Three simple structures were considered to be candidates for precipitate strengthening of NiAl: A2 (disordered bcc), $L2_1$ (Heusler) and DO_3; all are crystallographically related to the B2 structure and thus could form as coherent particles (Figure 6). Table 2 shows some of the A2 phases (all refractory metals), their lattice parameters and lattice misfit with NiAl. The ternary Ni-Al-X (X = Cr, Mo, W and V) phase diagrams indicate a NiAl + X two-phase field. Thus, it is possible to precipitate these refractory metals in NiAl. However, because of the relatively large lattice mismatch of these elements with the matrix, lattice coherency is not expected except in the case of Cr for which the lattice mismatch is less than 1 percent. Therefore, Cr was selected for study in this program.

A second structure of interest for coherency strengthening in NiAl is the $L2_1$ (Heusler Phase) of which there are about 50 known compounds. The Heusler phase compounds are ternary compounds of the Cu_2MnAl-type. Those of interest in the proposed program are of the Ni_2XAl type where X are the Groups IVB and VB transition metals. The crystal structure of Ni_2XAl, illustrated in Figure 6,

consists of eight NiAl unit cells with ordered substitution of X for Al in the Al sublattice. The lattice parameters of selected $L2_1$ compounds, listed in Table 3 are about twice that of NiAl. Formation of any one of these compounds in NiAl is quite possible based on the Ni-Al-X ternary diagram (Figure 7). Ni_2TiAl appears to be most suitable because of its lowest lattice mismatch with NiAl and the relatively large NiAl + Ni_2TiAl phase field. As mentioned earlier, the promise of Ni_2TiAl as a strengthener in NiAl has been demonstrated by Polvani et al.

The third family of structure which could be considered a potential strengthener in NiAl is DO_3 of which there are about 17 known compounds with A_3B compositions (A = Li, Mg, Cd, Fe and Cu). Among these DO_3 phases, only the Fe compounds, in particular Fe_3Al, appear to be viable candidates. The unit cell of Fe_3Al, shown in Figure 6 consists of 8 FeAl unit cells with Fe substituting for Al at alternate Al sublattice sites. The Fe-Ni-Al ternary phase diagram at 950°C, the lowest temperature studied (Figure 9), shows a large FeAl/NiAl phase field. However, no Fe_3Al phase is indicated in the ternary diagram even at the Fe-25 a/o Al composition. Either this phase was overlooked or, more likely, Fe_3Al if indeed formed in NiAl at lower temperatures, may have a solvus below 950°C. The latter assumption is based on the observed thermal stability of Fe_3Al in Fe-Al binary alloys in which the solvus temperature is below 550°C. Therefore, both the possibility of creating a coherent DO_3 precipitate and the subsequent effectiveness of such a precipitate are doubtful.

Other types of strengthening that could be considered for this program include solution hardening and dispersion hardening. Refractory and transition metals are primary candidates for solid solution hardening. The promise of these elements can be inferred from Grala's study in which the strength of NiAl was found to increase with increasing Mo content (Reference 21).

1.4 PROGRAM OVERVIEW

The program was divided into three phases. In Phase I, binary NiAl alloys of different stoichiometry were prepared using both casting and rapid solidification techniques. The brittle to ductile transition temperature and deformation and fracture modes were determined and contrasted to define certain inherent characteristics for subsequent studies. In Phase II - Task I, of the program alloys were screened with modified compositions in an attempt to improve ductility. The approaches behind the alloy formulation were outlined in Section 1.2 and the specific alloy compositions studied are given in the following Section 1.5. Selected compositions were characterized in terms of fractographic and microstructural features and dislocation behavior. Phase II - Task II, conducted in parallel with Task I, studied methods of creating structures with increased strength. Again, the basic approaches outlined in Section 1.2 were followed. Selected alloys were evaluated in more detail in Phase III.

1.5 ALLOY FORMULATION

1.5.1 Phase I Baseline Alloys

The compositions of baseline alloys selected for Phase I evaluations, given in Table 4, lie in the beta phase (B2) field of the Ni-Al phase diagram. Alloy numbers 1 and 7 were chosen based on the maximum stoichiometric hardening observed in previous studies (Reference 1). A small amount of boron was added to some of the selected alloys because this addition has been successful in producing ductility in Ni_3Al. The boron level in Phase I alloys was selected based primarily on prior experience with Ni_3Al alloys.

1.5.2 Phase II - Task I Alloys for Ductility Improvement

As described in Section 1.2, two rather different approaches were selected in an attempt to ductilize NiAl. One approach was to modify the basic slip behavior of NiAl with selected substitutional solutes. To facilitate analysis single phase ternary alloys were formulated to study the effectiveness of this approach. The second approach attempted to exploit ductilizing effects of Ni_3Al and martensitic phases which form in NiAl alloys with low aluminum contents. The alloys formulated to study these two approaches are designated as Substitutional Alloys and Multiphase Alloys in the following.

1.5.2.1 Substitutional Alloys

As described in Section 1.2, the atomic radius ratio and the APB/bond energy are two alloy parameters considered important in determining the slip mode in NiAl. Increasing R_A/R_B favors <111> slip over <001>, while decreasing the APB/bond energy increases the propensity of slip due to the 1/2a<111> superpartials. The operation of <111> slip increases the number of independent slip systems and removes a major obstacle to ductility. It was also indicated that alloying NiAl with the early transition elements Cr, Mn, Fe and Co tends to decrease the heat of formation in NiAl, which is directly related to the ordering energy of the alloy. Because of the significantly smaller atomic radius of beryllium as compared to Al, substitution of Be for Al may be an effective means for increasing R_A/R_B. Substitution of gallium for aluminum was expected to have a similar effect on R_A/R_B. In the initial screening studies, relatively simple ternary alloys were chosen to define general trends. However, as the compound NiAl can exist over a range of compositions a complication was the selection of base alloys from which to start. Two were chosen: one slightly hypo- and the other slightly hyper-stoichiometric.

For convenience, the alloys formulated are grouped into three series depending on the substitutional behavior of the solute. Specific compositions are listed in Table 5. The first series is the Ni substitutional alloy series in which Cr, Mn, Fe and Co were assumed to reside in the nickel sublattice. The second series is the Al substitutional alloy series in which Mn, Ga and Be were assumed to be aluminum substituting solutes. Manganese forms B2 compounds with both Ni and Al and its substitutional behavior is not known in any detail. It is assumed to substitute exclusively for Ni in the first series, for Al in the

second series and equi-partition to both Al and Ni sites in the third series. The concentration levels selected were arrived at from the following considerations. To modify the slip behavior of NiAl to an appreciable extent using substitutional alloying, a high solute concentration was considered necessary with the upper limit determined by solubility. Since there is continuous solid solution in the pseudo-quarternary NiAl-CoAl and NiAl-FeAl systems, relatively high concentrations of Fe and Co were selected for this study. Each alloying element, except Be, in the first two alloy series was studied in three concentration levels, using a hypostoichiometric composition (Ni-48.5 a/o Al) as a base. Little is known about the solubility of Be in the base compound and it is difficult to find melting sources for Be containing alloys. The two Be-containing alloys were chosen to explore the limits of the NiAl hypostoichiometric stability range with Be levels that it was hoped were within the solubility limit. As another variant, alloys 77 and 78 included 5 a/o copper as this element may act synergistically with Be.

1.5.2.2 Multiphase Alloys

The fourth alloy series studied consisted of $B2+Ll_2$ alloys selected from binary and ternary Ni-Al-Fe, Ni-Al-Co, Ni-Al-Mn and Ni-Al-Cr systems. Specific alloy compositions are listed in Table 6. The selection was based on some toughening of NiAl alloys resulting from precipitation of the Ni_3Al phase in binary alloys initially observed by Russell and Edington (Reference 19) and more recent observations in rapidly solidified Ni-Al-Fe and Ni-Al-Co alloys (Reference 20). A comprehensive survey was therefore undertaken in this program to study the effects of alloy composition and processing on the ductility behavior of $B2+Ll_2$ alloys. Alloy numbers 79 and 82 are binary Ni-Al alloys with aluminum contents spanning the $B2+Ll_2$ phase field of Ni-Al phase diagram (Figure 8).

Alloy numbers 84 and 85 are examples of the ductile $B2+Ll_2$ alloys identified by Inoue and Matsumoto (Reference 20). As indicated in the Ni-Fe-Al ternary phase diagram (Figure 9), the equilibrium phases present in alloy No. 84 were expected to be of the NiAl and Ni_3Al type.

1.5.3 Phase II - Task II Alloys for Strength Improvement

Alloys formulated to increase strength include solid solution alloys and alloys containing precipitates of the types $L2_1$, Al, Ll_2 and other intermetallic compounds. These phase regions were explored in eight ternary systems Ni-Al-X, where X=Ti, Cr, Nb, Hf, Ta, Si, V and Zr. A comprehensive study was undertaken on the Ni-Al-Ti system and, to a lesser degree, the Ni-Al-Cr system because of the possibility of obtaining coherent precipitate strengthened NiAl alloys and because the phase fields of interest show wider compositional ranges in these ternary systems. The information gained from these systems could be applicable to other ternary systems. Alloys selected for strength evaluations are given in Table 7. Figure 10 shows the phase diagrams of some of the alloys selected for this phase. Boron was added to

most of the alloys with the aim of improving the grain boundary strength (by analogy with the Ni_3Al). Previous studies showed that small molybdenum additions produced fine grain size and improved the strength and ductility of NiAl alloys (Reference 12). Molybdenum at a concentration of 0.3 a/o was added to Alloy numbers 11, 19, 23 and 30.

2.0 EXPERIMENTAL

2.1 PREPARATION OF MATERIALS

2.1.1 Phase I NiAl Baseline Alloys

Phase I alloys were produced as castings and in powder form. Ten kilogram ingots of Alloys No. 1 through 8 were produced using a vacuum induction melting (VIM) technique. To reduce the casting porosity, the VIM ingots, enclosed in stainless steel jackets, were hot isostatically pressed (HIP) at 1093°C under a stress of 103 MPa for 3 hours. The HIP ingots were subsequently extruded at the Air Force Materials Laboratory. The extrusion cycle consisted of controlled heating at a rate of 80°C per hour to 600°C, soaking at that temperature for several hours, followed by heating at a more rapid rate (200°C per hour) to the extrusion temperature, 1000°C. An extrusion ratio of 9:1 was used for all of the alloys. The Phase I alloys in powder form were produced by Homogeneous Metals, Inc. (HMI). The powder was processed in an inert atmosphere during screening to -100 mesh. For consolidation, the powder was transferred in an inert atmosphere to cylindrical stainless steel containers followed by evacuation, hot-out gassing for one hour at 600°C, and sealing. Extrusion of the powder containers was performed under conditions similar to those used for the ingots.

2.1.2 Phase II NiAl Alloys

Phase II alloys were produced by nonconsumable arc melting in an argon atmosphere and cast into a water-cooled copper mold. The dimensions of the cast ingots were 12.7 by 25.4 by 83.8-mm (0.5 by 1.0 by 3.3-inches).

2.1.3 Melt Spinning

Melt spinning was conducted using a Model 2M Melt-Spinner manufactured by Marko Materials, Inc., Billerica, Massachusetts. Prealloyed charges were melted in a fused quartz crucible by induction heating in an argon atmosphere. The molten alloy was then ejected by pressurized argon as a stream through an orifice at the bottom of the crucible and directed onto a rotating copper quenching disk. The solidified alloy, in the form of ribbon of approximate dimensions 3-mm wide and 0.03-mm thick, was deposited in the ribbon collection chute 1.2-m long, avoiding ribbon fragmentation by impact with the melting chamber wall. The orifice was 0.5-mm in diameter and placed at a distance of 5-mm from the quenching disk. A surface speed of 18 meter/sec was used for quenching.

2.2 CHARACTERIZATION OF ALLOYS

2.2.1 Ductility Measurement

To characterize the ductility of the alloys, a computer-controlled wire electrical discharge machining technique was used to machine small tensile specimens from the castings and extruded bars. The specimens were 22-mm (0.87-inch) long with 6-mm (0.24-inch) long tapered grip sections and a 10-mm (0.4-inch) long, 3-mm (0.12-inch) wide, 1-to 2-mm (0.04-to 0.08-inch) thick gage section. The specimen configuration is shown in Figure 11a. Although the tensile tests provided useful assessment of plastic flow, the stress for the onset of plasticity was too imprecise for yield stress determination.

2.2.2 Strength Measurement

Yield strengths of selected alloys were determined in compression at 0.2 percent offset strain. The configuration of the specimen is shown in Figure 11b. The specimens, 5 by 5 by 13-mm (0.2 by 0.2 by 0.5-inch), were compressed between two alumina plattens, the displacement of which were measured using a linear voltage differential transformer (LVDT). The displacement and load, continuously recorded by an X-Y recorder during the tests, were used to define the stress-strain behavior of the alloys.

2.2.3 Electron Microscopy

The deformation behavior of selected Phase II - Task I alloys at room temperature was studied using transmission electron microscopy (TEM) techniques. Selected alloys were deformed about 2 percent in compression at room temperature prior to the TEM studies. Thin foils for TEM were cut with the foil plane normal to the compression stress axis. The Burgers vectors of dislocations produced by room temperature deformation were established using the g.b=0 "effective invisibility" criterion which involves examination of the visibility of dislocations at various g vectors and comparing the observations with the predictions. Burgers vectors used for the dislocation visibility calculations are <001>, <011> and <111>. The dislocation character and slip plane were identified from results of Burgers vector determination and dislocation slip trace analyses.

3.0 RESULTS AND DISCUSSIONS

Because of the large number of alloy conditions involved in this study, it is obviously not possible to illustrate and describe all features in detail. For completeness, microstructures, which may be of interest in the future but do not contribute to the main thrust of the following discussion are also included.

3.1 PHASE I NiAl BASELINE ALLOYS

All the Phase I alloys, in VIM ingot and powder form were extruded without difficulty. The extrusions were sectioned, both in the longitudinal and transverse directions, for metallographic examination. It was immediately clear that the hyperstoichiometric Alloy numbers 1 and 2, were extensively cracked. All other alloys appeared sound. Etched sections for both material forms revealed single phase alloys with an equiaxed microstructure, although duplex grain sizes were evident which were often distributed in bands as illustrated in Figure 12 for the VIM and Figure 13 for the powder alloy, number 3. The grain sizes of the powder alloys are generally smaller than those of the VIM alloys by up to a factor of 2.

3.1.1 Ductility

Tensile tests were conducted to assess ductility rather than strength of the Phase I alloys in the as-extruded condition. Tensile specimens could not be machined from Alloy number 1 because of its extreme brittleness. Ductility results for Alloy numbers 2 to 7 are shown in Figures 14 (a through f). At low temperatures failure occurred with no evidence of plastic flow; fracture sometimes occurring at the slight stress concentration at the shoulder of the specimen. As the temperature increased, the failure location tended to switch to the gage section. The onset of ductility occurs over quite a narrow temperature range, and the transition from brittle to ductile behavior can be designated by a temperature, T_{BD}, defined as the maximum temperature at or below which no plastic flow is measured at fracture. A tabulation of T_{BD} for alloys 2 to 7 is given in Table 8. In the case of the extruded VIM alloys, the observed brittle-ductile transition temperatures are 500°C for Alloys 3 and 7 which do not contain boron and 675°C for all the boron-containing alloys. No major effect of aluminum concentration in the brittle-ductile transition temperature can be observed in the VIM alloys. Most of the VIM materials fractured by transgranular cleavage at all temperatures tested. However, Alloy number 3 fractured intergranularly below and with a mixed transgranular-intergranular mode above the transition temperature.

The fracture behavior and the effect of boron in the P/M alloys follow similar trends as with the VIM alloys. It is interesting to note the considerably lower T_{BD} in the case of the boron-free stoichiometric Alloy number 3. The significance of this observation is not clear as no general trends emerge when all data are considered in terms of alloy stoichiometry and product form. It is known that the T_{BD} of bcc metals can be changed by metallurgical features such as grain size and dislocation substructure (References 32, 33). The observed differences could be due to the latter variations resulting from extrusion.

To study such effects in more detail, experiments were conducted on one of the P/M alloys (number 4) which involved a small amount of plastic deformation (3 percent) at 50°C above the transition temperature prior to tensile testing at lower temperatures. Results given in Figure 15 show that the brittle-ductile transition temperature of the prestrained alloy was lower than the parent material by about 200°C, an indication that the lower transition temperature in the P/M alloy, number 3, could be of similar origin. Attempts were made to further reduce the T_{BD} in P/M Alloy number 3 by swaging at 600°C, but the bar fractured in the first pass. The thermomechanical working approach was discontinued in favor of the alloying approach as a means for ductilizing NiAl alloys at ambient temperatures.

3.1.2 Hardness and Yield Strength

The hardness numbers and yield strength at room temperature of the boron-doped binary alloys in the as-extruded condition have been plotted in Figures 16 and 17 as a function of aluminum content. Hardness variations indicate that a minimum value occurs in the equiatomic alloy and increases in both nickel- and aluminum-rich alloys. These results are in agreement with previous studies (Reference 4). Compressive yield strength values were obtained over a range of temperatures (Figure 18). (Note that the hyperstoichiometric alloys could not be tested due to the extensive cracking.) The results show that at temperatures up to 600°C (1110°F), the strength increases as deviation from the equiatomic composition increases. This trend obviously parallels the hardness changes. However, above 600°C (1110°F) not only do the strength values fall to quite low levels, but the compositional trend reverses because at higher temperatures the equiatomic alloy has the highest strength. It was found that boron had a strong effect on strength; alloys containing 0.25 atom percent (a/o) of this element were about 60 percent stronger than boron-free alloys. Alloy 6 (Ni-43Al-0.25B) exhibited yield values over 830 MPa (120,000 psi) at room temperature and retained strength to quite high temperatures, being over 550 MPa (80,000 psi) at 600°C (1110°F). These values approach those of intermediate strength superalloys such as Waspaloy; however, the ductility values are poor, as described in the previous section.

3.2 PHASE II - TASK I NiAl ALLOYS

The alloys listed in Tables 5 and 6 were produced as drop cast ingots (12.7 by 25.4 by 83.8-mm) at Pratt & Whitney, except for the four beryllium-containing alloys. To reduce the casting porosity, the ingots were hot isostatically pressed at 1200°C (2200°F) under a stress of 100 MPa for 3 hours. The beryllium-containing alloys were produced as 8.9-by 57.2-mm diameter arc melted buttons at Livermore Lab, (courtesy of Dr. Jacobson). The buttons were studied in the as-cast condition. Selected alloys in Tables 5 and 6 were also prepared using melt spinning techniques.

3.2.1 Microstructure

The compositions of alloys given in Table 5 were selected to be B2 single phase from available phase diagrams. To verify the phase structure X-ray analyses were conducted on selected alloys. X-ray results showed the presence of only the B2 phase in the alloys containing iron, cobalt and gallium. For alloys containing chromium, an A2 phase, identified as alpha-chromium, was also observed when the chromium content exceeded 10 atom percent (Alloy numbers 41, 42 and 60.) In alloys containing manganese, a second B2 phase, identified as MnAl was also observed when the manganese level exceeded about 10 atomic percent.

To determine the effect of rapid solidification on ductility, several alloys including the chromium and manganese modified NiAl (numbers 40 and 52) and the baseline alloys (numbers 69, 74 and 75) were produced as ribbons using a melt spinning technique. The microstructures of alloy numbers 40 and 52 are given in Figure 19 which shows a grain structure consisting of columnar grains between equiaxed grained surface layers.

3.2.2 Ductility and Fracture

Ductility inferences could be drawn from the mechanical integrity of the drop cast ingots and the machining behavior of the densified materials. These observations are summarized in Table 9, which shows that most of the materials were cracked either in the as-cast condition and/or during machining. An example of the cracks observed is shown in Figure 20 for the case of the beryllium-containing alloy number 59. Extreme brittleness was observed in alloys which contained a second phase, for example, numbers 41, 42, 45, 60 and 61. Some of the single phase alloys also appeared to be rather brittle as cracks were found in the ingots. Only 7 out of 32 alloys could be machined without extensive cracking. It was considered, initially, that the extreme brittleness of some of the alloys was in part due to the method of alloy preparation. The specific hearth configuration utilized for melting resulted in a rather uneven solidification profile which in turn caused the formation of large grains. To produce more rapidly solidified castings, a new hearth configuration was subsequently utilized to remelt some of the alloys. Finer grain structures were indeed produced in the new castings, however, the brittleness persisted. Another attempt to modify the ductility behavior was by rapid solidification using a melt spinning technique. Several alloys including the chromium and manganese modified NiAl (numbers 40 and 52) and the baseline alloys (numbers 69, 74, and 75) were produced as ribbons. The ductility of the melt-spun alloys was assessed by bending the ribbons at room temperature. Results indicate that rapid solidification has little if any, effect on the room temperature ductility of this series of alloys.

Tensile testing similar to that for the Phase I alloys was conducted to determine the effect of substitutional alloying on brittle-ductile transition behavior. Densified alloys which could be machined (see Table 9) were tested and results are given in Table 10. The transition temperature of the baseline alloy (Ni-48.5 a/o Al) was found to be 500°C and those of the gallium or manganese modified alloys were 75°C to 275°C higher. Since the processing and the grain sizes of the alloys tested are rather similar, the observations indicate an adverse effect of gallium or manganese additions on ductility.

3.2.3 Deformation Behavior

Transmission electron microscopy (TEM) was used to determine the effect of substitutional solutes on deformation behavior of ternary NiAl alloys. Alloys which could be machined without extensive cracking were studied including alloys containing Cr, Mn, Ga, and the baseline NiAl (see Table 9).

Dislocations were generated in selected alloys primarily by compressive deformation at room temperature. For the chromium and manganese-modified alloys dislocations produced by compression deformation at 775°C, a temperature above the brittle-ductile transition for both alloys, were also studied. Attempts were made to determine the effect of deformation modes (uniaxial tension versus compression) on dislocation behavior in the manganese-modified alloy, which was partially successful as the tensile specimen failed in brittle manner at 20°C without introducing sufficient dislocations for analysis. However, a direct comparison of dislocations features in tensile and compressive deformation at 775°C was made.

3.2.3.1 Baseline NiAl Alloy (Ni-48.5 a/o Al)

The general appearance of dislocations in the alloy produced by room temperature deformation is illustrated in Figure 21a which shows dense dislocation clusters aligned along [110] directions. Analysis of dislocations in the clusters using the invisibility criterion shown in Table 11 indicates that the Burgers vectors of these dislocations are [001]. The slip plane is then found to be (110) by slip trace analysis based on [001] Burgers vector (Figure 21b). Long dislocation segments within clusters lie predominantly along [110] direction and therefore are mostly edge in nature. Upon imaging some of these edge dislocations, using +g and -g with deviations $s > 0$, the dislocation spacings changed indicating that they are dislocation dipoles.

Previous electron microscopy studies of slip systems in NiAl were conducted primarily on single crystals. Results summarized by Fraser, et al (Reference 34) show that NiAl compressed along <001> at temperatures below room temperature deforms by the operation of <111> {112} and <111> {110} slip systems, and that plastic deformation of crystals compressed along any other direction is caused by the <100> {110} and <100> {001} slip systems. These results imply that the preferred Burgers vector in NiAl is <001> and that slip along <111> occurs rarely; only below room temperature and when stressed along an <001> axis for which there is no resolved shear stress along the <001> directions. Unlike single crystal specimens, each crystal (grain) in a polycrystalline aggregate is subject to a complex state of stress because of the constraints of the neighboring grains, even if the applied stress is uniaxial. Thus most, if not all, potential slip systems would be stressed and the dislocations with the lowest energies and highest mobility would contribute toward the deformation. The observation of the <001> {110} slip system in polycrystalline NiAl is therefore consistent with previous single crystal studies.

3.2.3.2 Chromium Modified NiAl (Ni-48.5 a/o Al-5.2 a/o Cr)

The general appearance of dislocations produced by room temperature compressive deformation and phases present in this alloy are illustrated in Figure 22a. Small spherical precipitates with sizes ranging from 1600Å to 3200Å and parallel slip bands (traces denoted as A) are the obvious features. Using X-ray energy spectroscopy and micro-micro diffraction with a spot size of about 1000Å, the spherical precipitates in Figure 22a were identified as alpha-chromium with a lattice parameter of 2.84Å which is the same as that determined for the matrix using a similar technique. An analysis of Burgers vectors of dislocations inside the slip bands is shown in Table 12 which indicates that they are of the [111] type. The slip plane is then found to be (112) by slip trace analysis based on the [111] Burgers vector (Figure 22b). The dislocation line traces are perpendicular to slip trace A and the dislocation line direction was identified as [111] showing the dislocations are screw in nature. When imaging these screw dislocations by reversing the operating g vector with deviation $s > 0$, the dislocation spacings change (Figure 23), indicating a dislocation dipole configuration. These closely spaced dipoles when steeply inclined from the top to the bottom of the foil, show a characteristic center of inversion which can also be observed in Figure 23.

It is interesting to note that the addition of Cr indeed changes the basic slip behavior of NiAl from the <001> to <111> slip. Further, the formation of dislocation bands in the Cr-modified alloy indicates difficulty in cross slip. Both of these observations are consistent with the hypothesis advanced in Section 1.2 that addition of early transition metals to NiAl would reduce the antiphase boundry energy which contributes to the stabilization of the 1/2a<111> superpartials and the difficulty in cross slip. The fact that the Cr-modified alloy is still brittle in spite of the operation of <111> {112} dislocations could indicate a lack of mobility in such dislocations. Support of this view can be inferred from the several fold increase in strength of NiAl crystals when deformation is by the <111> {112} slip system (Reference 35).

The appearance of dislocations produced by compressive deformation above the brittle-ductile transition temperature is shown in Figure 24. A homogeneous distribution of dislocations resulted from the elevated temperature deformation. Analysis of the matrix dislocations using the "invisibility" criterion shown in Table 13, leads to the conclusion that the Burgers vector is <010>. The slip plane and average dislocation line direction were found to be (001) and [100], respectively. Therefore, the dislocations are predominantly of the edge-type. No dislocation dipoles were found, in contrast to the room temperature deformation which produced numerous dipoles.

The above observations show that the Cr effect on slip behavior on NiAl does not extend to high temperatures. This may be rationalized by the fact that the stability of the B2 lattice in NiAl decreases with decreasing temperature and shows a tendency to undergo martensitic type lattice transformation at low temperatures. Thus, the stability of NiAl is more readily purturbed at low

temperatures by alloying additions than at high temperatures. Another puzzling observation is the high ductility of the Cr-modified NiAl in polycrystalline form in spite of the operation of the <001> {100} slip system which violates the Von Mises Criterion. Similar questions had been raised by Baker and Schulson (Reference 36) in the case of binary polycrystalline NiAl, which was observed to deform with high ductility by <001> dislocations. Detailed study by Baker and Schulson shows that the high ductility was made possible by the operation of an hko <001> slip system plus diffusion-assisted deformation processes. The high ductility of the Cr-modified and other NiAl alloys at temperatures above the brittle-ductile transition could perhaps be explained in a similar manner.

3.2.3.3 Manganese Modified NiAl (Ni-43.7 a/o Al-4.9 a/o Mn)

The dislocation structure in this alloy, produced by compressive deformation at room temperature, shown in Figure 25 appears to be somewhat similar to the baseline alloy (Figure 21a). Analysis of dislocations, similar to those already described, led to the identification of [111] as the Burgers vector and (112) as the slip plane. In this case, it was determined that the dislocations are predominantly edge in nature.

The dislocation structures produced by deformation above the brittle-ductile transition are shown in Figure 26. The dislocation structures produced in compressive deformation (Figure 26a) and tensile straining (Figure 26b) appear rather similar. Further, diffraction analysis showed that the nature of the dislocations and slip systems in both types of deformation are essentially similar, predominantly edge dislocations with <011> and <001> slip directions observed in tension and <001> in compression.

The observations show that Mn has a similar, but perhaps less pronounced effect on the dislocation behavior of NiAl at low temperatures as compared to Cr. The operation of <111> {112} dislocations again did not lead to ductility improvement in the Mn-modified alloy which could perhaps be attributed also to lack of mobility.

3.2.3.4 Gallium Modified NiAl (Ni-48.0 a/o Al-0.5 a/o Ga)

As shown in Figure 27, the dislocation appearance is rather similar to the baseline NiAl alloy. The slip traces denoted as A are diffuse in this alloy. Analysis of dislocations inside the slip bands using the "invisibility criterion" show that the Burgers vectors are [010]. The slip plane and dislocation line direction were identified as (101) and [101] indicating that the dislocations are edge in nature. Similar studies conducted on the alloy containing a higher concentration of Ga (2.4 a/o) gave essentially the same results.

As described in Section 1.2, additions of Ga and Be to NiAl are made to increase the atomic radius ratio which may improve the mobility of <111> dislocations if such dislocations were indeed produced. No <111> dislocations were found in the Ga-modified alloys. It would appear that addition of Be or Ga in combination with Cr may produce more desirable results.

Results of all dislocation analysis on selected substitutional alloys for Phase II - Task I studies are summarized in Table 14.

3.2.4 Ductility and Strength of Multiphase Alloys

The fourth series of alloys studied are nickel-rich binary and ternary alloys numbers 79 through 87 which are listed in Table 6. The alloys were produced as 2.4 cm diameter, 10 cm long arc-melted drop castings and as ribbons using a melt spinning technique. The melt-spun alloys were studied in four conditions: as-spun and after heat treatments for two hours at 800°C, 1000°C and 1200°C. The drop castings were studied in as-cast condition and after a heat treatment for 2 hours at 1200°C.

The ductility of the melt-spun alloys at various heat treatment conditions was determined using room temperature bend tests. The results are summarized in Table 15. Except for alloy number 82, other alloys showed some ductility at room temperature in the as-solidified and/or after heat treatment condition. Alloy number 82 contained the highest aluminum content and was brittle in all conditions. From this observation together with previous results of the program, it may be concluded that in polycrystalline binary NiAl alloys with aluminum content exceeding about 37 a/o, ductility at room temperature cannot be induced by control of microstructure. It is also important to note that the ductility of some alloys (Numbers 80, 81, 86 and 87) was improved by heat treatment while the the ductility of other alloys (Nos. 79, 82, 84 and 85) was not affected by heat treatment even though significant changes in microstructure occurred in these alloys as described in the following section. For the alloys not affected by heat treatment, it is probable that ductility is governed by more fundamental properties of the alloys such as the nature of atomic bonding, which clearly cannot be modified by heat treatment.

The tensile ductility of the cast alloys was measured in both the as-cast condition and after 2 hours at 1200°C, a heat treatment which resulted in room temperature ductility improvements in some of the melt-spun alloys. The elongation of the cast alloys at fracture is given in Table 16 which, for comparison, also includes the more qualitative results on the alloys in ribbon form. Several interesting observations regarding the effect of solidification rate on ductility at ambient temperatures can be made from Table 16.

- Some alloys (numbers 79, 84 and 85) are relatively ductile in either the rapidly solidified or cast form.

- For all other alloys, except the virtually completely single phase alloy number 82, rapid solidification appears to enhance the ductility. Interestingly, the ductility enhancement occurs not in the as-solidified condition, except for alloy number 81, but rather after a high temperature heat treatment. This indicates that the ductility enhancement is an indirect consequence of rapid solidification resulting from a more favorable phase mixture in subsequent heat treatment. A microstructure comparison of some alloys in ribbon and cast form will be made below.

The fact that Alloy number 79 showed some ductility at room temperature is remarkable since the Ni_3Al phase in this alloy is expected to be hyperstoichiometric (Al > 25 a/o) and that the alloy does not contain boron, conditions which have been shown to lead to extreme brittleness in polycrystalline Ni_3Al. The ductility of number 79 at 600°C is also surprising in view of the fact that polycrystalline Ni_3Al is rather brittle at this temperature. Similar observations can also be made from the 600°C ductility data of Alloy numbers 84 and 85 which consist of Ni_3Al, and NiAl phases. For comparison, a binary Alloy number 83 containing similar aluminum content as numbers 84 and 85 and consisting of Ni_3Al and Nickel solid solution phases showed no ductility to 600°C (Table 16).

The tensile fracture strength of the cast nickel-rich NiAl alloys are given in Table 17 which shows that the addition of Fe and Co to the base alloy Ni-20 a/o Al, not only enhances the 600°C ductility but also provides significant strengthening. Among the alloys which fracture before plastic yielding, the Cr-modified NiAl (number 87) showed the highest fracture strength.

3.2.5 Microstructure of Multiphase Alloys

The general microstructure features in these alloys are described first followed by a more detailed analysis of microstructures in Alloy numbers 84 and 86. As described in the preceding section Alloy number 84 is one of the alloys which show good ductility irrespective of solidification rate and heat treatment. In contrast, Alloy number 86 is one of the alloys the ductility of which is influenced by solidification rate and heat treatment.

The general microstructures and room temperature tensile fracture modes of the nickel-rich alloys in cast form are illustrated in Figures 28 through 32 and the corresponding microstructures of these alloys in rapidly solidified condition in Figures 33 through 40. The fracture modes of the cast alloys are summarized in Table 18.

The most prominent microstructural feature in the cast binary alloy with the lowest aluminum content (number 79) is the highly irregular Ni_3Al dendrites (Figure 28). In contrast, dendritic structures are absent in the higher aluminum alloys (numbers 80, 81, and 82, Figures 29, 30, and 31). The Ni_3Al phase precipitates with a spaghetti-like morphology in Alloy number 80. Alloy numbers 81 and 82 appear to be predominently single phase and have undergone a complete transformation to martensite in the case of Alloy number 81. A lamellar structure consisting of NiAl and Ni_3Al phases has been observed in both the iron and cobalt-modified ternary Alloy numbers 84 and 85 (Figures 32, 33 and 34). It should be pointed out that the formation of the lamellar structure is probably not responsible for the enhanced ductility observed in these two alloys, as the rapidly solidified counterparts which are also ductile do not show any lamellar structure.

The microstructure of the cast manganese-modified alloy (number 86) consists of equiaxed grains and a spaghetti-like precipitate nucleated from grain boundaries which has grown into the grains (Figure 35a). Electron microprobe chemical analysis showed that the composition of the precipitate phase contains more manganese and less aluminum than the matrix, indicating the

possibility of a Ni_3Al type precipitate in a NiAl matrix. The high temperature heat treatment of this alloy resulted in some grain growth and formation of more precipitate (Figure 35b). The as-cast microstructure of the chromium-modified Alloy (number 87) consists of "blocky" dendrites (grey regions in Figure 36a.) Electron microprobe chemical analysis showed that the interdendritic regions (light areas in Figure 36a) contain more chromium and less aluminum than the dendrites suggesting Ni_3Al and NiAl types of phase, respectively. The high temperature treatments resulted in homogenization of the cast structure and a uniform precipitation of a spaghetti-like phase which has a similar composition to the interdendritic regions in the as-cast structure (Figure 36b).

The microstructure of melt-spun B2 + $L1_2$ alloys at various heat treatment conditions, shown in Figures 37 through 44, reveal major changes in grain size and grain structure occurring in some alloys that were heat treated at 1200°C. For example, Figures 39, 40, 41 and 44 show the development of "bamboo" grain structure from small equiaxed grains in the as-solidified condition. Changes in phase morphology and distribution in the melt-spun alloys also occurred during the heat treatment. Figure 37 shows, for example, a lamellar arrangement of the B2 and $L1_2$ phases in Alloy number 79 in the as-solidified condition developed into equiaxed grains of the two phases during the 1200°C heat treatment (Figure 37). Although no detailed phase structure determination has been made on the melt-spun alloys, it is obvious that some of the microstructural changes were results of structural (martensitic) transformations (e.g. Figures 38, 43 and 44).

Detailed analysis of Alloy number 84 in the as-rapidly solidified ribbon form revealed that the columnar grains (see Figure 41) are of two different compositions, one having more iron and less aluminum than the others. Electron micro-diffraction analysis showed that high iron-low aluminum grains consist of a high volume fraction of fine Ni_3Al type particles of dimensions about 25-nm in a disordered fcc (γ phase) matrix (Figure 45b). The other type of grains were found to be a single phase NiAl.

The volume fraction of NiAl phase was determined to be about 54 percent in the as-solidified condition. Heat treating the alloy for two hours at 1200°C did not have any appreciable effect on the phase composition and distribution. However, considerable grain coarsening occurred as shown in Figure 45c. The microstructure of Alloy number 84 in ribbon form is significantly different from that of its cast counterpart which consists of a lamellar structure (Figures 32 and 33). Further, the as-solidified microstructures in this alloy appear to be rather stable; not significantly changed by the high temperature heat treatment used.

An effect of solidification rate on microstructure can also be observed in Alloy number 86. Detailed microstructural features of this alloy in the as-rapidly solidified ribbon form is shown in (Figure 46). Extensive micro-twinning was observed and the alloy appears to consist of a single phase as no compositional differences were detected at various regions. Electron micro-diffraction analysis showed that the crystal structure was noncubic, the

exact lattice cannot be established from the diffraction patterns obtained. The microstructure of the rapidly solidified material was found to undergo major changes during heat treatment. The typical microstructure after 2 hours at 1200°C is shown in Figure 47, which clearly reveals a two-phase structure. Transmission electron microscopy studies showed that in addition to the twinned noncubic phase, a moderate amount of Ni_3Al phase was formed during the heat treatment. These microstructural changes may account for the enhanced ductility observed in the heat treated melt-spun ribbon.

3.3 PHASE II - TASK II NiAl ALLOYS

Thirty-one alloys were formulated in an attempt to enhance the strength of the binary NiAl over a useful temperature range. The alloy compositions are given in Table 7. The potential for strengthening of NiAl produced by solute hardening, precipitation of coherent and incoherent phases of the A2, $L2_1$, and Ll_2-type were explored in eight ternary systems; Ni-Al-(Ti, Cr, Nb, Hf, Ta, Si, V and Zr). The most comprehensive study was undertaken on the NiAl-Ti system, while a somewhat less extensive study was also undertaken on the Ni-Al -Cr system.

The alloys were produced using arc melting and drop casting techniques. It was observed that a majority of the castings contained one or more cracks in the as-cast condition. About one-third of the alloys cracked extensively during machining of compression specimens. A summary of cracking tendencies is given in Table 19. All alloys containing $L2_1$ type phase were too brittle for machining. Two-thirds of the alloys given in Table 7 were successfully machined and compressive yield strengths over a temperature range of 20°C (70°F) to 900°C (1650°F) were determined. The results are described in the following sections.

3.3.1 Ni-Al-Ti Alloys

The compressive yield strengths of single phase NiAl alloys as a function of temperature are given in Figure 48. The range of yield strengths observed at low temperatures is very high (15 ksi (100 MPa) to 200 ksi (1380 MPa) at room temperature) but converges at high temperatures to about 20 ksi (137 MPa) at 900°C (1650°F). As expected the unalloyed single phase NiAl (number 13) exhibited the lowest strength. Doping unalloyed NiAl with boron (number 14) provided considerable strengthening. The addition of titanium was observed to provide a more dramatic increase in strength (numbers 18 and 19). However, the strengths of these solute hardened alloys decreased rapidly with increasing temperature. Both good strength and strength retention to intermediate temperatures were observed in NiAl alloys (numbers 9 and 10) containing Ll_2-type precipitation (Figure 49). Figure 49 also indicates that the yield strength of the Ll_2 precipitate hardened alloy (number 10) can be changed by solutioning and aging heat treatments in a similar manner to the Ll_2 precipitation strengthened nickel base superalloys.

Some interesting microstructural observations have been made on selected alloys of the Ni-Al-Ti system. Figure 50 shows the microstructure of the binary NiAl alloy containing 36 atom percent aluminum (number 13) in various heat treatment conditions. NiAl alloys with this aluminum content undergo thermoelastic martensitic transformation with an M_s temperature of about 150°C (300°F) (Reference 37). Figure 50a shows that Alloy number 10 is fully martensitic after a heat treatment at 1260°C (2300°F). Heat treatment of this alloy at a lower temperature 1040°C (1900°F) resulted in decoration of grain boundaries with Ni_3Al phase in addition to the formation of martensite (Figure 50b). Slow furnace cooling from the 1040°C (1900°F) led to precipitation of additional Ni_3Al phase which was located also intragranularly (Figure 50b). The slow cooling treatment also appears to have reduced the propensity for the martensitic transformation. Doping of Ni-36 a/o Al with boron was found to produce dramatic microstructural effects which are illustrated in Figure 51. Two microstructural differences can be observed in the boron-doped alloy (number 14) after the 1260°C (2300°F) heat treatment: incipient melting at the grain boundaries is evident and the martensitic transformation has been suppressed (Figure 51a). Martensite is also absent in the boron-doped alloy after the 1040°C (1900°F) heat treatment (Figures 51b and 51c).

The variety of microstructures observed in Alloy number 13 (Figure 52) indicates that low temperature ductility of this type of alloy may be manipulated by heat treatment. Simple bend tests were conducted on Alloy number 13 at room temperature to survey the fracture mode as a function of microstructure. Results are illustrated in Figure 52. Transgranular fracture was observed in the martensitic structure resulting from the 1260°C (2300°F) heat treatment (Figure 52a) and the NiAl-Ni_3Al two-phase structure produced by the slow furnace cooling from 1040°C (1900°F) (Figure 52c). Mixed inter- and trans- granular fracture was found in the martensitic structure with grain boundaries decorated by Ni_3Al phase (Figure 52b). The bend ductility associated with these microstructures was observed to be limited, but varied with microstructure, the highest ductility being found with the martensitic structure.

The microstructures of the NiAl-Ni_3Al two-phase alloys (numbers 9 and 10) were also examined. Figure 53 shows that the Ni_3Al phase (dark contrast) in Alloy number 9 formed a lamellar structure with NiAl and the volume fraction of the lamellar colonies is about 0.6. In contrast, the Ni_3Al phase in Alloy number 10 (Figure 54) appears as grains with highly irregular boundaries which are delineated by the NiAl phase. Rather small NiAl phase particles can be observed within the Ni_3Al grains.

3.3.2 Ni-Al-Cr Alloys

The compressive yield strength versus temperature results for the chromium-modified NiAl alloy are illustrated in Figure 55. As in the Ni-Al-Ti system, NiAl alloys strengthened with Ni_3Al phase (numbers 12 and 24) have better yield strength characteristics than alloys containing the A2 (alpha-chromium) phase. The yield strengths of the Ni-Al-Cr two-phase alloys

(numbers 21, 22 and 23) are similar to the solute hardened single phase Alloy (number 25) indicating that the A2 phase is not an effective strengthener in NiAl. In an attempt to strengthen the Ni-Al-Cr two-phase alloys, a solutioning and aging heat treatment cycle was also included for selected alloys. However, the additional heat treatment resulted in no yield strength improvements compared with the alloys in the HIP condition.

3.3.3 Ni-Al-V Alloys

The compressive yield strength versus temperature curves for the vanadium-modified NiAl alloys in the as-cast condition are given in Figure 56. There appears to be a correlation of vanadium content with strength. The microstructural features responsible for the strengthening in this alloy system have not been studied.

3.3.4 Other Ternary NiAl Alloys

The compressive yield strength versus temperature curves for NiAl alloys in other Ni-Al-X ternary systems (X=Nb, Hf, Si and Zr) are given in Figure 57 in which data from nominally single phase alloys containing about 1 atom percent solute were compared. In this figure, hafnium appears to provide the largest increase in yield strength per atom percent of solute.

3.4 PHASE III ALLOYS

Results of Phases I and II studies showed that among the various ternary alloys studied, only the nickel-rich alloys containing either iron or cobalt exhibited acceptable ductility behavior. Accordingly, iron and cobalt modified Alloy numbers 88 and 89 with compositions given in Table 20 were selected for Phase III studies. These alloys were produced as 7.6-cm (3-inch) diameter vacuum induction melted ingots which were then encapsulated in steel jackets and extruded following similar procedures as those for Phase I alloys. Alloy numbers 88 and 89 were studied after a heat treatment for 2 hours at 1150°C.

3.4.1 Microstructure of Phase III Alloys

The microstructures of Alloy numbers 88 and 89 in the transverse section of the extruded bar are given in Figure 58. The microstructure of Alloy number 88 consists of grains of two different size distributions. The large grains which comprise 85 percent were found, using electron diffraction analysis, to be a B2 phase. The composition of the B2 phase, given in Table 21, was determined using an electron microprobe technique. The small grains which are distributed in the grain boundary regions of the B2 phase were found to consist of two coherent Al and $L1_2$ phases with the $L1_2$ phase appearing as very fine (15-nm) particles (Figure 59a). The average composition of the two phases is given in Table 21. The Al phase is likely to be an iron-nickel solid solution.

The microstructure of Alloy number 89 (Figure 58b) was found to consist of about 80 percent striated grains in an apparently single phase matrix. Electron microscopy studies revealed microtwin bands in the striated grains and complex diffraction patterns one of which was found to fit a rhombohedral lattice with parameters a = 3.08Å and α = 45°. The striated grains are likely to be a martensitic phase which was produced from the B2 phase during cooling to room temperature following the high temperature heat treatment. It is known that the B2 lattice of hypostoichiometric NiAl alloys with low aluminum contents tends to be unstable at low temperatures and transforms to martensite with lower crystal symmetry. The matrix of Alloy 89 was found to be an Al phase containing coherent Ll_2 particles about 72nm in size (Figure 59b). The composition of the striated grains and the average composition of the matrix phases are indicated in Table 22.

3.4.2 Mechanical Properties

Standard test specimens were used to measure properties of the extruded bar stock. Cylindrical specimens with dimensions given in Figure 60a were used to determine tensile and creep properties and center cracked panels (Figure 60b) to assess fatigue crack growth properties. Testing procedures prescribed by ASTM were followed in evaluating mechanical properties of Alloy numbers 88 and 89.

The tensile properties of Alloy numbers 88 and 89 are given in Figure 61 which show that the strength levels of the NiAl alloys are similar to nickel superalloys with a low volume fraction (0.1 to 0.2) of the strengthening Ll_2 phase. Interestingly, the NiAl alloys show tensile ductility at room temperature of 5 to 10 percent elongation at fracture. The ductility of both alloys increases slowly with temperature up to almost 700°C after which it increases at a rapid rate. The iron-modified NiAl alloy (number 88) was found to be stronger than the cobalt-modified alloy (number 89) at low temperatures but it's strength decreased more rapidly with increasing temperatures and became weaker than the cobalt-modified alloy above about 400°C. Tensile fracture occurred transgranularly at low temperatures and intergranularly at high temperatures for both alloys.

Constant load creep testing was conducted at 760°C under initial stress levels equal to 50 percent of the tensile yield strengths and at 980°C under 33 percent of the yield strengths of the respective alloys. Creep rupture occurred within 2 hours at 760°C and less than 5 hours at 980°C for both alloys, indicating that the alloys lack creep resistance. Creep failures were observed to be intergranular in all cases.

Fatigue crack growth measurements were conducted at a stress ratio R of 0.1, frequency of 60 cycles per minute at room temperature and at 650°C. Results for Alloy numbers 88 and 89 are given in Figure 62 which show that the cobalt-modified NiAl alloy is slightly better at both temperatures. For comparison, the crack growth data of an IN-100 type turbine disk alloy determined at 650°C and similar stress conditions were also included in Figure 62. The crack growth behavior of the NiAl alloys is similar to a current advanced disk alloy.

4.0 CONCLUSIONS

Although no breakthrough in the form of a new alloy that meets the rather challenging requirements of turbine disks occurred in this study, certain alloying/process options were defined more clearly. Not surprisingly the major drawback in NiAl alloys is the lack of ductility (or impact resistance) at ambient temperatures. Although there are several approaches to moving the brittle-to-ductile transition temperature, T_{BD}, the onset of ductility always seems to occur suddenly over a narrow temperature range. It can be speculated that these changes are produced by factors that influence the thermally activated flow processes. This in turn indicates that rather radical changes in the alloys will be necessary to modify other athermal behavior.

The main areas of progress in this project can be summarized as follows:

- The transition temperature in binary NiAl alloys produced from either cast or P/M preforms ranged between 375 and 625°C. No clear trends could be discerned although the T_{BD} value of 375°C for the 50 percent Al P/M alloy may indicate an advantage for this product form.

- T_{BD} can be reduced by prior straining above the initial transition temperature. Specifically, a tensile strain of 3 percent at 50°C above the transition reduced the T_{BD} value by 200°C. This behavior pattern has been observed in other body center cubic alloys.

- Boron additions (0.25 percent) increase the strength of binary alloys by up to 200 MPa at room temperature and the higher strength is sustained to 600°C. Such additions raise the T_{BD} by at least 150°C. Boron has no effect on the fracture mode at low temperatures, which occurs by a cleavage mechanism.

- Alloys containing 29 to 35 percent Al show some bend ductility when produced as melt-spun ribbon, and this seems to be retained after high temperature exposure. In contrast, arc melted material containing 35 percent Al was completely brittle.

- The martensitic transformation that occurs in alloys containing around 36 percent Al does not appear to induce any ductility in cast alloys The transformation may have contributed to the bend ductility observed in RST ribbon although the details are unclear.

- Single element additions did not improve ductility characteristics. For example, Ga and Mn had little effect on T_{BD}. Two elements, Mn and Cr were found to change the slip system at room temperature. Specimens tested in compression exhibited $\langle 111 \rangle \{112\}$ slip in contrast to the $\langle 100 \rangle \{010\}$ slip in the base compound. This could prove to be an important finding, but methods of increasing dislocation mobility must also be defined before the more isotropic slip characteristics can be exploited.

- Several methods of increasing the strength of NiAl alloys were examined.
  - Ti is an effective solid solution hardener, producing strength increases of up to 500 MPa at low and intermediate temperatures.
  - Formation of $L1_2$ (Ni_3Al) precipitates resulted in moderate strength increases and strength was retained to higher temperatures.
  - Formation of Al (alpha-Cr) precipitates did not seem to offer any strength advantage over solid solutions.
  - Alloys which formed the $L2_1$ (Ni_2AlTi) phases were too brittle to be tested.
- The best balance of strength and ductility was found in low Al containing alloys with Co and Fe additions. The major phase ir these alloys is the B2 phase.
- These alloys were produced as extruded bars and the mechanical properties were characterized in more detail.
  - Yield strength of up to 120 ksi (830 MPa) to temperatures of 600°C were obtained.
  - Creep rupture properties are inferior to current disk alloys.
  - Crack growth rates appear to be about equal to the most advanced superalloy disk materials.

REFERENCES

1. E. P. Lautenschlager, Jr., "Effects of Structure Upon the Mechanical Behavior of B-NiAl," Northwestern University Ph.D. Dissertation, 1966.

2. A. J. Bradley and A. Taylor: Proc. R. Soc. A, 1929, Vol. 159, p 232.

3. A. Lasalmonie, M. J. Lequeux and P. Costa, "Strength of Metals and Alloys," Proc. Int. Conf., 5th, p 1317, Ed. P. Haasen, V. Gerold and G. Kostroz, Vol. 2, 1979.

4. W. J. Yang and R. A. Dodd: Metal Sci. J., 1973, Vol. 7, p 412.

5. M. H. Loretto and R. J. Wasilewski: Strength of Metals and Alloys, Second International Conference, ASM, Metals Park, 1970, Vol. 1 pp 113-117.

6. A. K. Vandervoort, Mukherjee and J. E. Dorn: Trans. ASM 1966, Vol. 59, pp 930-944.

7. M. Rudy and G. Sauthoff: Mat. Res. Soc. Symp. Proc. Vol. 39, 1985, Materials Research Society, pp 327-333.

8. A. U. Seybolt: Trans. ASM, 1966, Vol. 59, pp 860-875.

9. A. Lasalmonie: J. Materials Sci, 1981, Vol. 17, pp 2419-2423.

10. G. M. Rowe, J. Ingram and P. R. Strutt: 29th Annual EMSA Meeting Proc. 1971, pp 118-119.

11. E. M. Schulson, Presentation at NASA-COSAM Workshop, NASA-Lewis, Oct. 1982.

12. E. M. Grala, "Mechanical Properties of Intermetallic Compounds," Ed. J. H. Westbrook, J. Wiley & Sons Inc., N.Y., 1960.

13. E. R. Stover, "Effects of Alloying and Deformation Processing in Mechanical Behavior of NiAl," WADC-TDR-60-184, Part VII Vol. II, Nov. 1966.

14. R. S. Polvani, W. S. Tzeng and P. R. Strutt: Metall. Trans, 1976, Vol. 7A, pp 33-40.

15. W. A. Rachinger and A. H. Cottrell: Acta Metall, 1956, Vol. 4, p. 109.

16. P. A. Flinn: Trans. TMS-AIME, 1960, Vol. 218, p 145.

17. K. I. Portnoy, V. L. Bogdanov, A. V. Ruban and D. L. Fuks: Russian Metallurgy No. 5, 1981, (UDC 669, 245:536,722) pp 95-97.

18. D. I. Potter: Materials Sci and Engr., 1969/70, Vol. 5, pp 201-209.

19. K. C. Russell, and J. W. Edington: Metal Science J., 1972, Vol. 6, pp 20-24.

20. A. Inoue, T. Masumoto: J. Materials Sci, 1984, Vol. 19, pp 3097-3106.

21. R. W. Guard and A. M. Turkalo: "Mechanical Properties of Intermetallic Compounds," Wiley & Sons, New York (1959) p 141.

22. Y. K. Au and C. M. Wayman: Scripta Metall., 1971, Vol. 6, pp 1209-1214.

23. V. V. Martynov, K. Enami, L. G. Khandros, A. V. Tkachenko and S. Nenno: Scripta Metall., 1983, Vol. 17, pp 1167-1171.

24. A. Taylor and R. W. Floyd: J. Inst. Metals, 1952-53, Vol. 81, p 25.

25. K. P. Myasnikova, V. Ya, L. I. Mazkiv, L. I. Pryakhina and G. Ya. Motrychuk: Russian Metallurgy, 1977, Vol. 3, pp 192-199.

26. A. Taylor and R. W. Floyd: J. Inst. Metals, 1952-53, Vol. 81, p 451.

27. K. W. Girard and E. A. Smith: J. Inst. Metals, 1959-60, Vol. 88, p 283.

28. L. Kauman and H. Nesor: Canadian Metall. Quarterly, 1975, Vol. 14 p 221.

29. V. Ya Markiv, V. V. Burnashova: UDC 669.297, 5'54' 71, pp 113-115.

30. J. S. Benjamin, B. C. Giessen, and N. J. Nicholas: Trans. TMS-AIME, 1966, p 224.

31. P. Nash and D. R. F. West: Metal Science, Dec. 1979, p 670.

32. G. T. Hahn: Metall. Trans. 1984, Vol. 15A, p 947.

33. M. F. Ashby and J. D. Embury: Scripta Metall., 1985, Vol. 19, pp 557-562.

34. H. L. Fraser, R. E. Smallman and M. H. Loretto: Phil. Mag. 1974, Vol. 28, pp 651-665.

35. R. T. Pascoe and C. W. A. Newey: Metal Sci J., 1968, Vol. 2, pp 138-143.

36. I. Baker and E. M. Schulson: Metall. Trans A, 1984, Vol. 15A, pp 1129-1136.

37. S. Chakravorty and C. M. Wayman: Metall. Trans. A, 1975, Vol. 7A, pp 555-568.

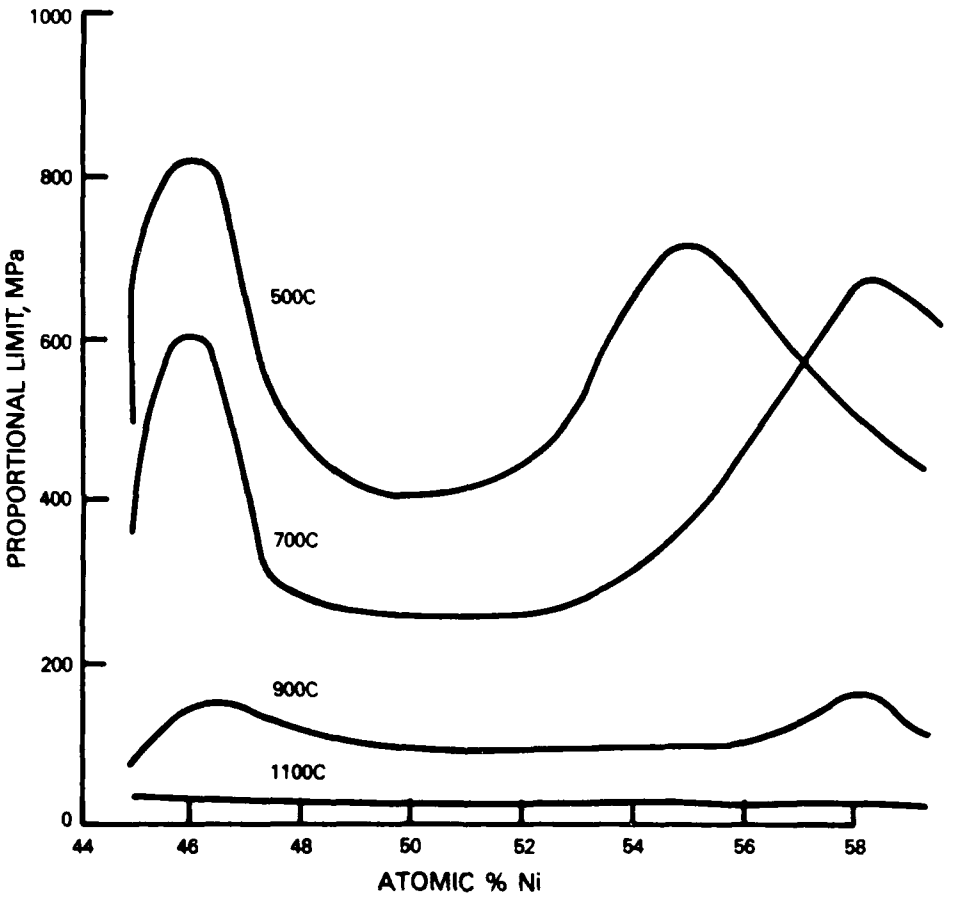

Figure 1 Proportional Limit of NiAl as a Function of Composition (Reference 1).

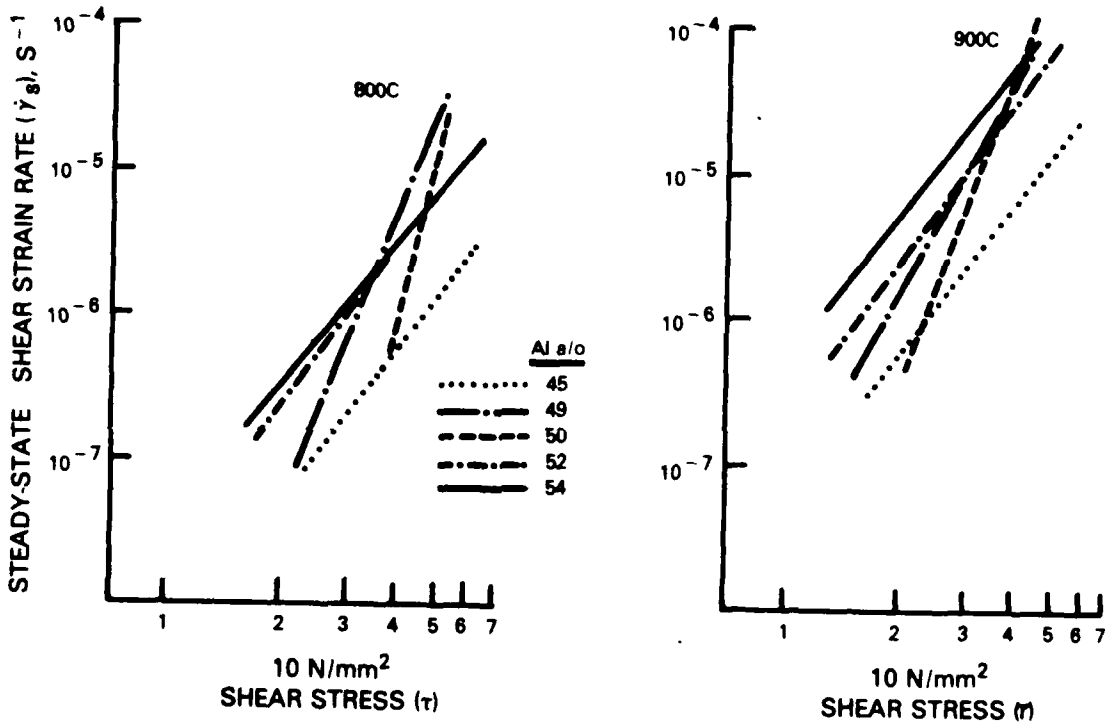

Figure 2 Steady-State Creep Rate of NiAl Alloys versus Stress (Reference 4).

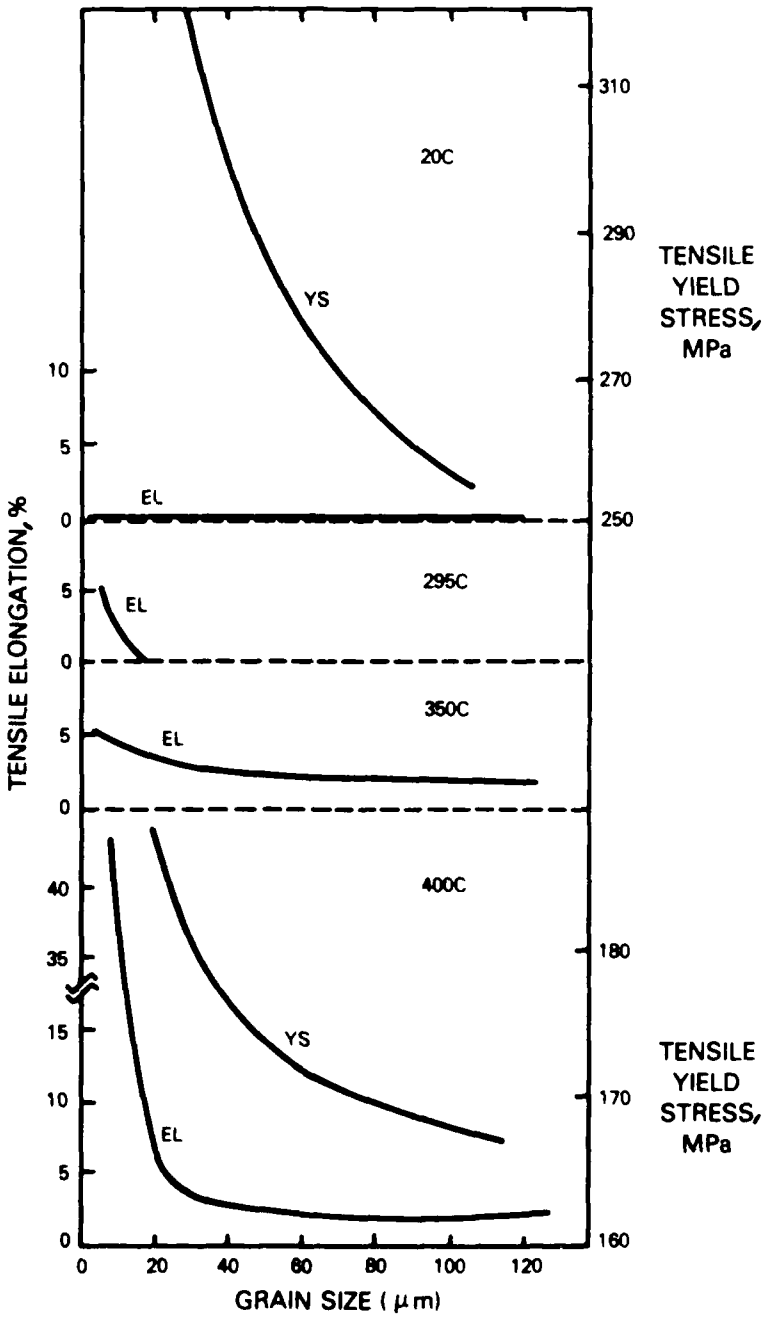

Figure 3 Tensile Strength and Ductility of Ni-49 a/o Al as a Function of Grain Size at Several Temperatures (Reference 3).

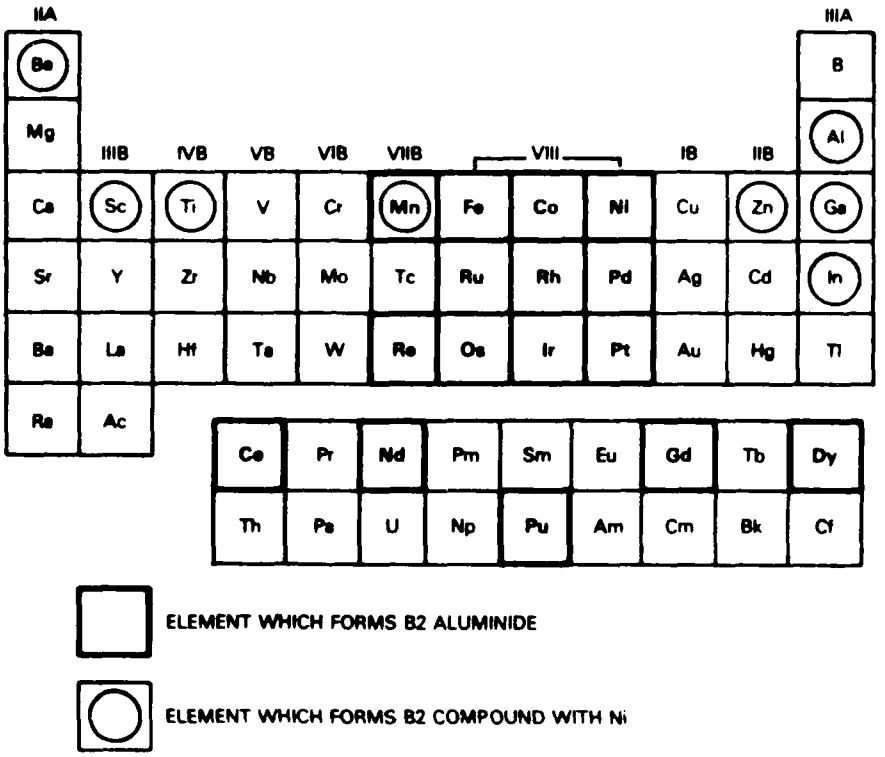

Figure 4 Occurrence of B2 Aluminides and Nickel-Containing B2 Compounds.

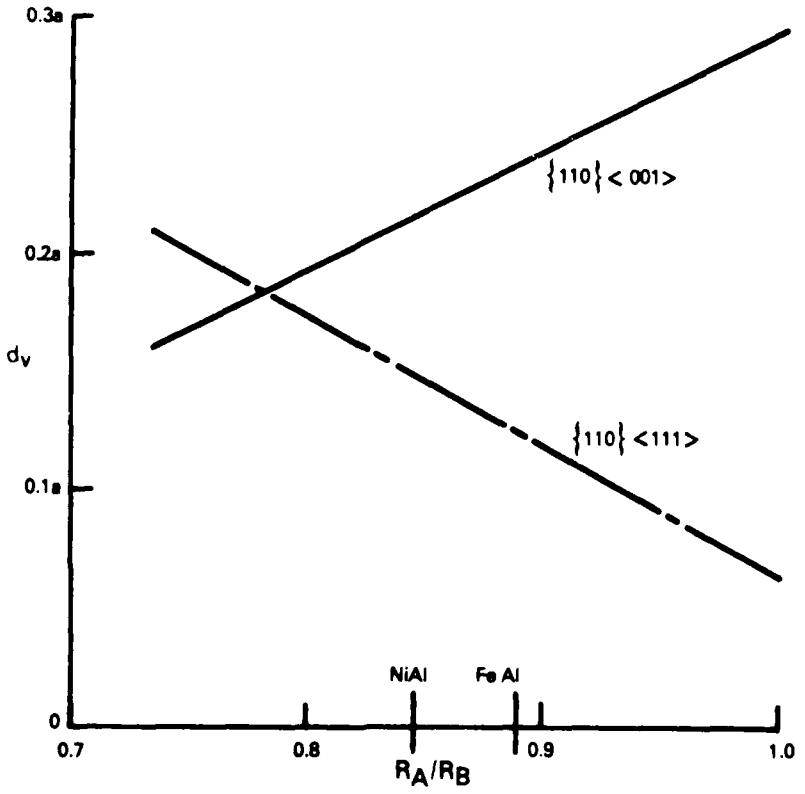

Figure 5 Vertical Displacement During Rigid Translation of {110} Planes Along <001> and <111> Directions as a Function of Atomic Radius Ratio of the Component A and B Atoms in the B2 Compound.

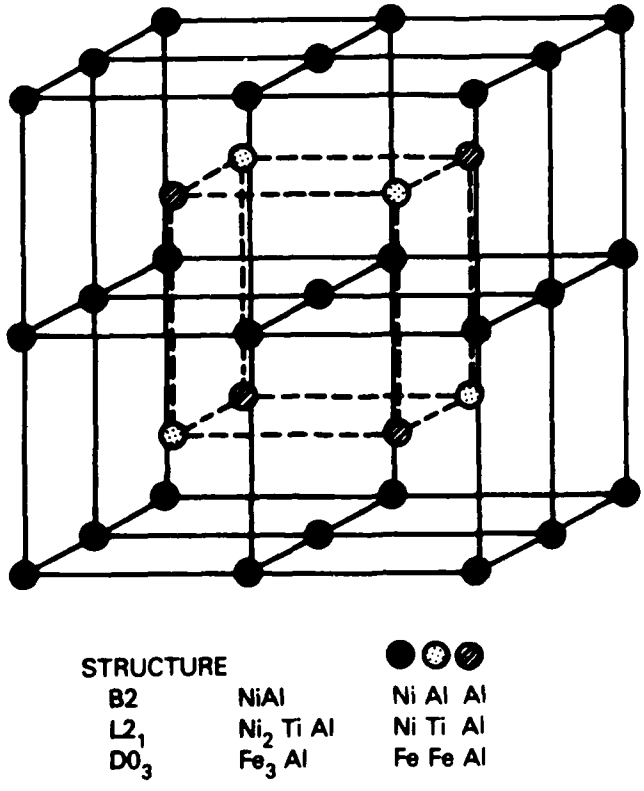

Figure 6 Crystallographic Relationship between the B2, L2, and DO_3 Structures.

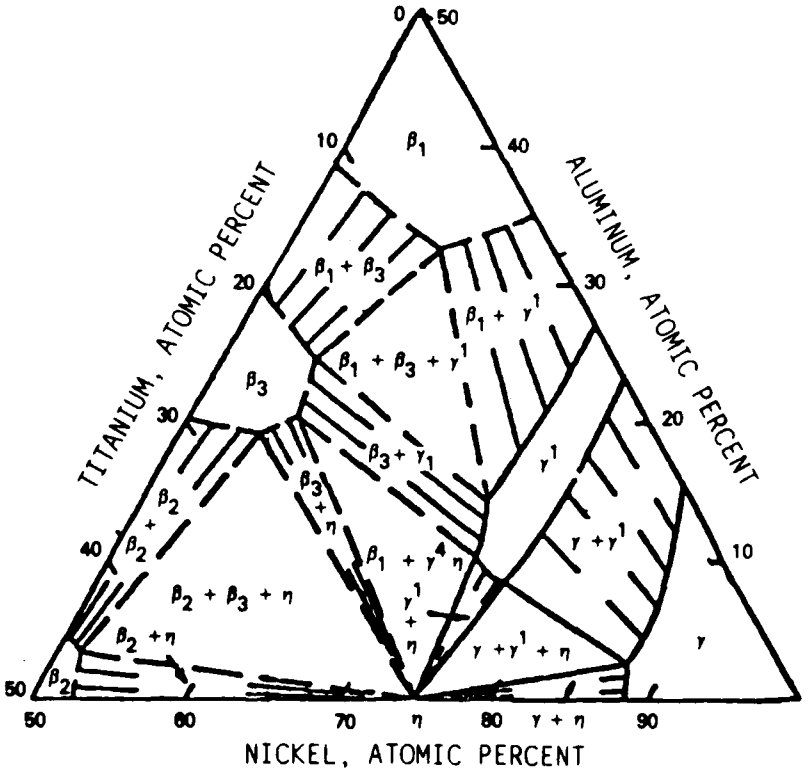

Figure 7 Suggested Form of the Ni-Ti-Al Phase Diagram for Alloys Containing More Than 50 a/o Ni (Reference 24) β_1 = NiAl, β_2 = NiTi and β_3 = Ni_2TiAl.

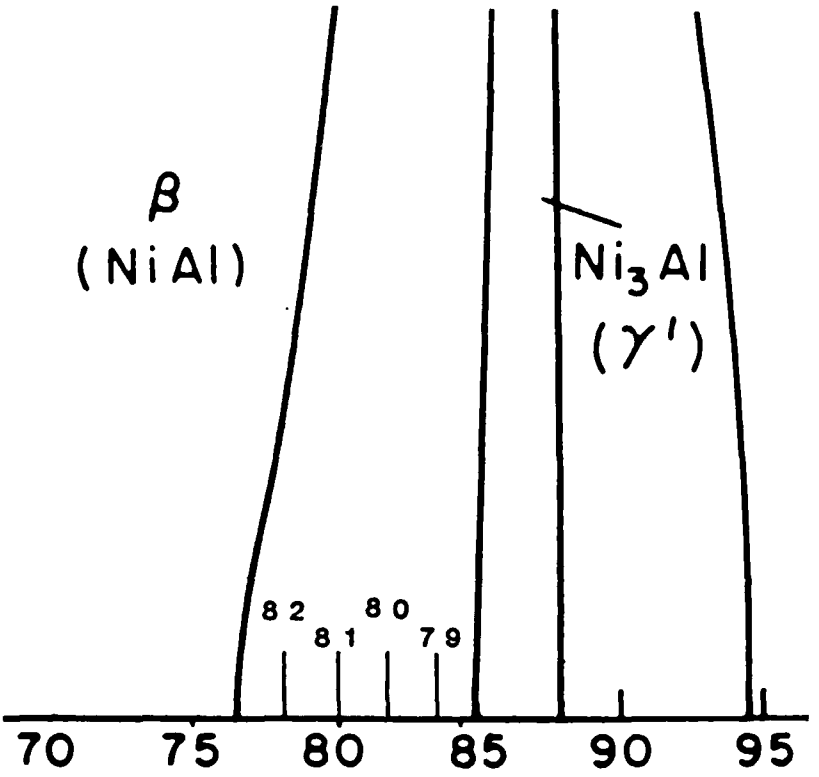

Figure 8 Ni-Al Phase Diagram Indicating the Locations of Some of the Nickel-Rich Alloys Relative to the B2 and $L1_2$ Phase Fields.

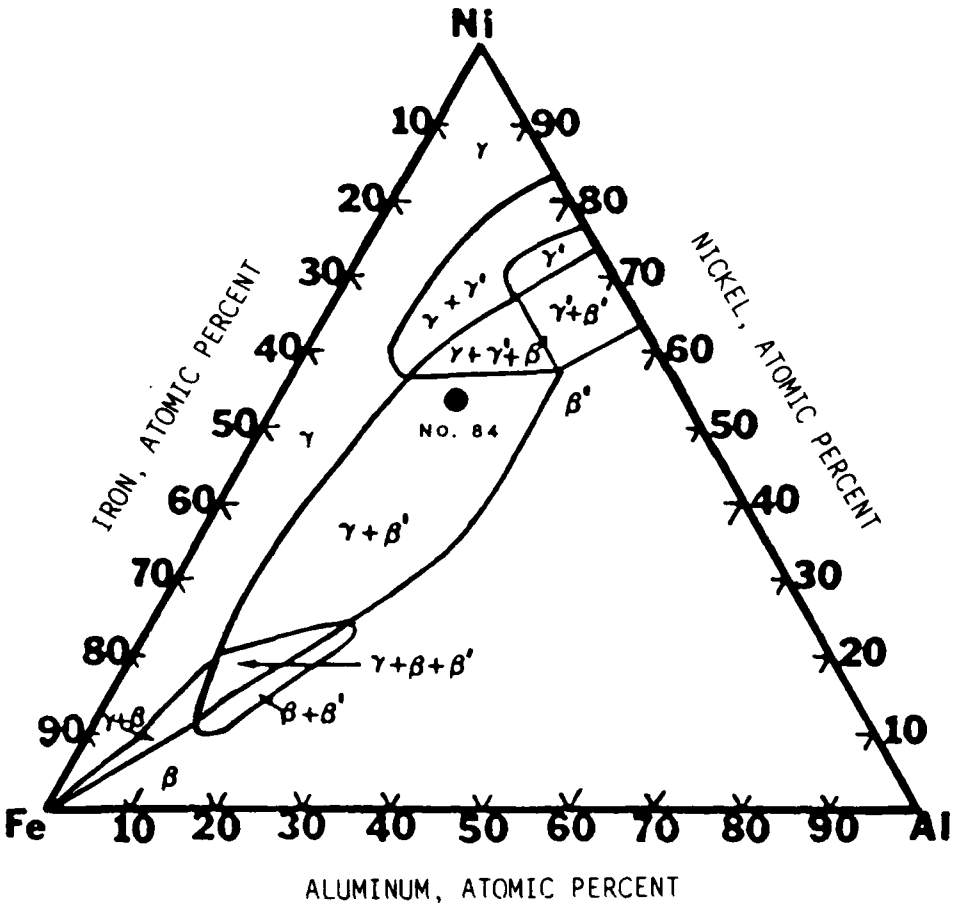

Figure 9 Fe-Ni-Al Ternary Phase Diagram at 950°C Indicating the Location of Alloy No. 84 (γ = fcc, γ' = Ni_3Al, β = bcc, β' = FeAl, NiAl).

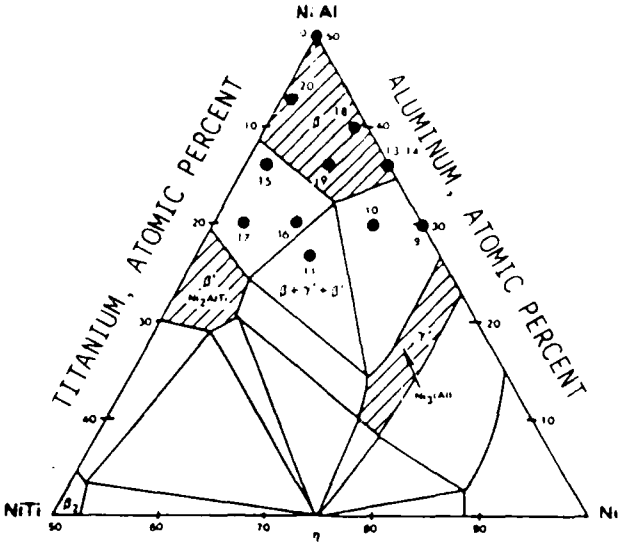

a

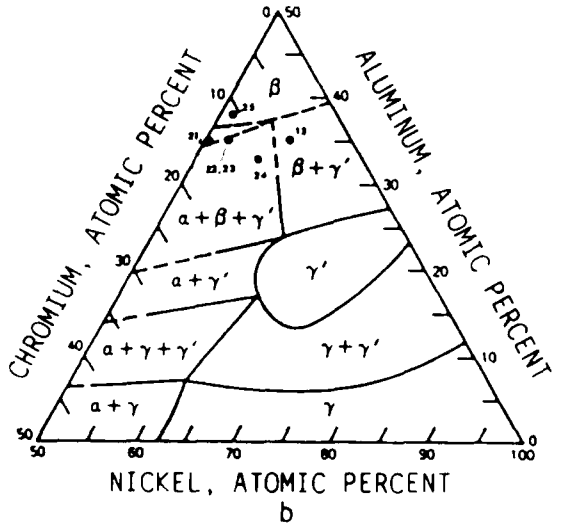

b

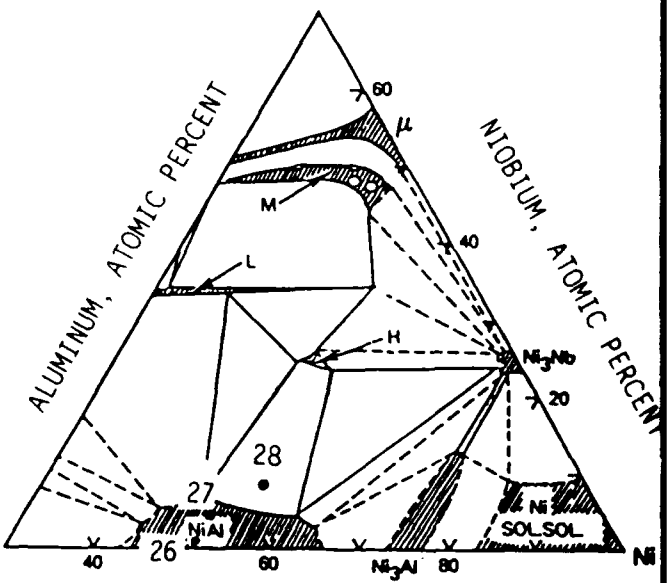

c

Figure 10 Ternary Phase Diagrams Indicating Some of the Alloys Selected for Phase II - Task II Strength Evaluation (a) Ni-Al-Ti Isothermal Section for 750°C (Ref. 24) (b) Ni-Al-Cr Isothermal Section for 750°C (Ref. 26) (c) Ni-Al-Nb Isothermal Section for 1140°C (Ref. 30).

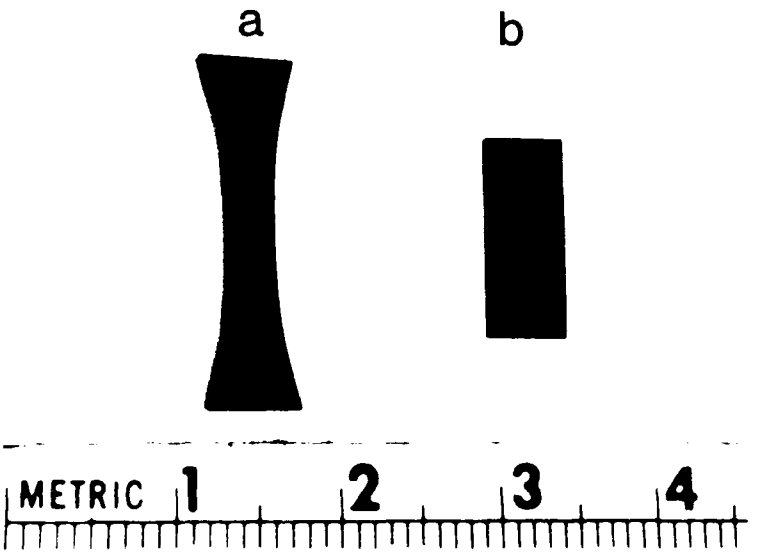

Figure 11 Specimen Configurations Used for Measurement of: (a) Tensile Ductility, and (b) Compressive Yield Strength.

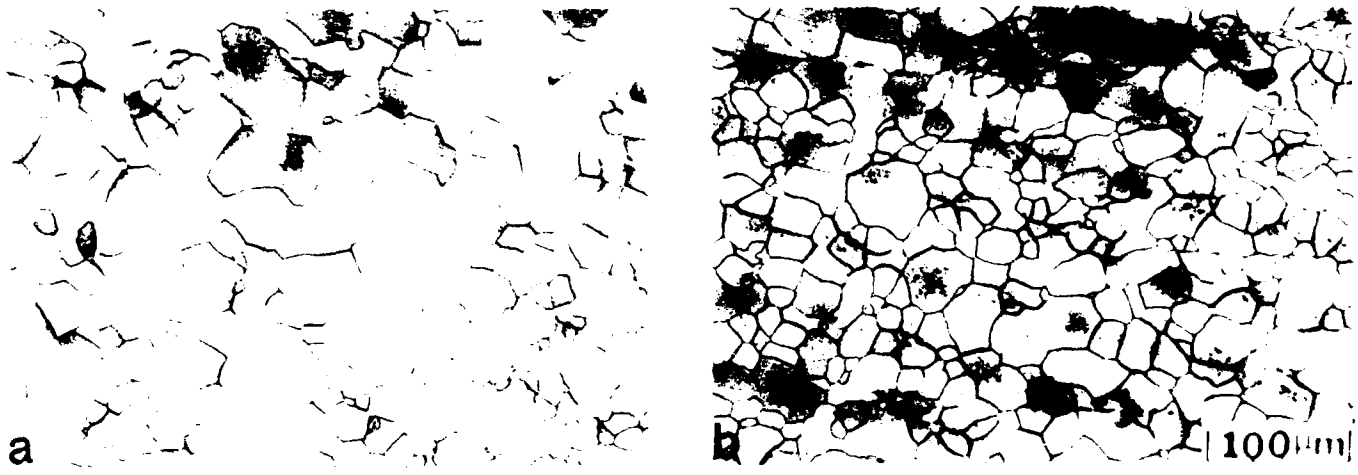

Figure 12. Microstructure of the Stoichiometric Ni-Al [illegible]
VIM Ingot and Extruded at 1000°C with an [illegible]
(a) Transverse Section, (b) Longitudinal [illegible]

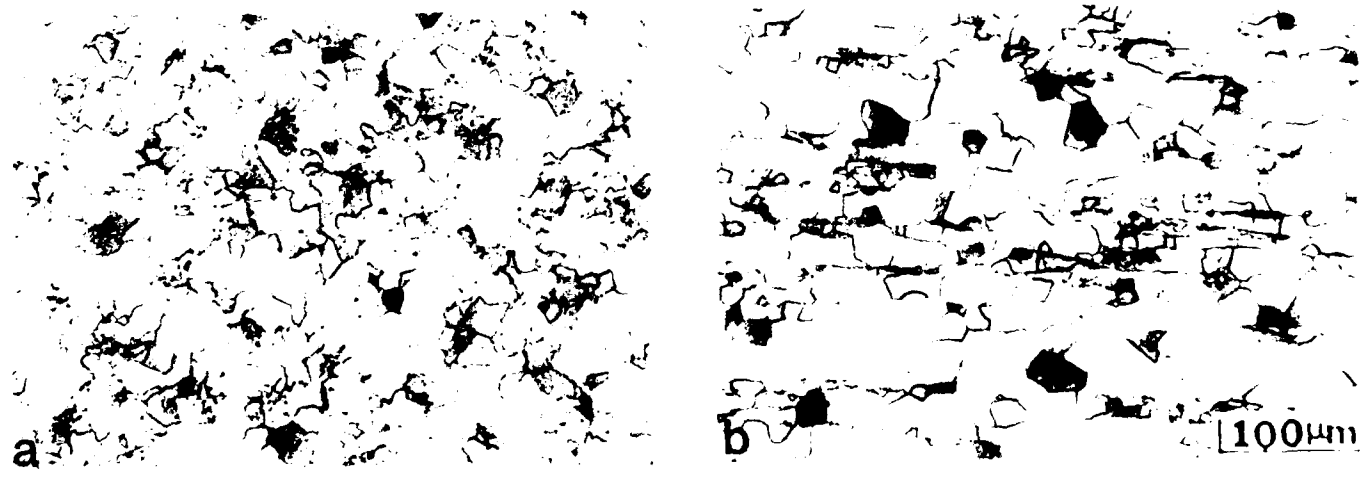

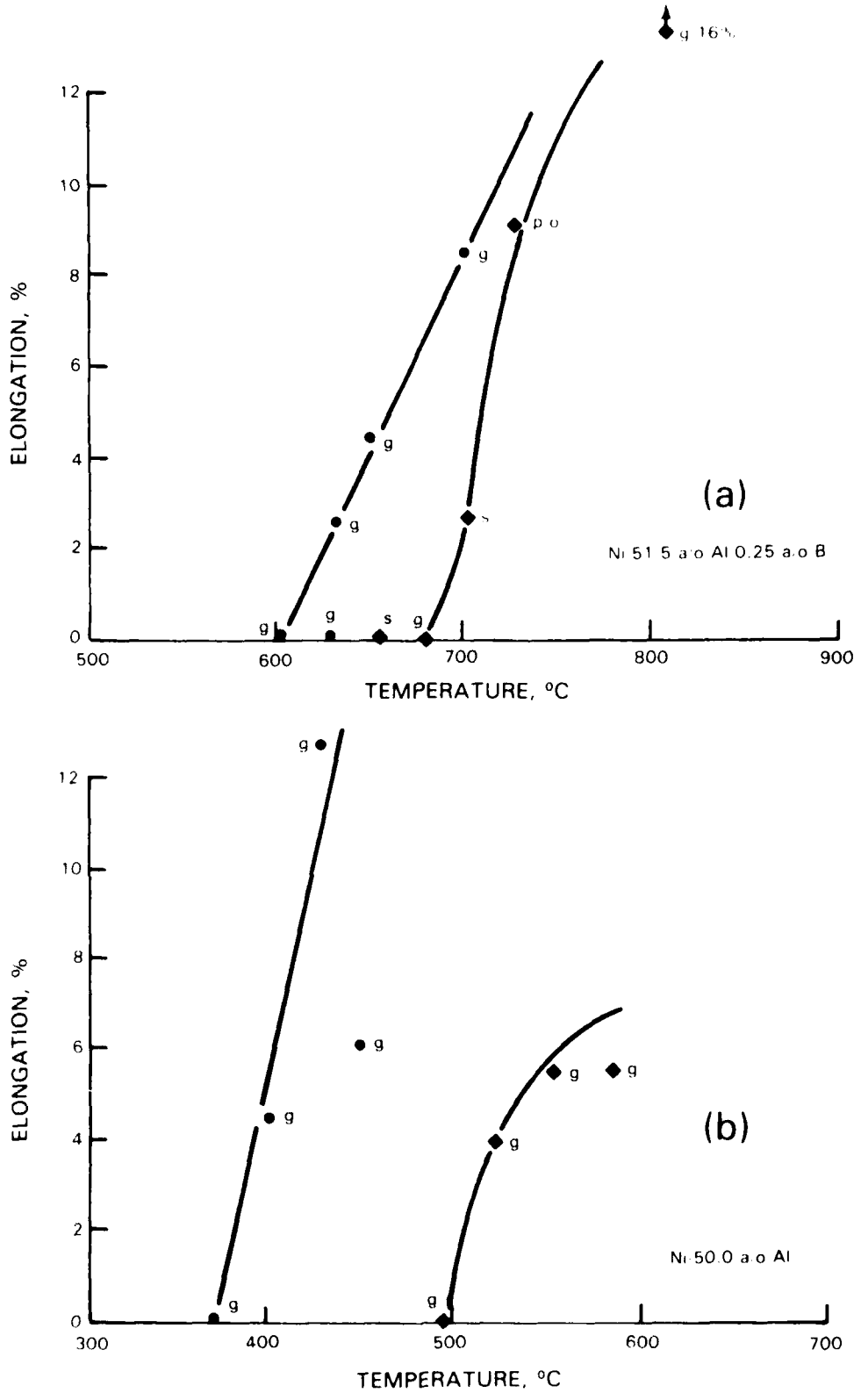

Figure 14 Tensile Elongation vs Temperature Curves for Phase I NiAl Alloys Produced as VIM Ingots (◆) and in Powder Form (●) and Extruded at 1000°C with an Extrusion Ratio of 9:1. The Fracture Locations in the Specimens are Indicated by "g" for Gage Fracture, "s" for Fracture at the Shoulder or Grip Section of the Specimen and P.O. for Specimens Deformed at the Shoulder and Pulled Out of the Grip Without Fracture.

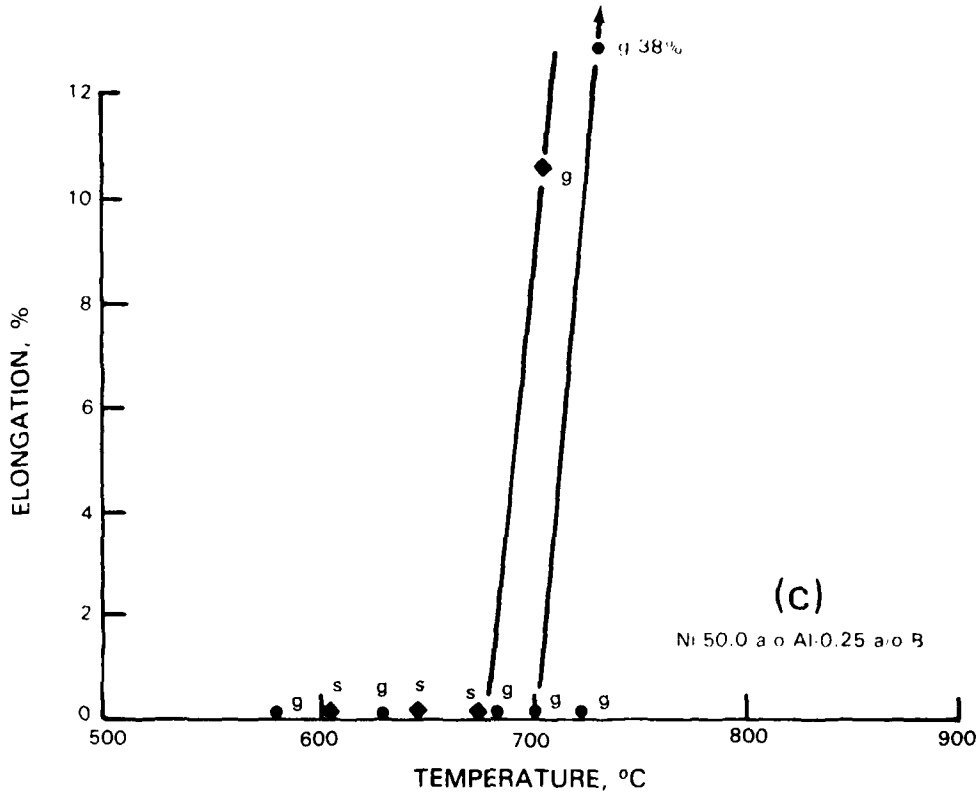

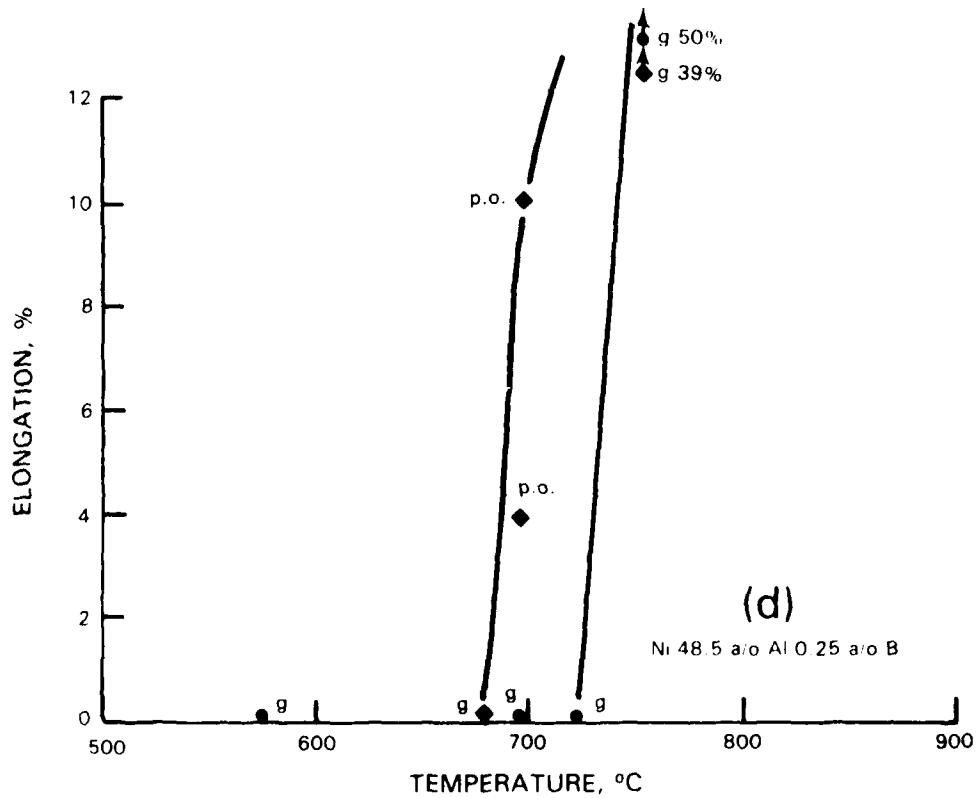

Figure 14 (Continued)

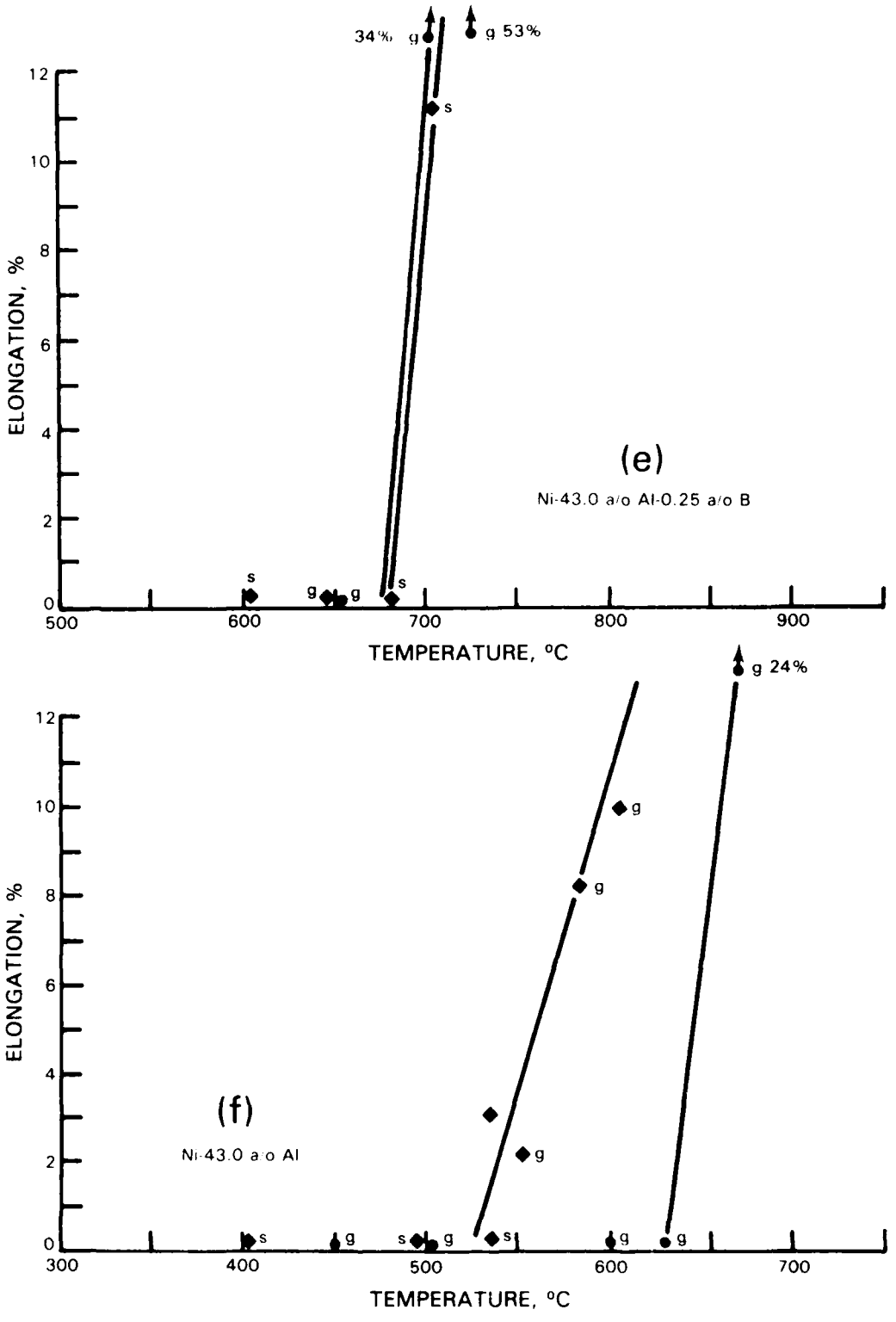

Figure 14 (Continued)

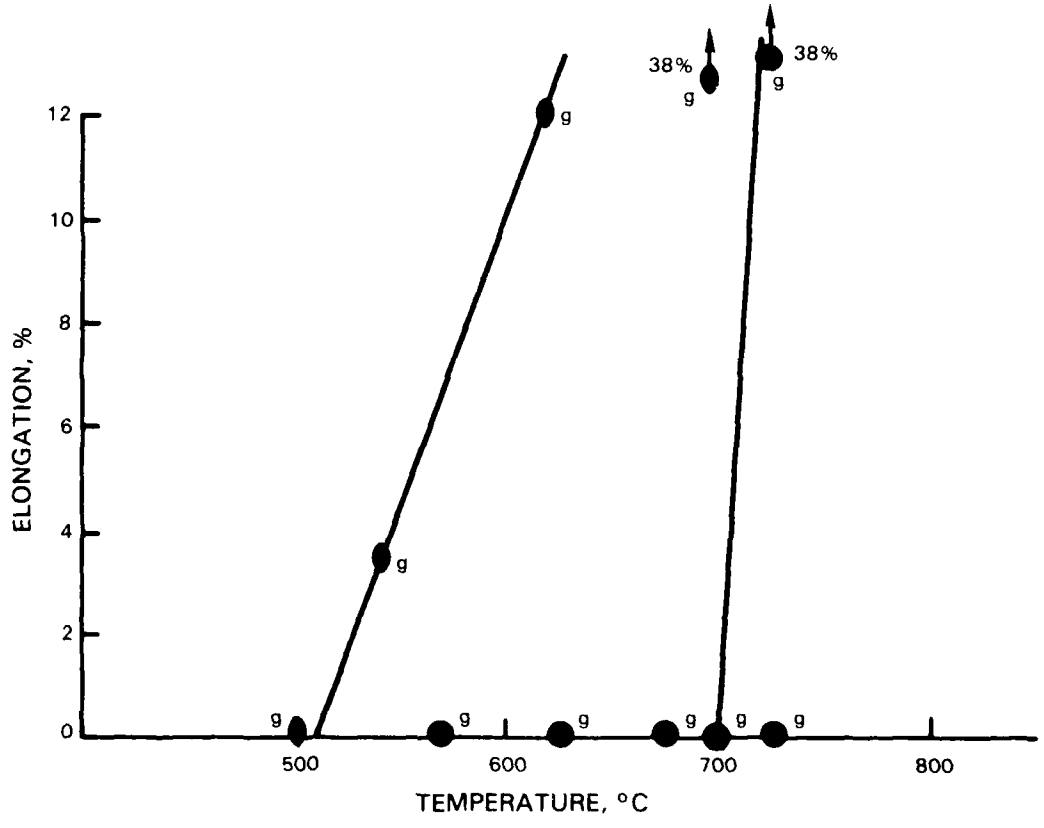

Figure 15 Tensile Elongation vs Temperature Curves for Ni-50 Al-0.25 a/o B (Number 4) Produced in Powder Form and Extruded at 1000°C With an Extrusion Ratio of 9:1. Tested in the As-Extruded Condition (●) and After 3 Percent Tensile Prestrain at 750°C (◖).

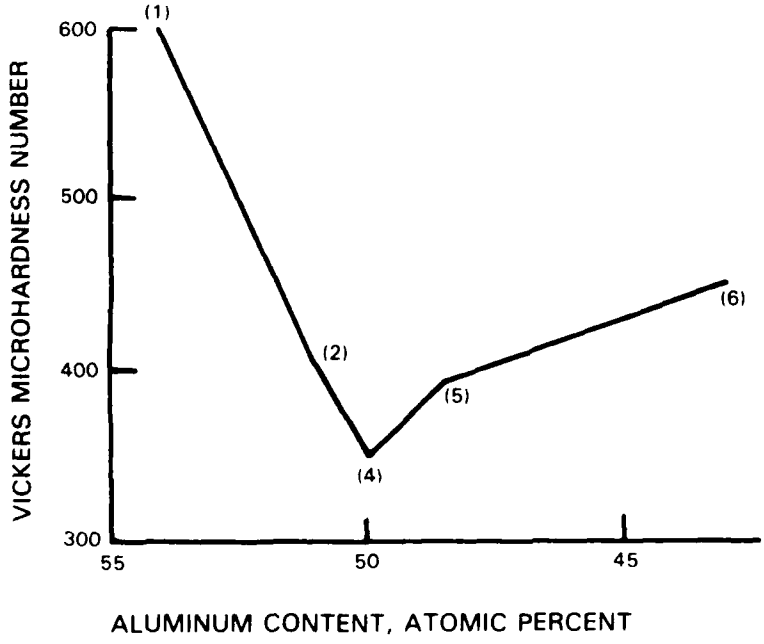

Figure 16 Room Temperature Hardness as a Function of Aluminum Content in Boron Doped NiAl Alloys. The Alloys Are Identified by Numbers in Parentheses.

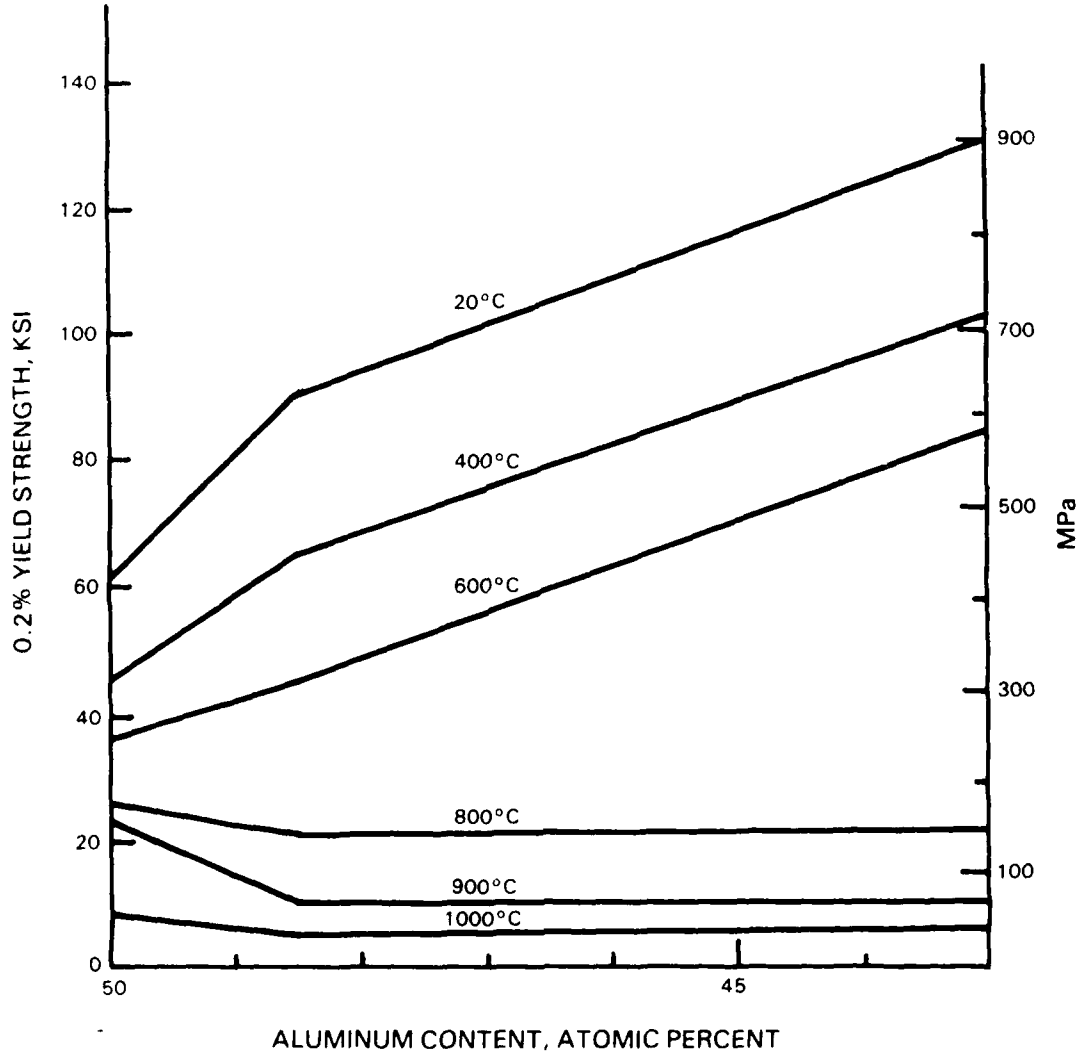

Figure 17 Compressive Yield Strength as a Function of Aluminum Content in Boron Doped NiAl Alloys.

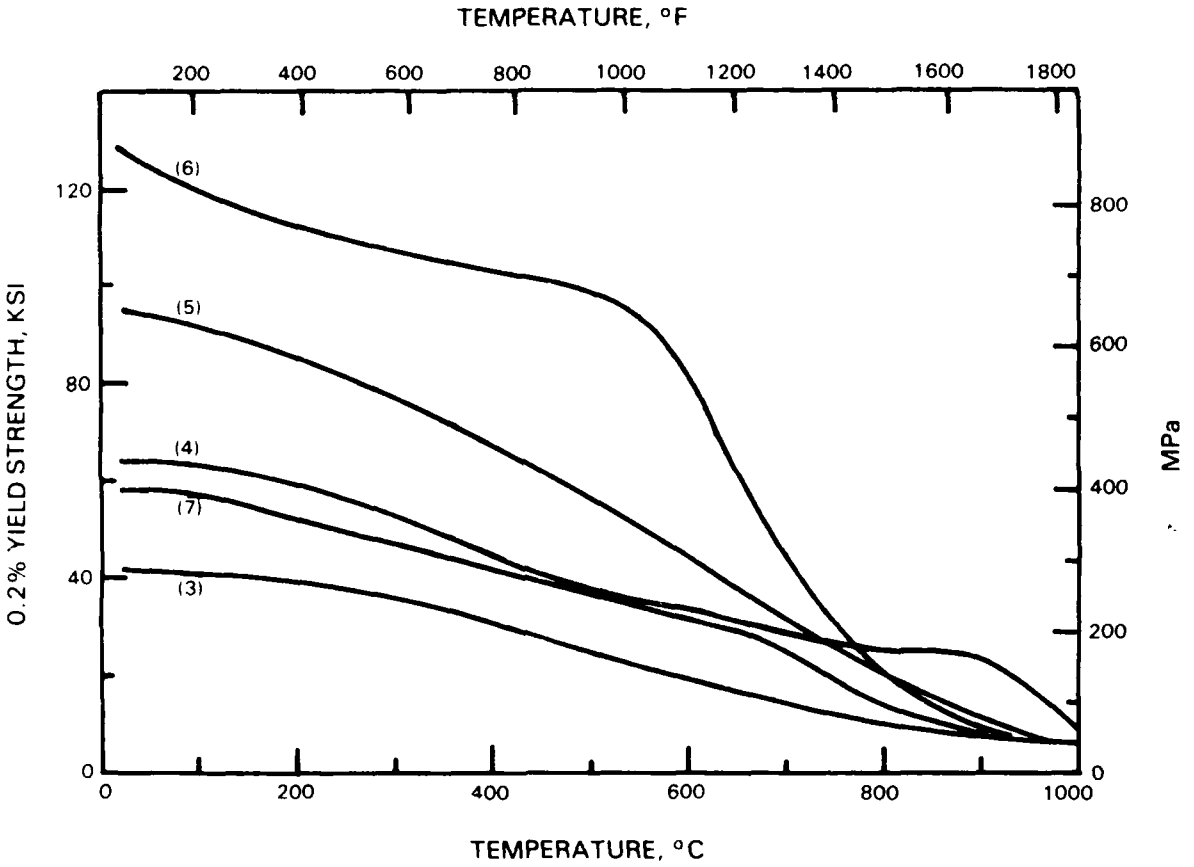

Figure 18 Compressive Yield Strength of NiAl Alloys as a Function of Temperature. The Alloys are Identified by Numbers in Parentheses.

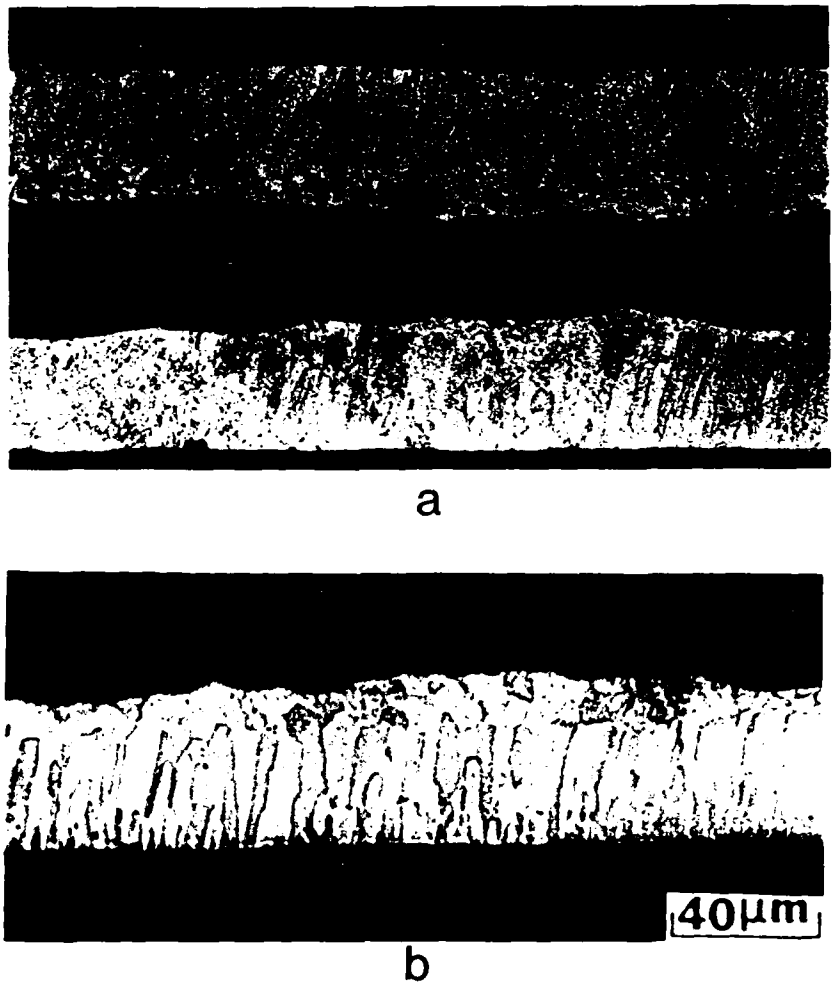

Figure 19 Microstructure of Alloys (a) Number 40 and (b) Number 52 in the As-Melt Spun Condition.

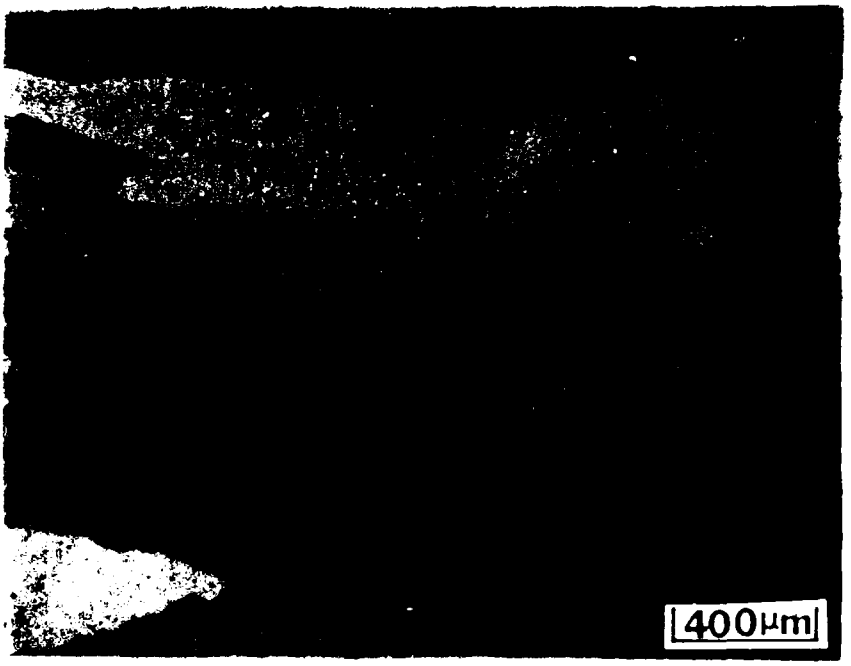

Figure 33. (a) General Appea nce of an Arc-Melted Button of Alloy Number 59 Ni-46.1 a/o Al-2.4 a/o Be (b) Cracks in the Arc-Melted Button.

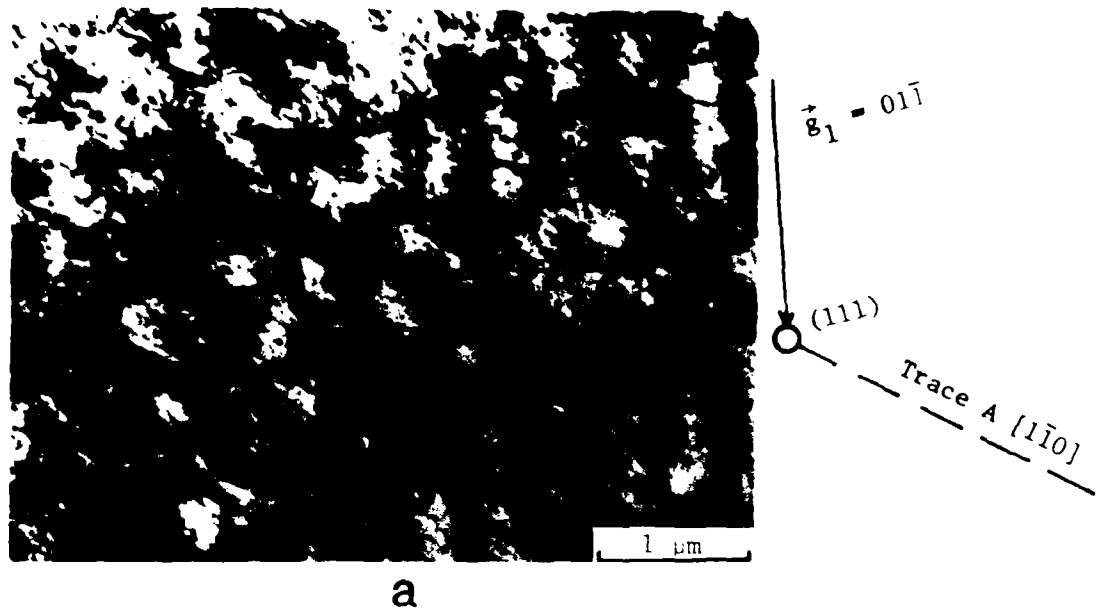

a

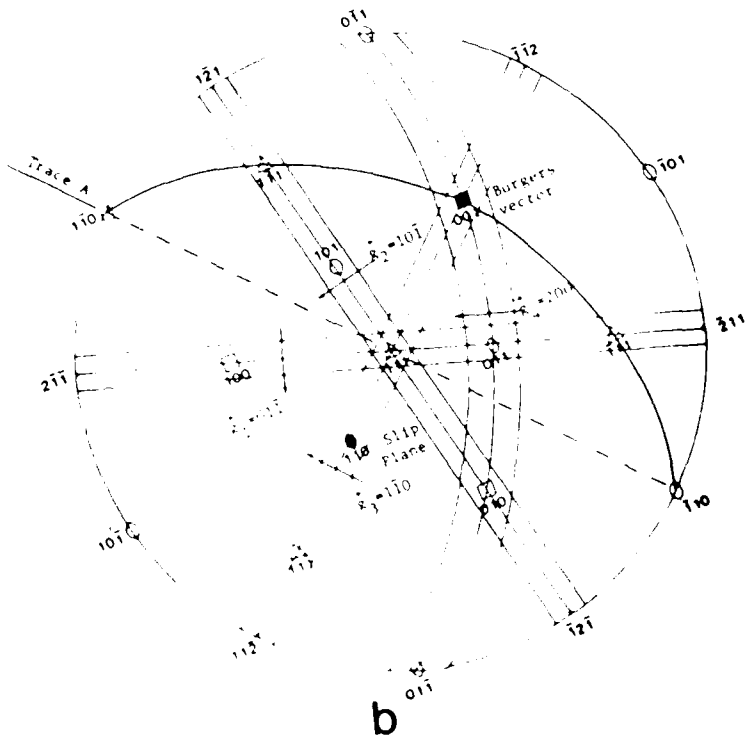

b

Figure 21 (a) General Appearance of the Dislocation Structure in Ni-48.5 a/o Al (Number 69) Resulting From Room Temperature Compressive Deformation (Strain 1.8 Percent). The Dashed Line Indicates the Slip Trace A as Observed on ⟨111⟩ Zone Axis. (b) ⟨111⟩ Stereographic Projection Illustrating the Trace Analysis and the g Vectors Used for the Burgers Vector Analysis.

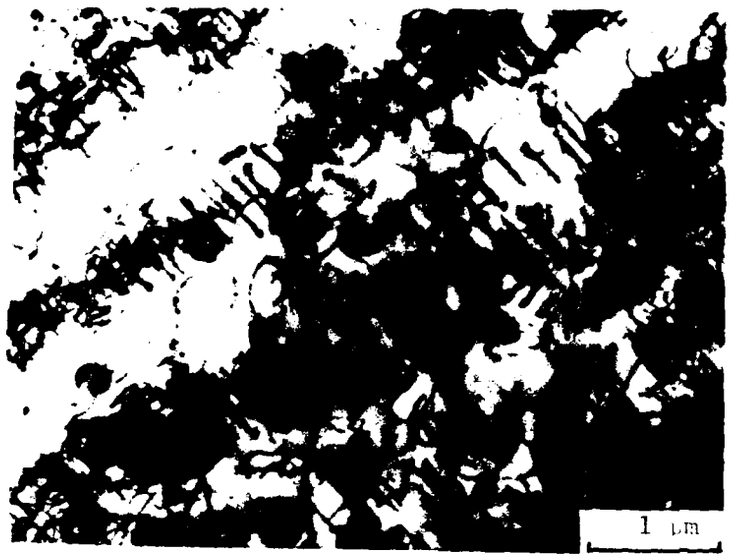

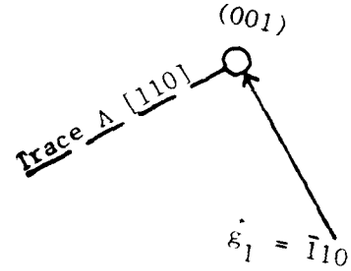

a

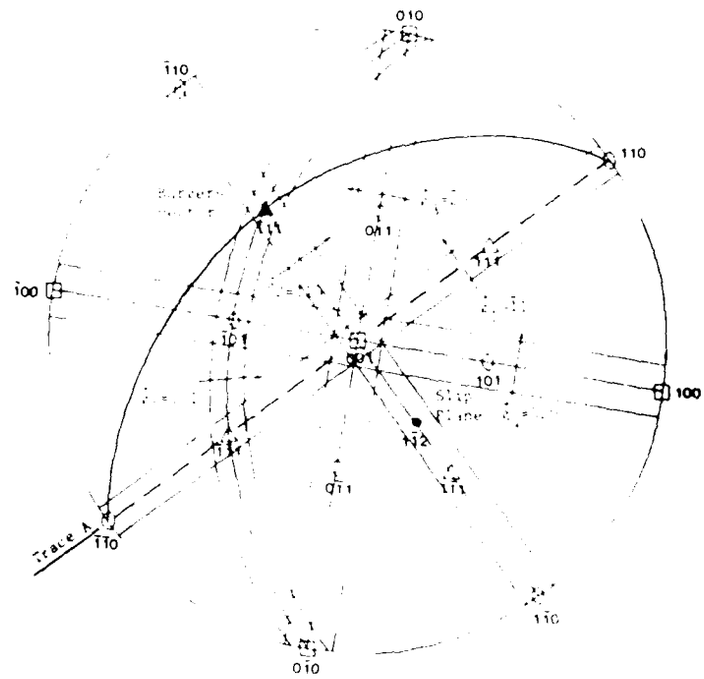

b

Figure 22 (a) General Appearance of the Dislocation Structure in Ni-48.5 a/o Al-5.2 a/o Cr (Number 40) Resulting From Room Temperature Compressive Deformation (Strain 1.8 Percent). The Dashed Line Indicates the Slip Trace A as Observed on (001) Zone Axis. (b) (001) Stereographic Projection Illustrating the Trace Analysis and the g Vectors Used for the Burgers Vector Analysis.

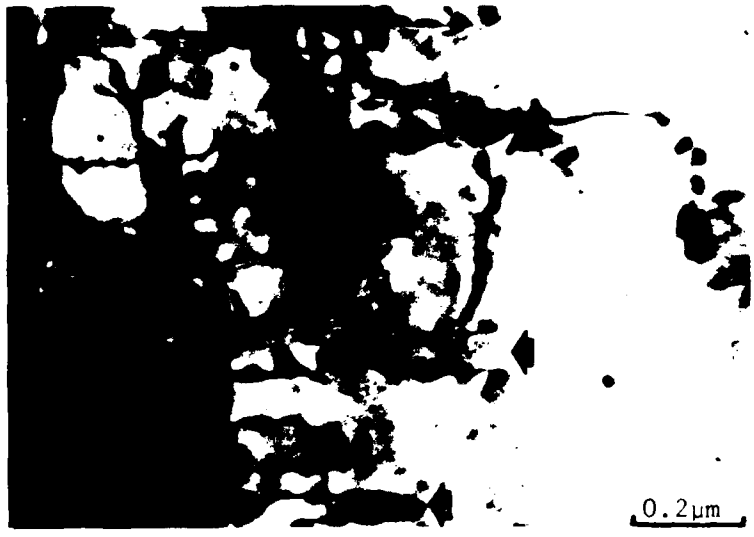

a

b

Figure 23 Detailed Appearance of the Dislocations in Figure 10 Showing Changes in Dislocation Spacings (Arrows) and Image Contrast (Center of Inversion) Under Imaging Conditions of (a) g=[$\bar{1}$10], s > 0 and (b) g = [110], s > 0. Observations are Characteristic of Dipoles.

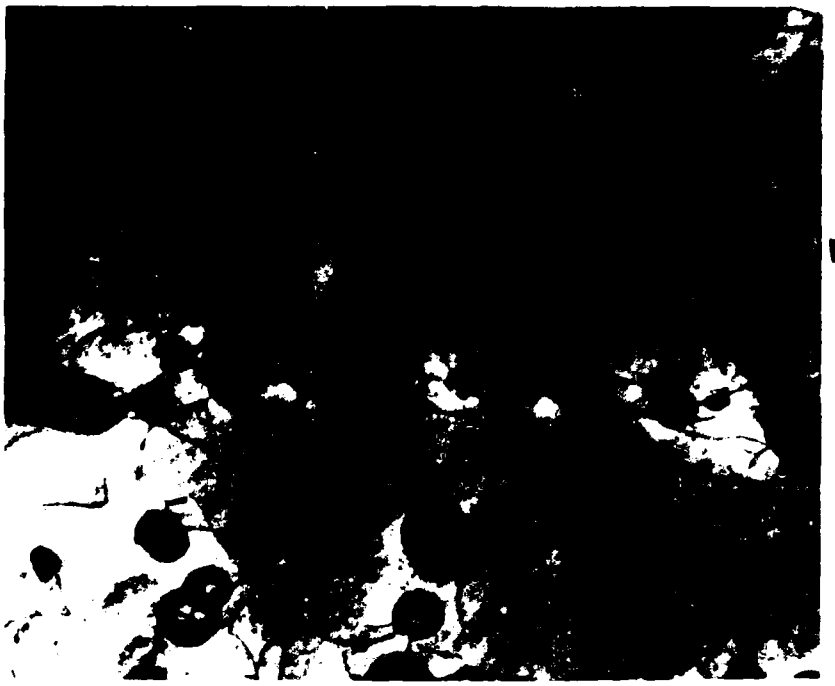

(a)

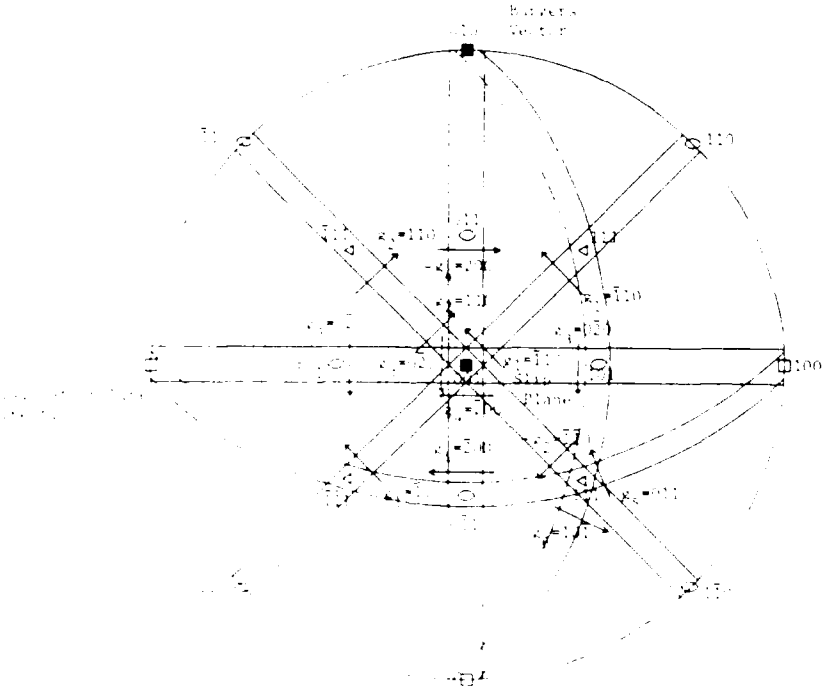

(b)

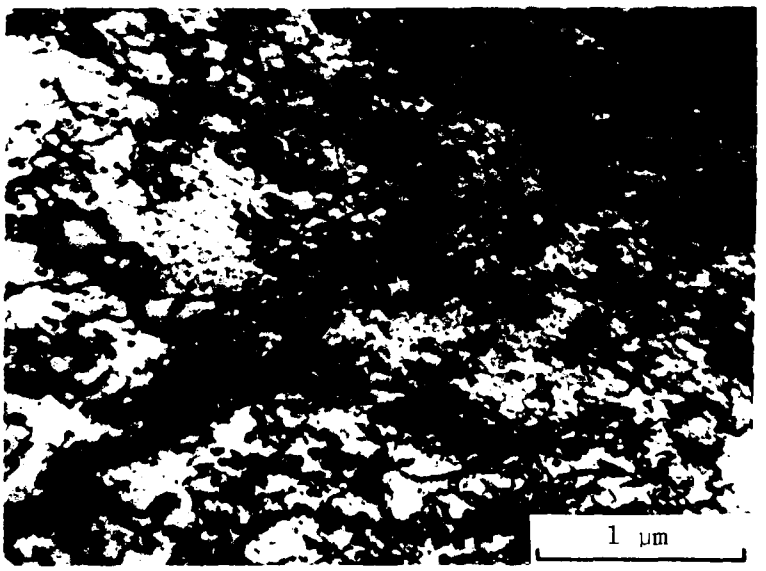

Figure 25 General Appearance of the Dislocation Structure in Ni-43.2 a/o Al-4.9 a/o Mn (Number 50) Resulting From Room Temperature Compressive Deformation (Strain 1.8 Percent). The Dashed Line Indicates the Slip Trace A as Observed on a [011] Zone Axis.

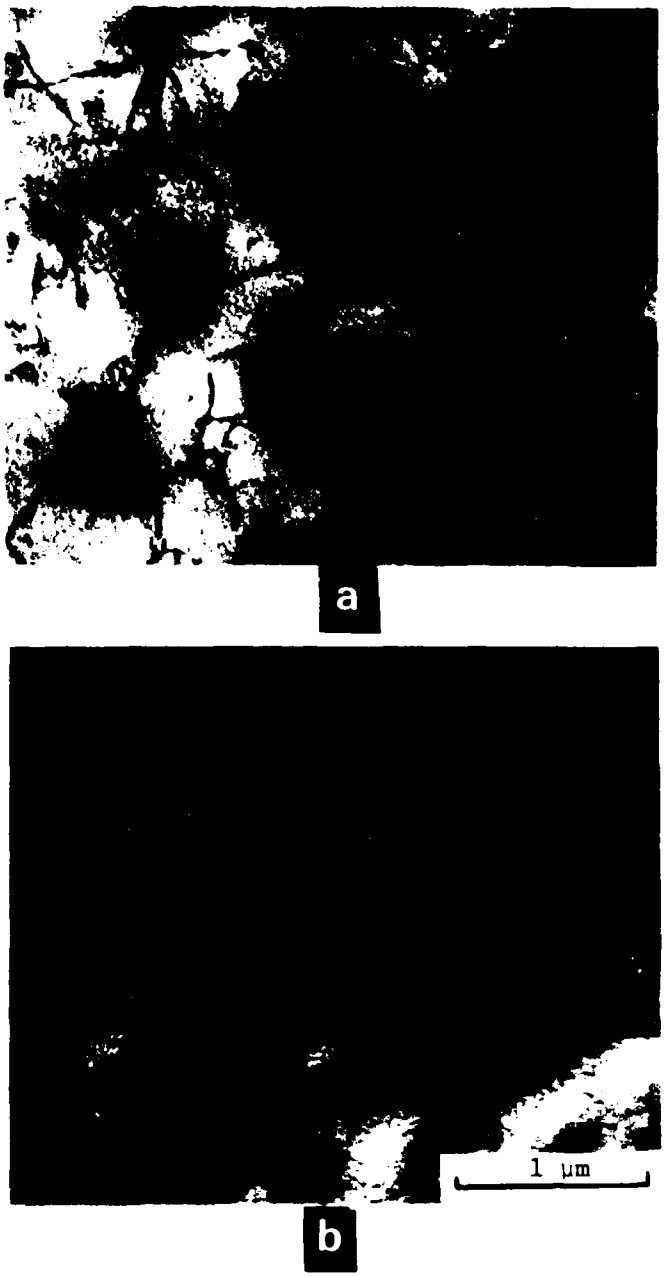

Figure 26 Appearance of the Dislocation Structure in Ni-43.7 a/o Al-4.9 a/o Mn (Number 52) Resulting From 775°C Deformation by (a) Compression and (b) Tension.

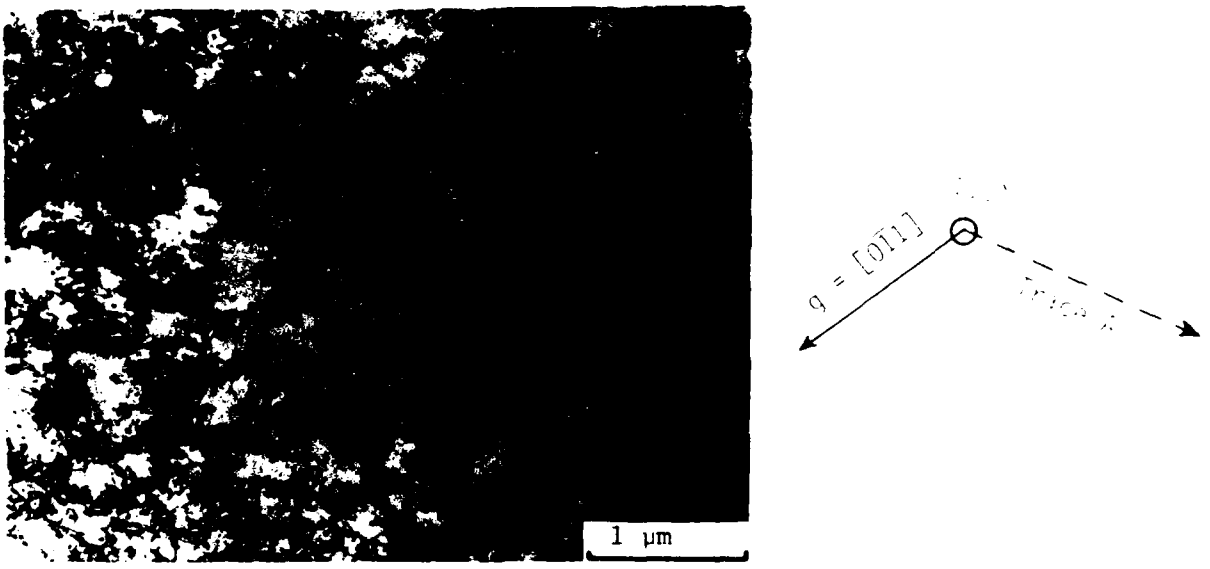

Figure 27 General Appearance of the Dislocation Structure in Ni 46.0 a/o Al-0.5 a/o Ga (Number 55) Resulting from Room Temperature Compressive Deformation (Strain 1.8 Percent). The Dashed Line Indicates the Slip Trace A as Observed on [111]-Zone Axis.

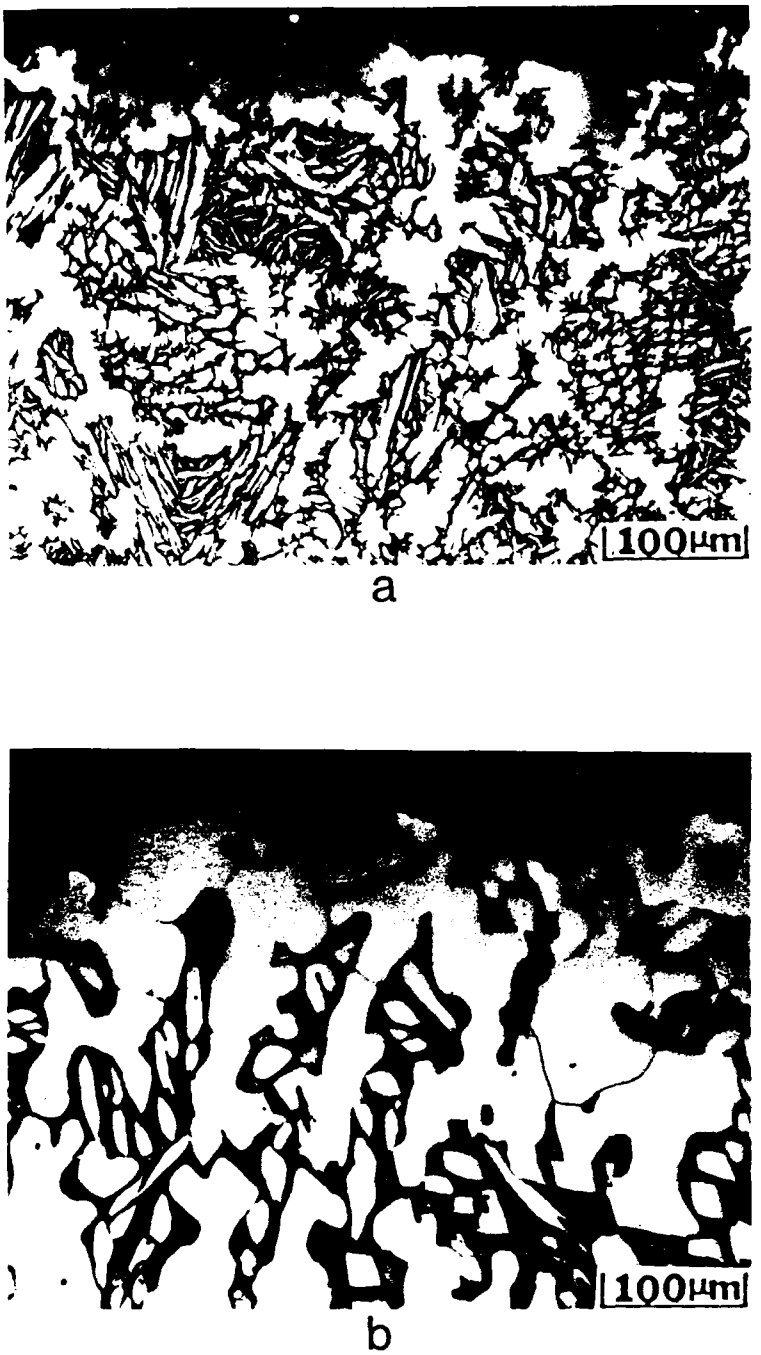

Figure 28 Microstructure and Tensile Fracture Path of NiAl Alloy Number 79 (Ni-29.3 a/o Al) Produced Using Arc Melting and Drop Casting Techniques (a) As-Cast (b) After Heat Treatment for 2 Hours at 1200°C.

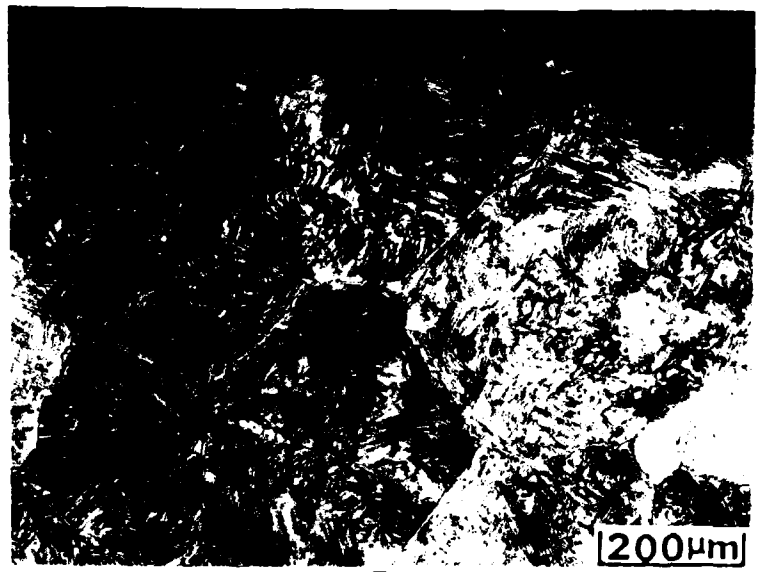

a

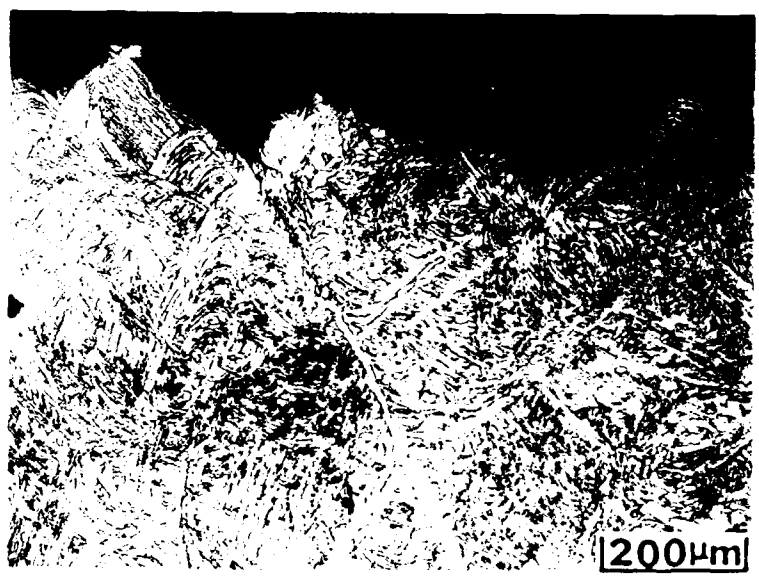

b

Figure 29 Microstructure and Tensile Fracture Path of NiAl Alloy Number 80 (Ni-32.3 a/o Al) Produced Using Arc Melting and Drop Casting Techniques. (a) As-Cast (b) After Heat Treatment for 2 Hours at 1200°C.

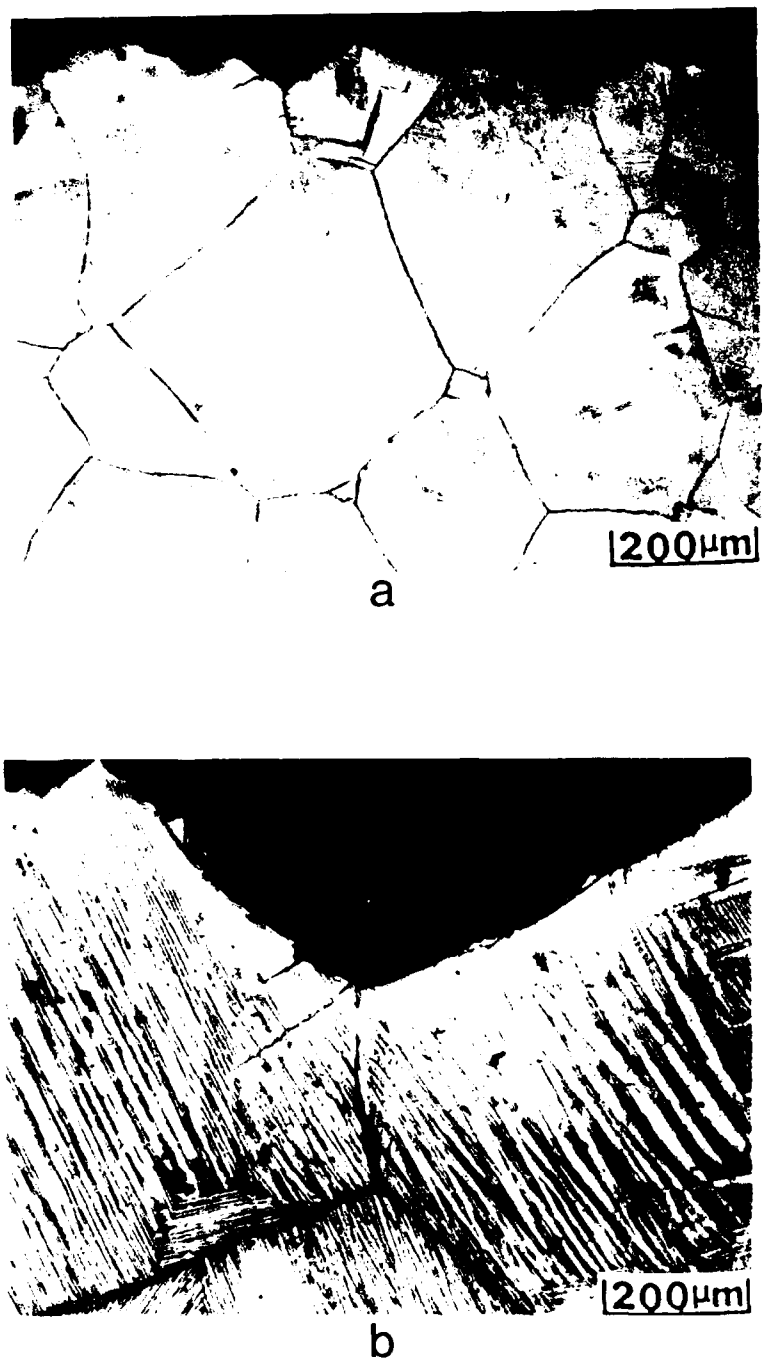

Figure 30 Microstructure and Tensile Fracture Path of NiAl Alloy Number 81 (Ni-35.2 a/o Al) Produced Using Arc Melting and Drop Casting Techniques. (a) As-Cast (b) After Heat Treatment for 2 Hours at 1200°C.

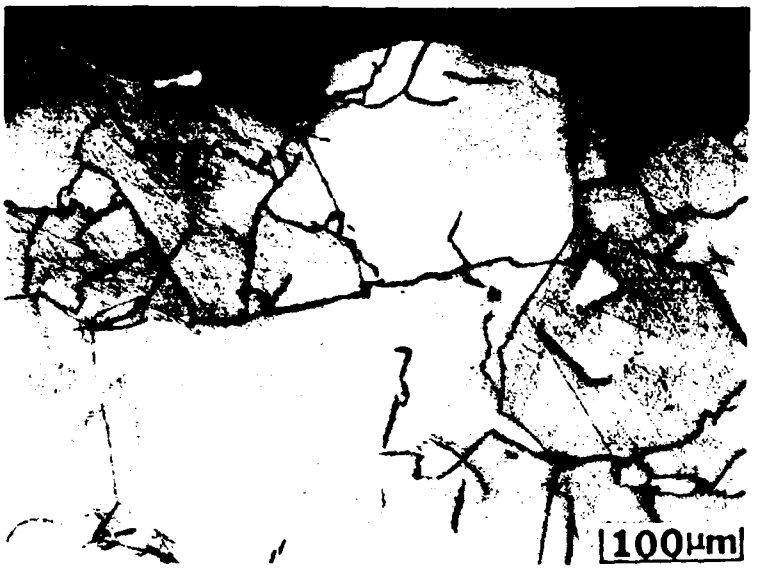

Figure 31 Microstructure and Tensile Fracture Path of NiAl Alloy Number 82 (Ni-38.0 a/o Al) Produced Using Arc Melting and Drop Casting Techniques. As-Cast.

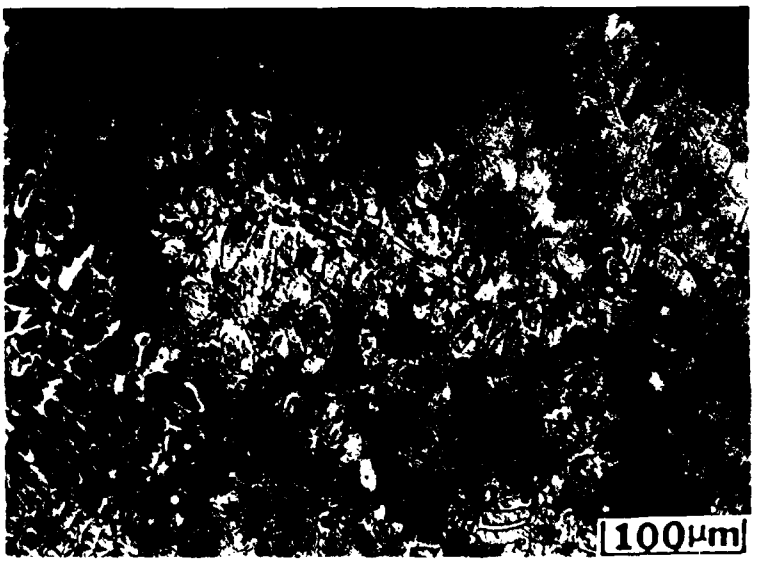

a

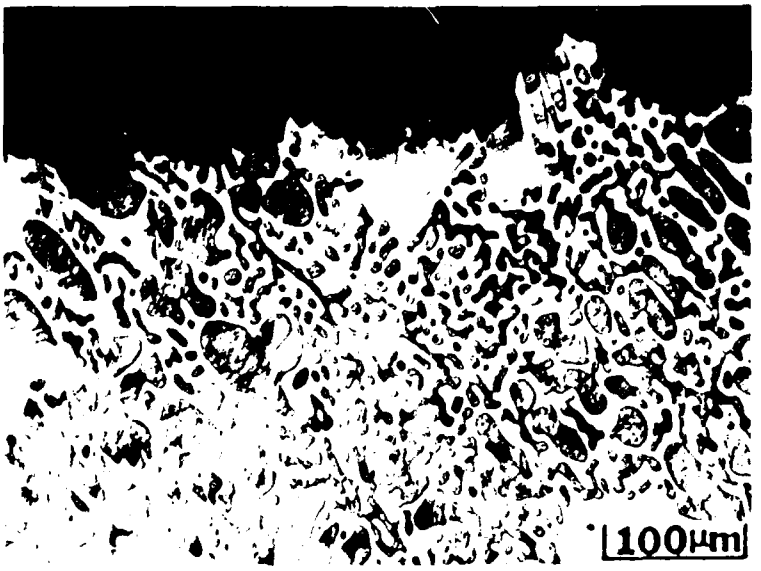

b

[illegible] Microstructure and Composition Along Path of NiAl Alloy Number 84 [illegible] Produced Using Arc Melting and Drop [illegible] Technique [illegible] As Cast (a) After Heat Treatment for 2 [illegible]

Figure 33 Microstructure of NiAl Alloy Number 84 (Ni-20 a/o Al-27.5 a/o Fe) in the As-Cast Condition Illustrating the Lamellar Structure.

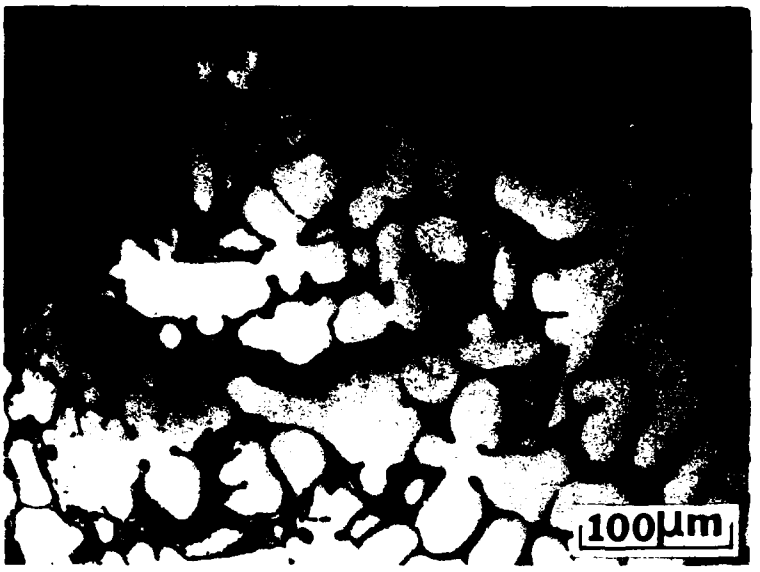

a

b

Figure 34. Microstructure and Tensile Fracture Path of NiAl Alloy Number 85 (50 Mole % Al Composition) Produced Using Arc Melting and Drop Casting Techniques (a) As Cast (b) After Heat Treatment for 2 Hours at 1200°C

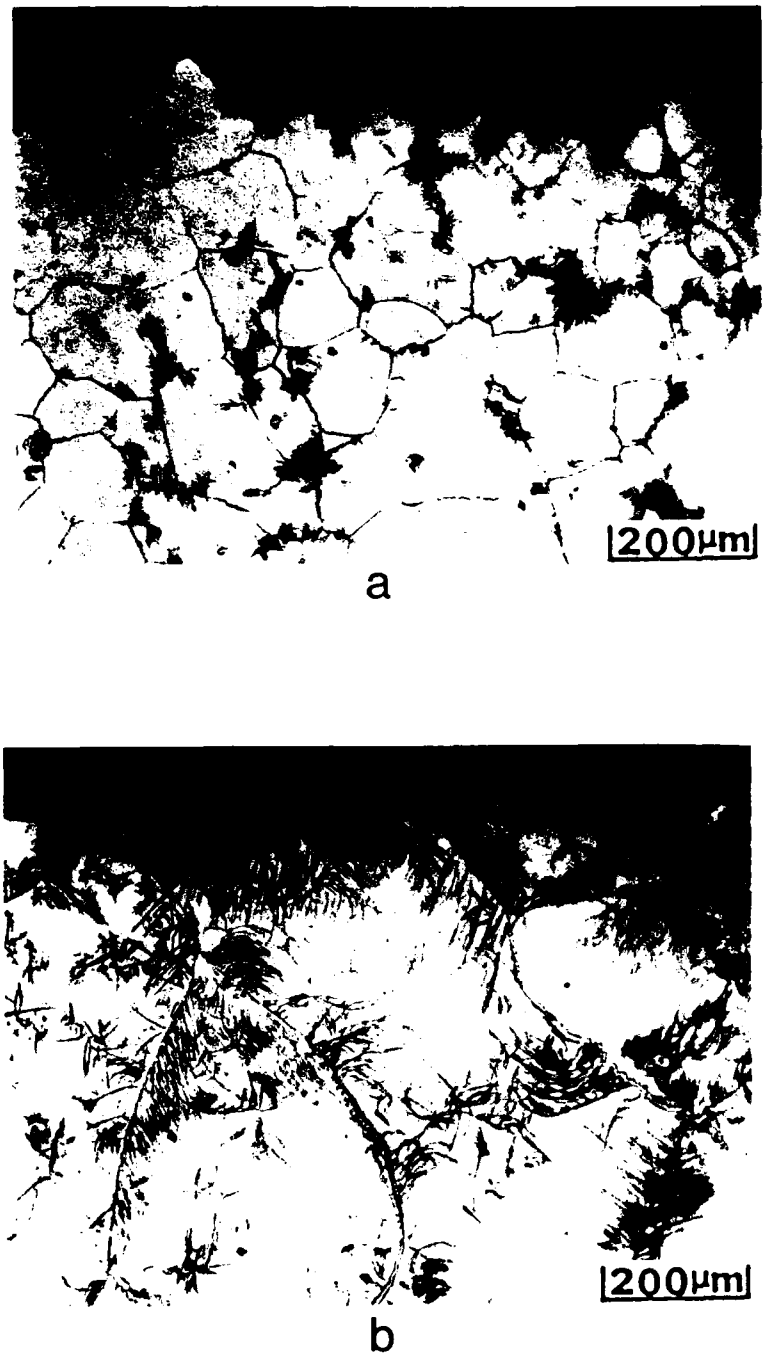

Figure 35 Microstructure of NiAl Alloy Number 84 (Ni-30.0 a/o Al-5.0 a/o Mn) Produced Using Arc Melting and Drop Casting Techniques. (a) As-Cast (b) After Heat Treatment for 2 Hours at 1200°C.

a

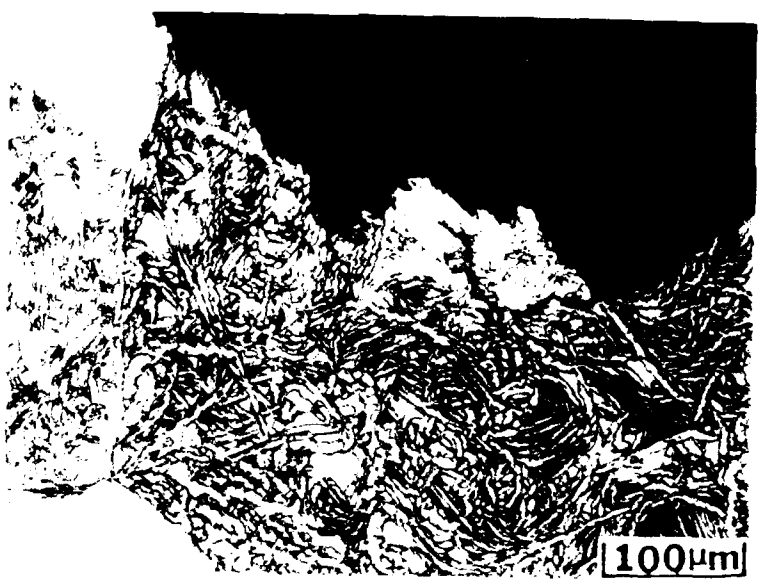

b

Figure 30. Microstructure of NiAl Alloy Number 82 (Ni-30.0 a/o Al-5.0 a/o Cr) Produced Using Arc Melting and Drop Casting Techniques. (a) As-Cast and (b) After Heat Treatment for 2 Hours at 1300°C

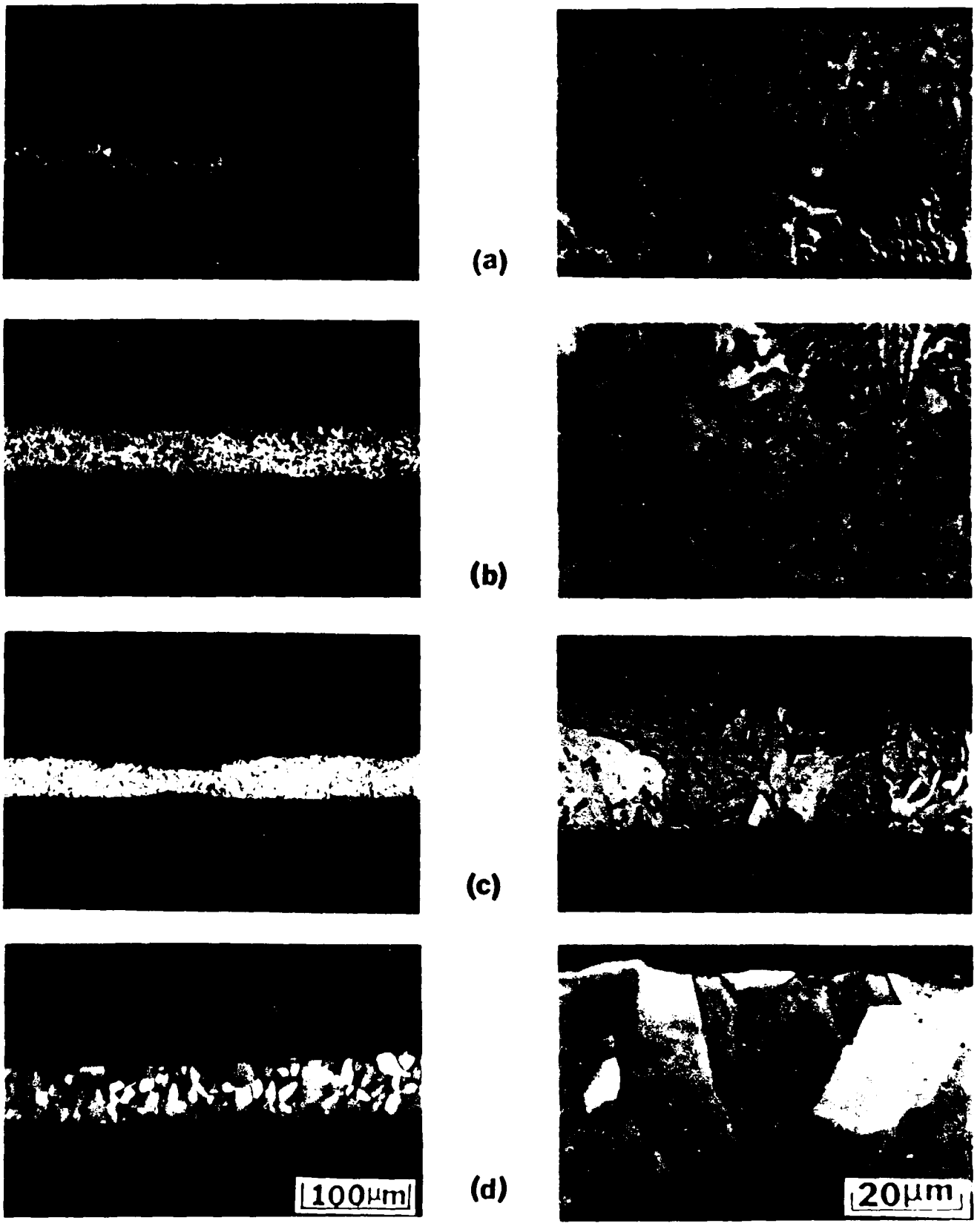
(a)
(b)
(c)
(d)
100μm
20μm

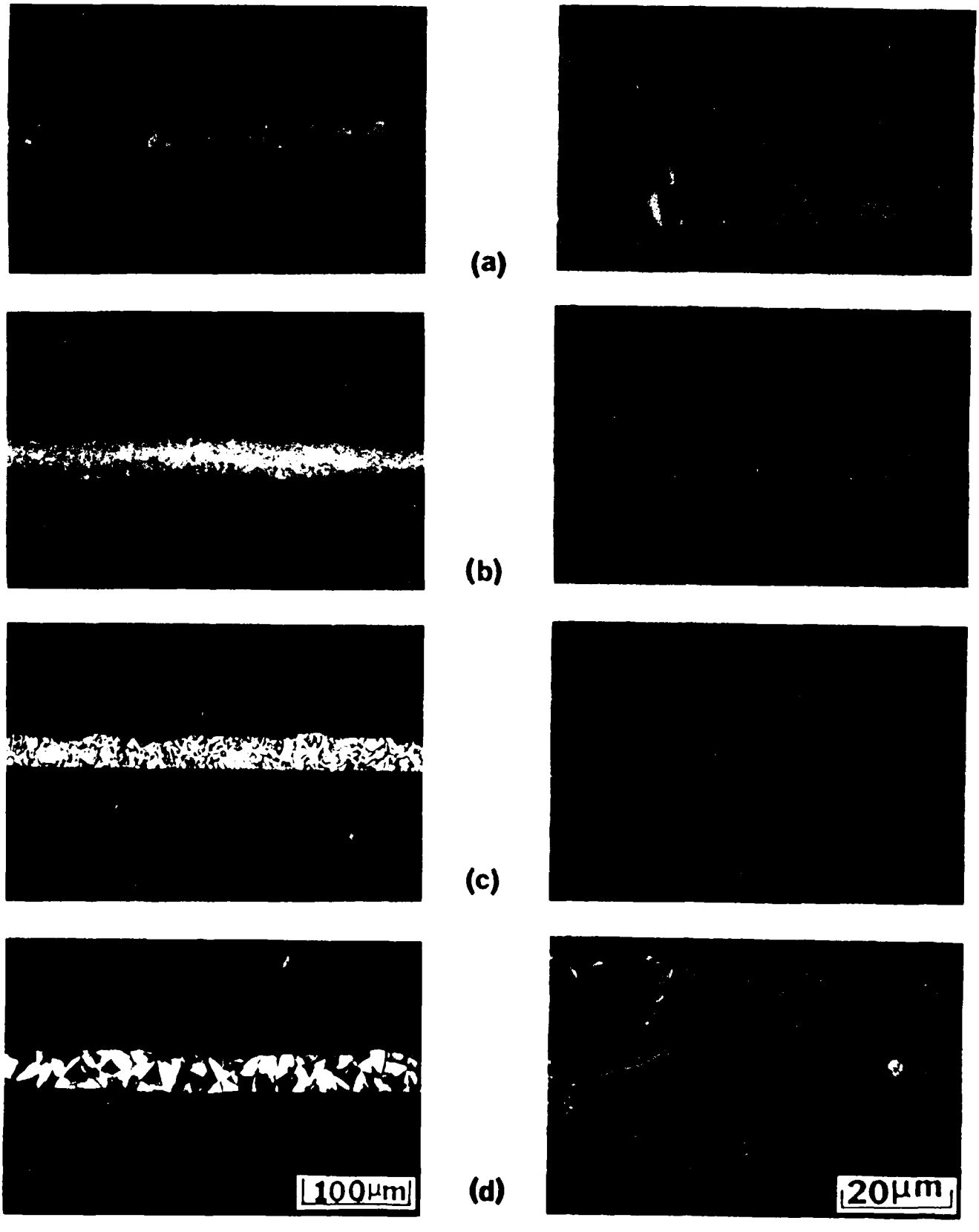
(a)
(b)
(c)
(d)
100μm
20μm

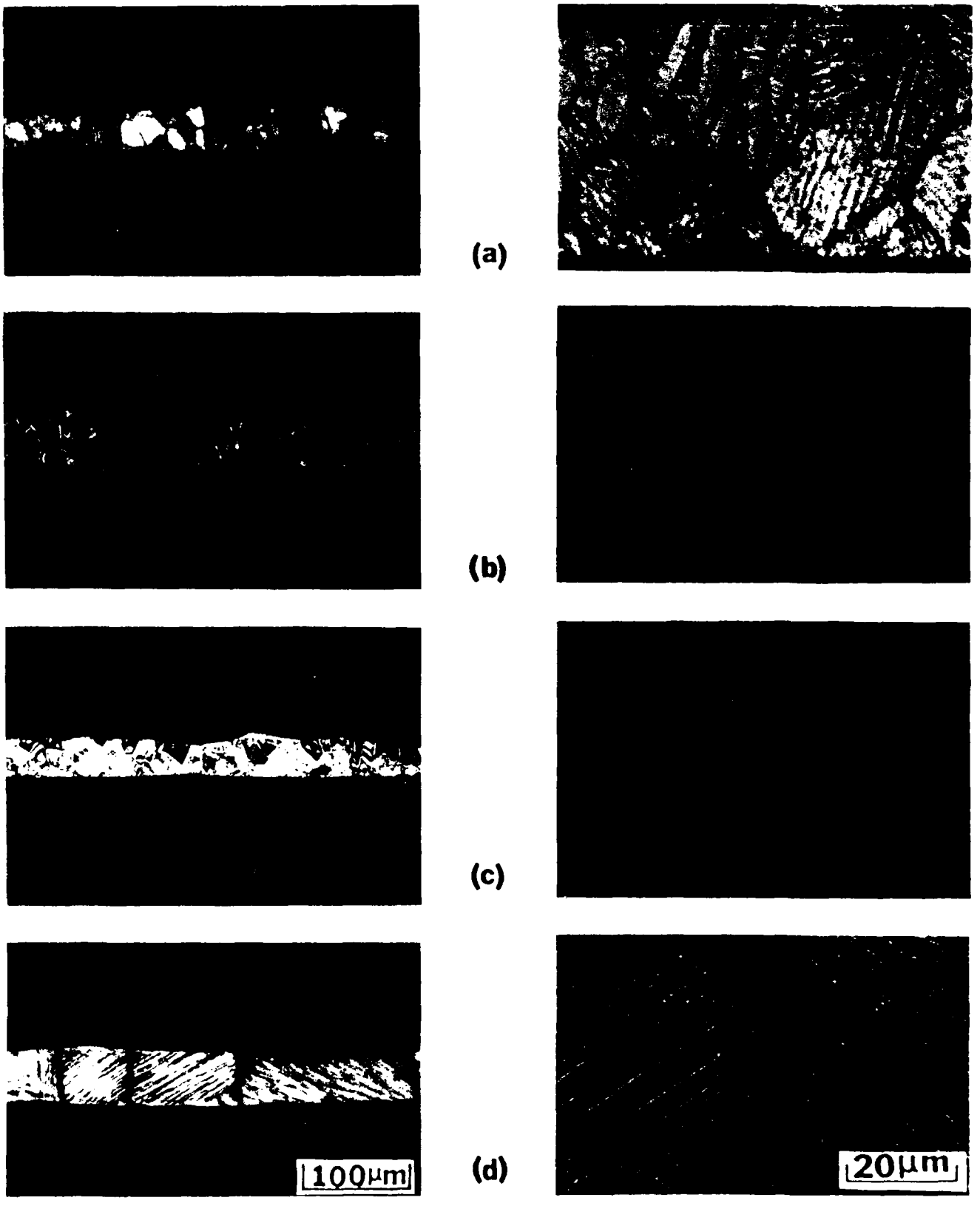

[illegible] Alloy Number 51 (Ni-35.2 a/o Al) Produced [illegible] Technique and in Various Heat Treatment [illegible] As Solidified, After 2 Hours at (b) 800°C, (c) 1000°C [illegible]

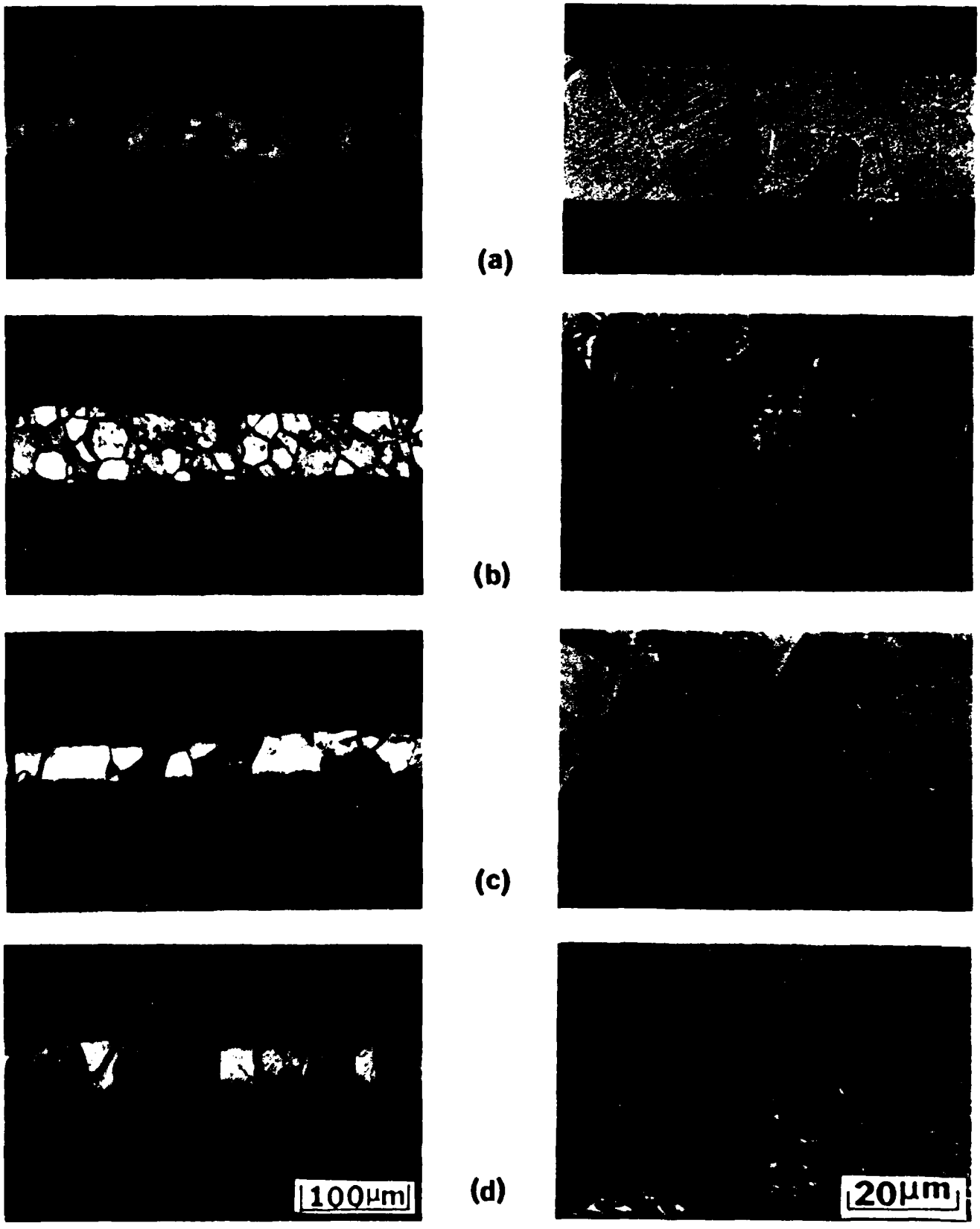
(a)
(b)
(c)
(d)
100μm
20μm

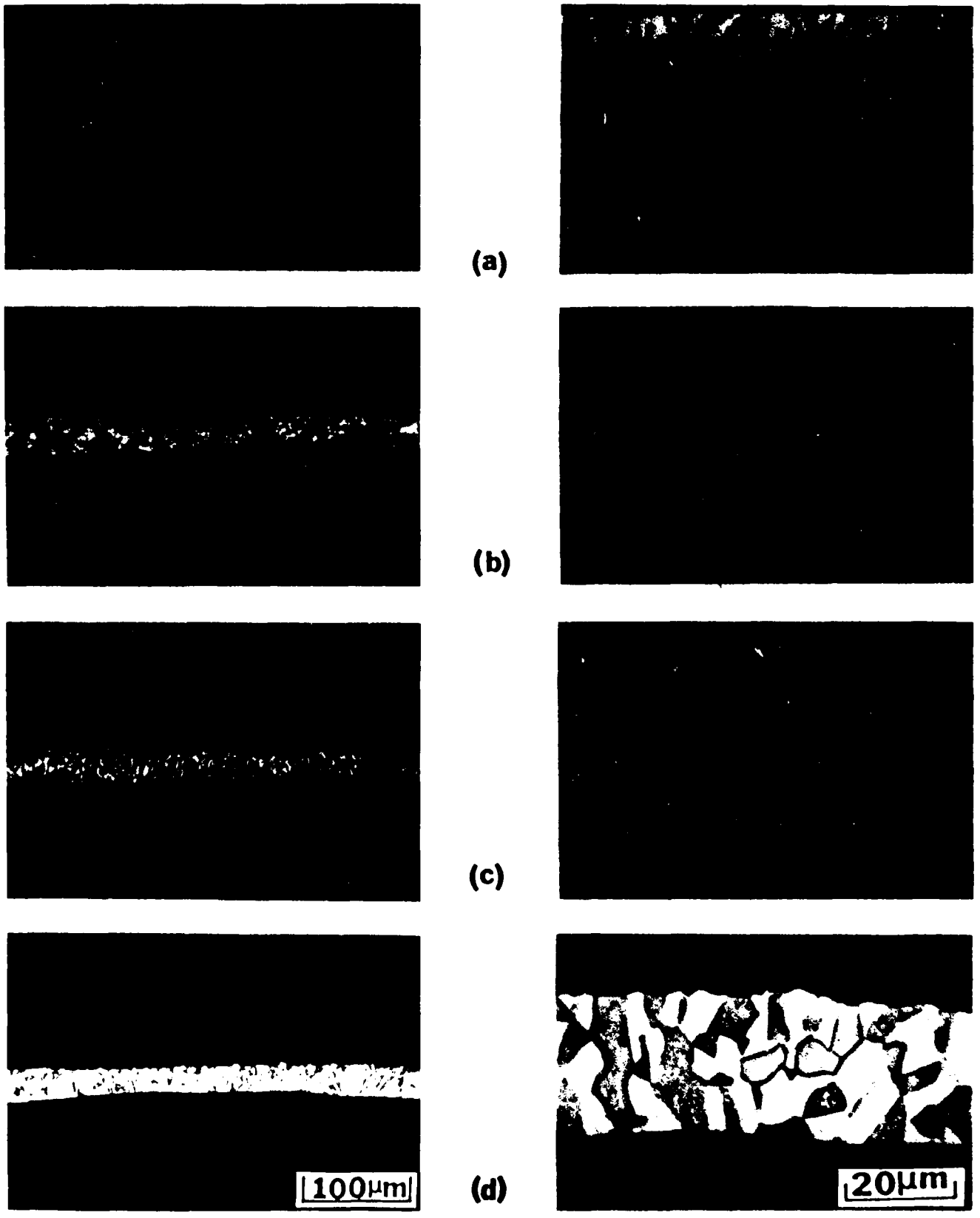

[illegible] NiAl Alloy Number 34 (At. [illegible] Al) Produced
[illegible] Melt Spinning Technique and in Various Heat Treatment
[illegible] As Solidified. After [illegible]

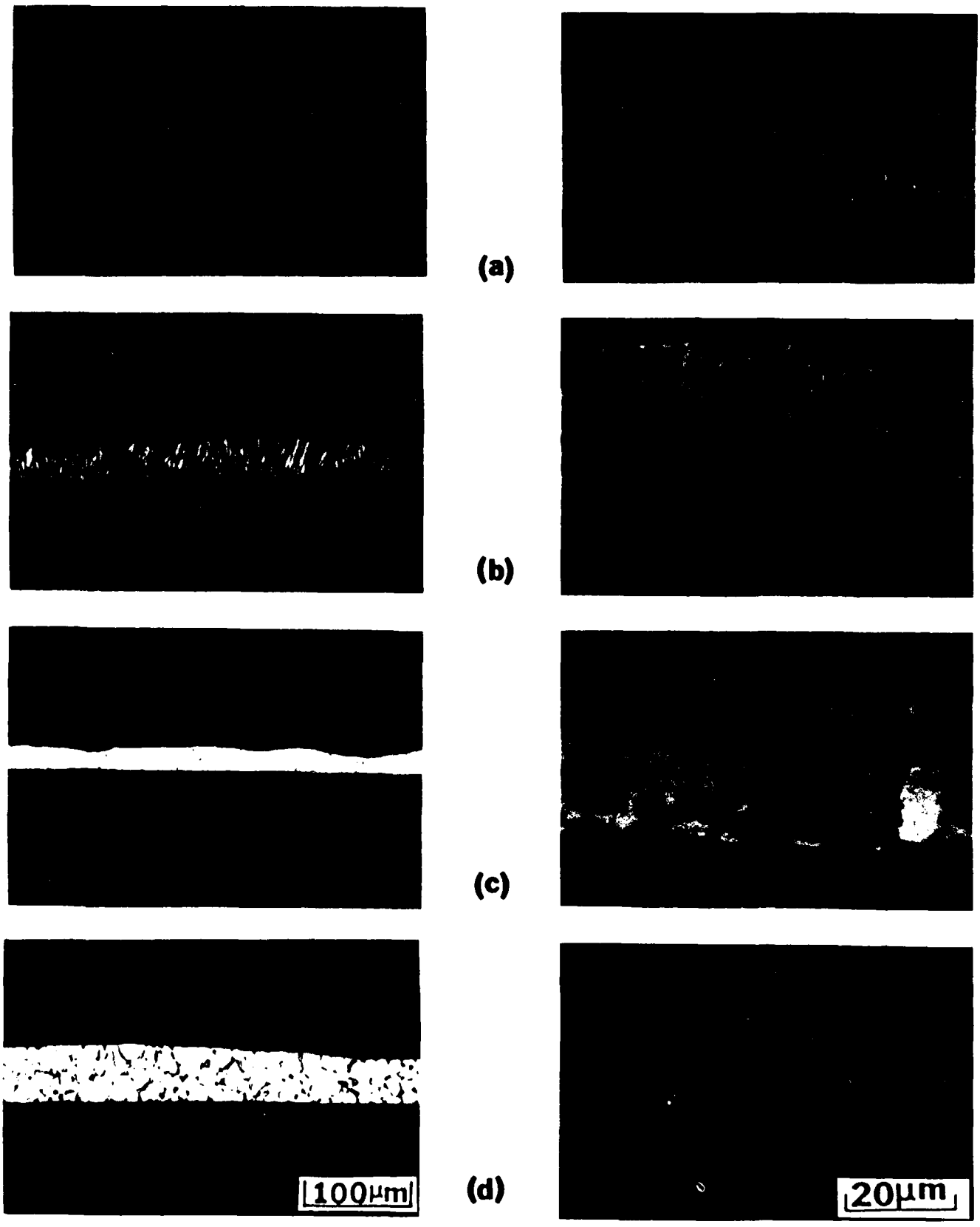

Figure 12. Microstructure of NiAl Alloy Number 85 (Ni-20.0 a/o Al-30.0 a/o Co) Produced Using a Melt Spinning Technique and in Various Heat Treatment Conditions (a) As-Solidified, After 2 Hours at (b) 800°C (c) 1000°C and (d) 1200°C.

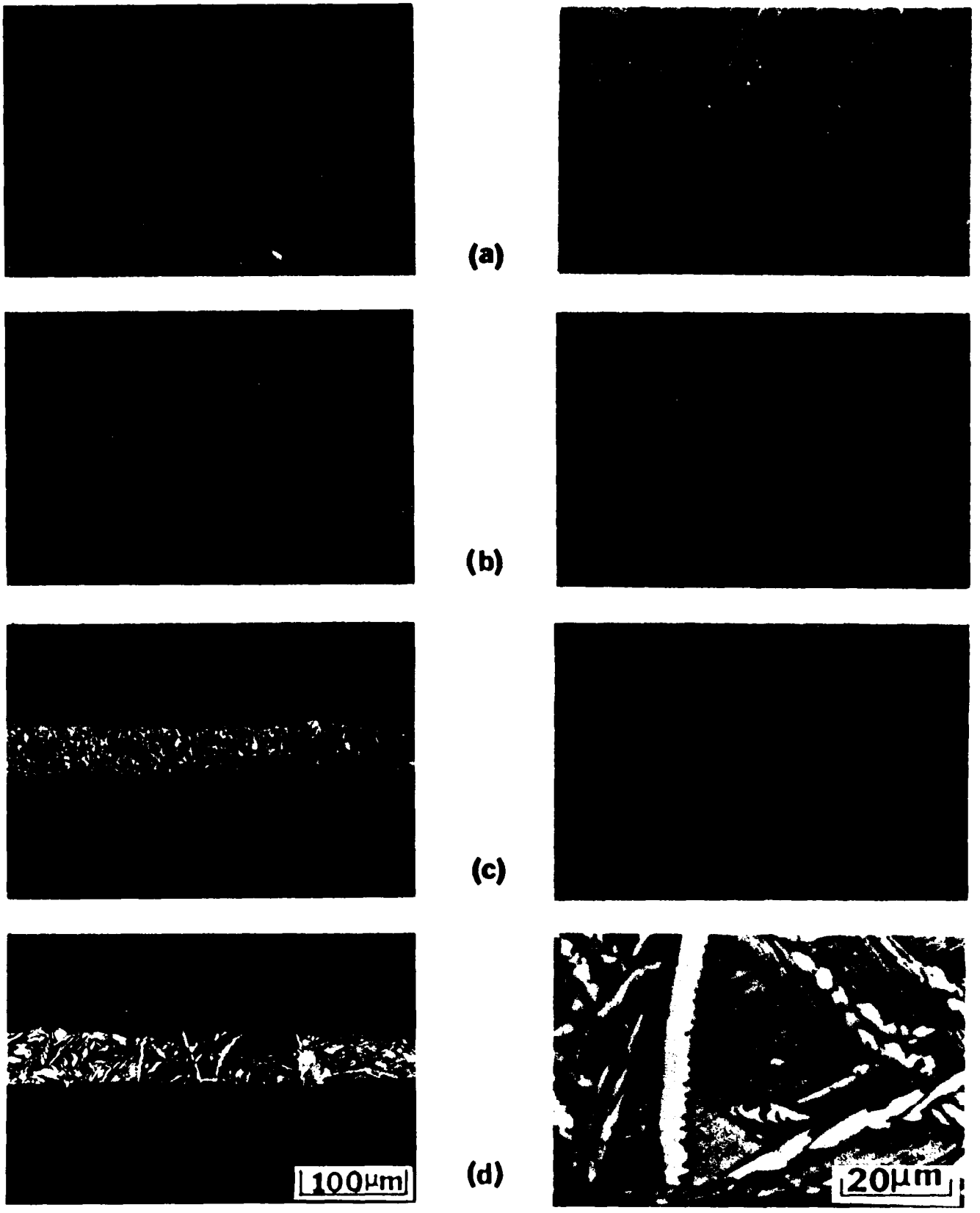

[illegible] NiAl Alloy Number 86 (Ni 50.0 a/o Al 50.0 a/o Mn) [illegible] Melt Spinning Technique and in Various Heat [illegible] Conditions, (a) As-Solidified. After 2 hours at [illegible] and (d) 1200°C.

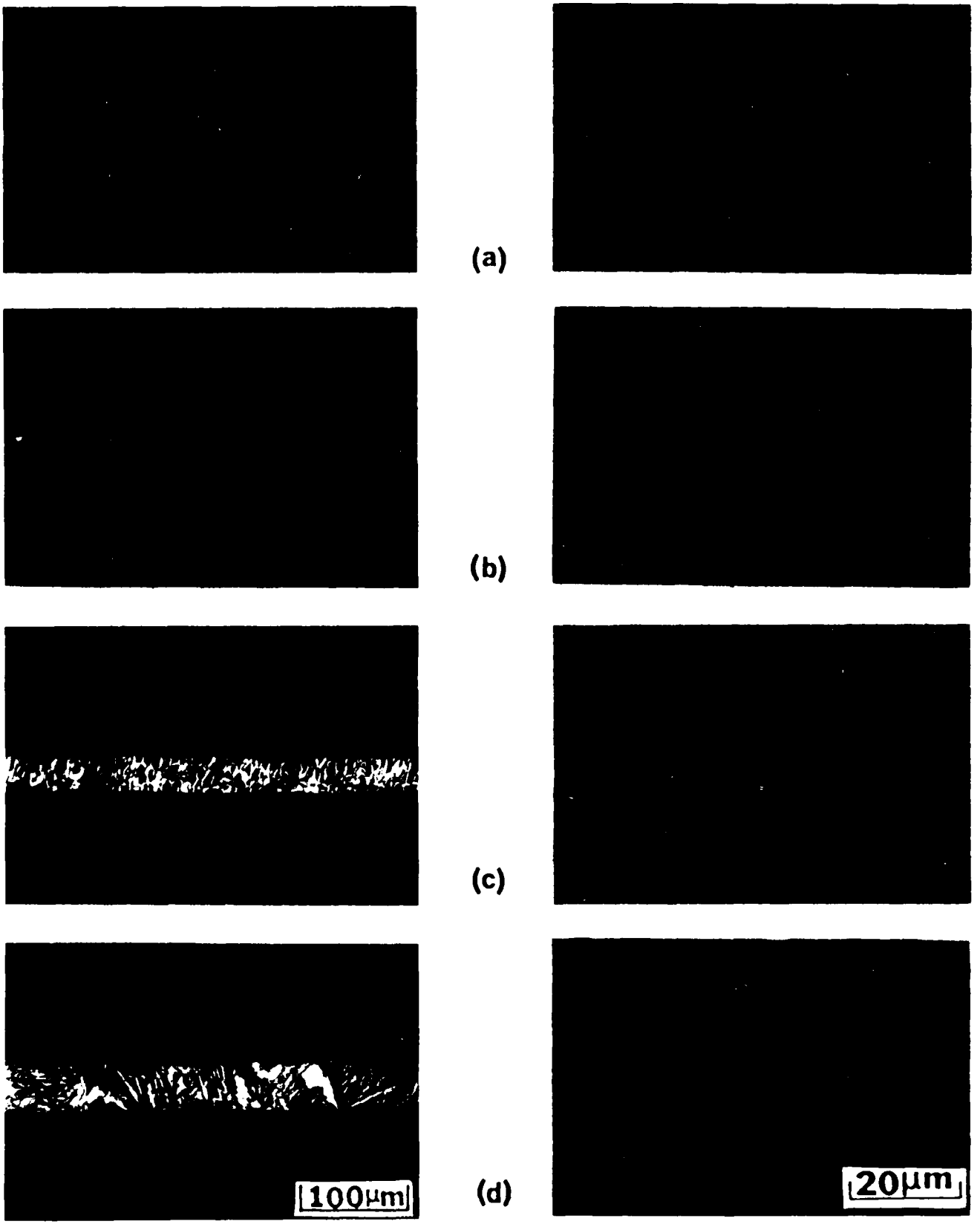

Figure 11. Microstructure of NiAl Alloy Number 87 CM [illegible] Al Produced Using a Melt Spinning Technique and in Various Heat Treatment Conditions: (a) As-Solidified, After 2 Hours at [illegible] and (d) 1200°C.

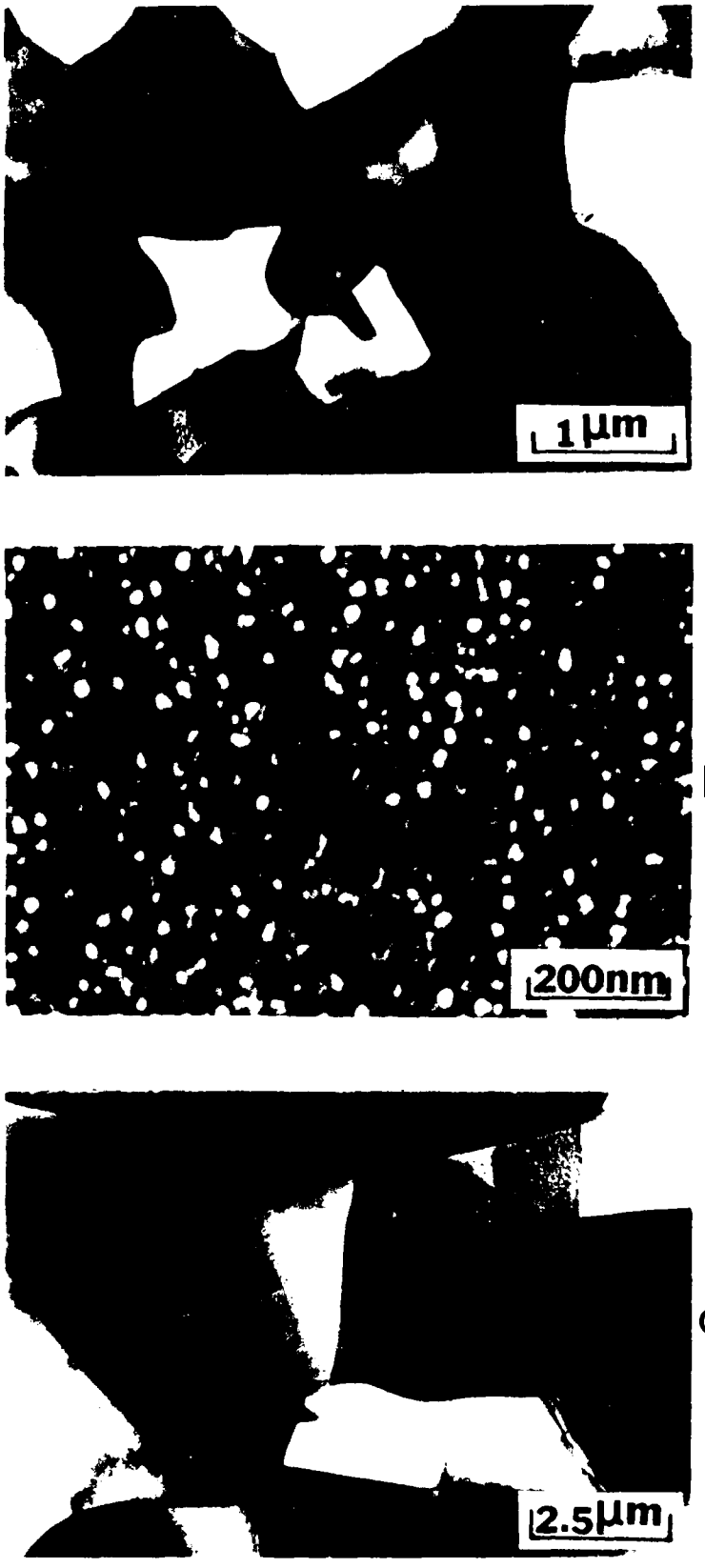
a
1μm
b
200nm
c
2.5μm

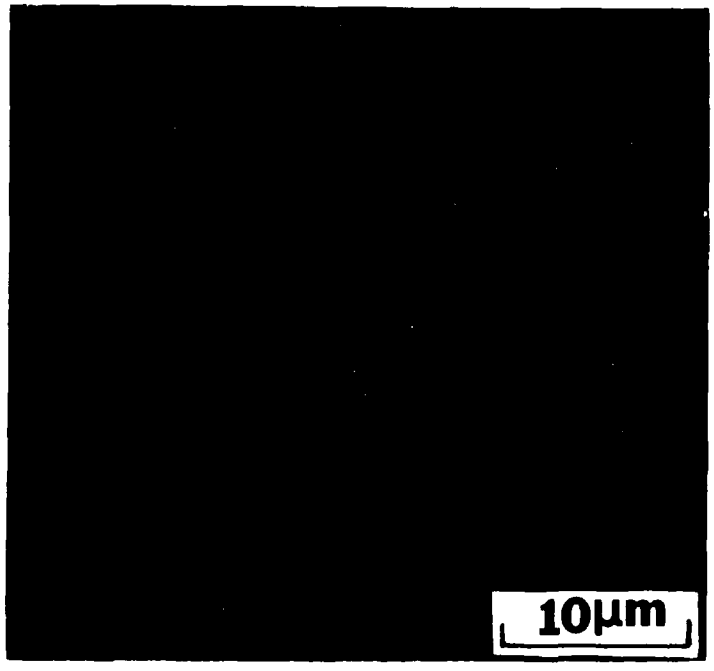

a

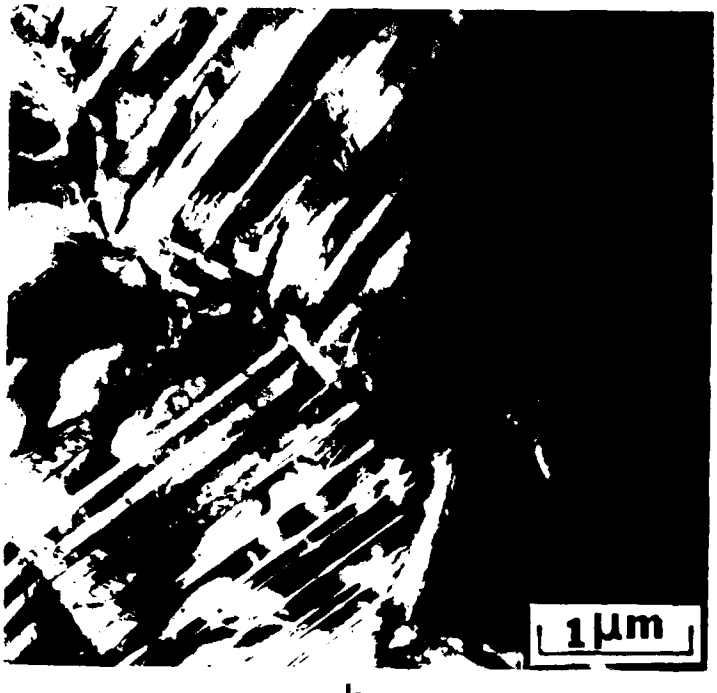

b

Figure 3. Microstructure of NiAl Alloy Number 8c (Ni-37.0 a/o Al-5.0 a/o Mn) Produced Using a Melt Spinning Technique and in As-Solidified Condition. (a) Secondary Electron Image Showing the General Appearance and (b) Transmission Electron Image Showing Extensive Microtwinning in this Alloy

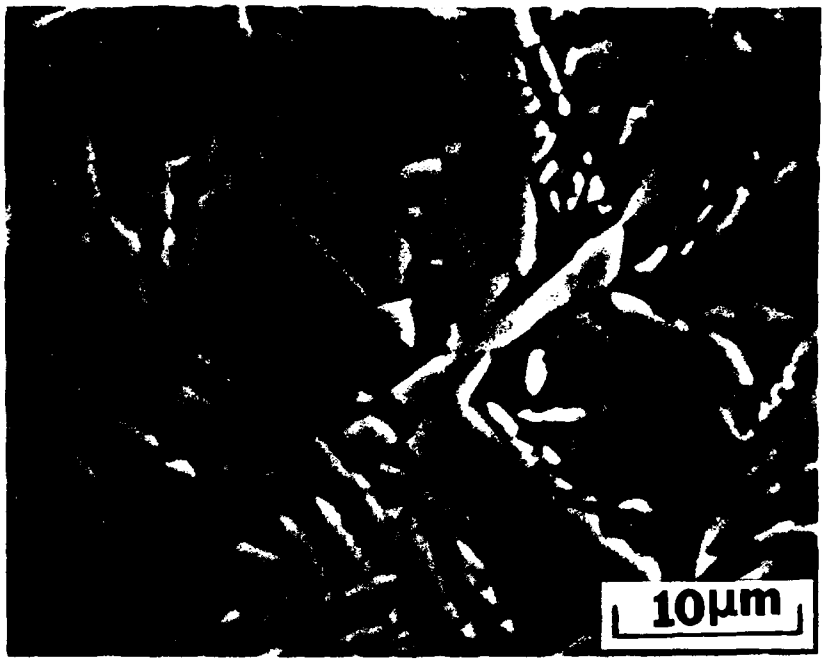

a

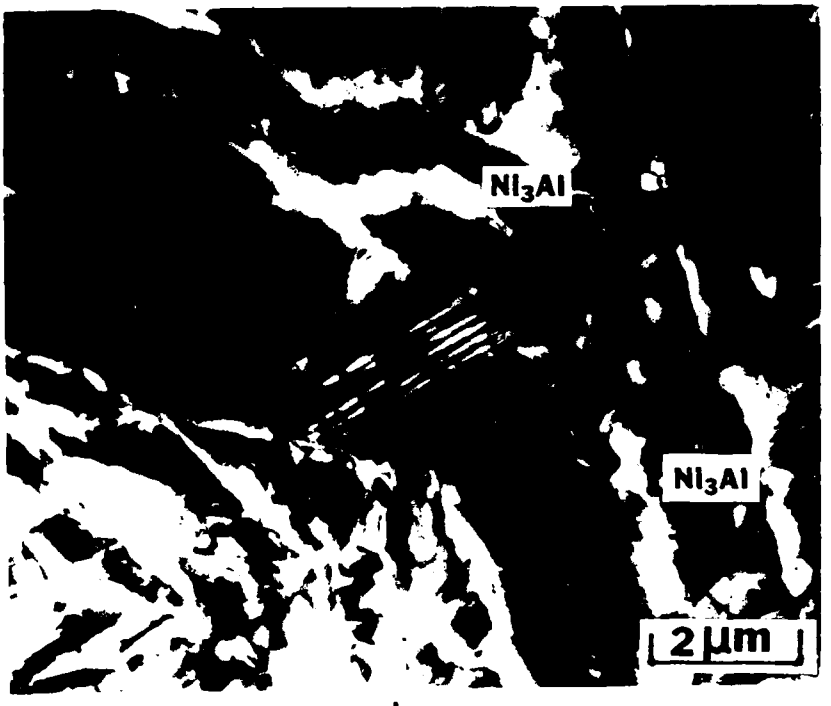

b

Figure 47 Microstructure of Ni-Al-Mn Number 86 (Ni 30.0 a/o Al-5.0 a/o Mn) Produced Using a Melt Spinning Technique and After Heat Treatment for 2 Hours at 1200°C (a) Secondary Electron Image Showing the General Appearance, (b) Transmission Electron Image Showing the Identified Ni_3Al Phase.

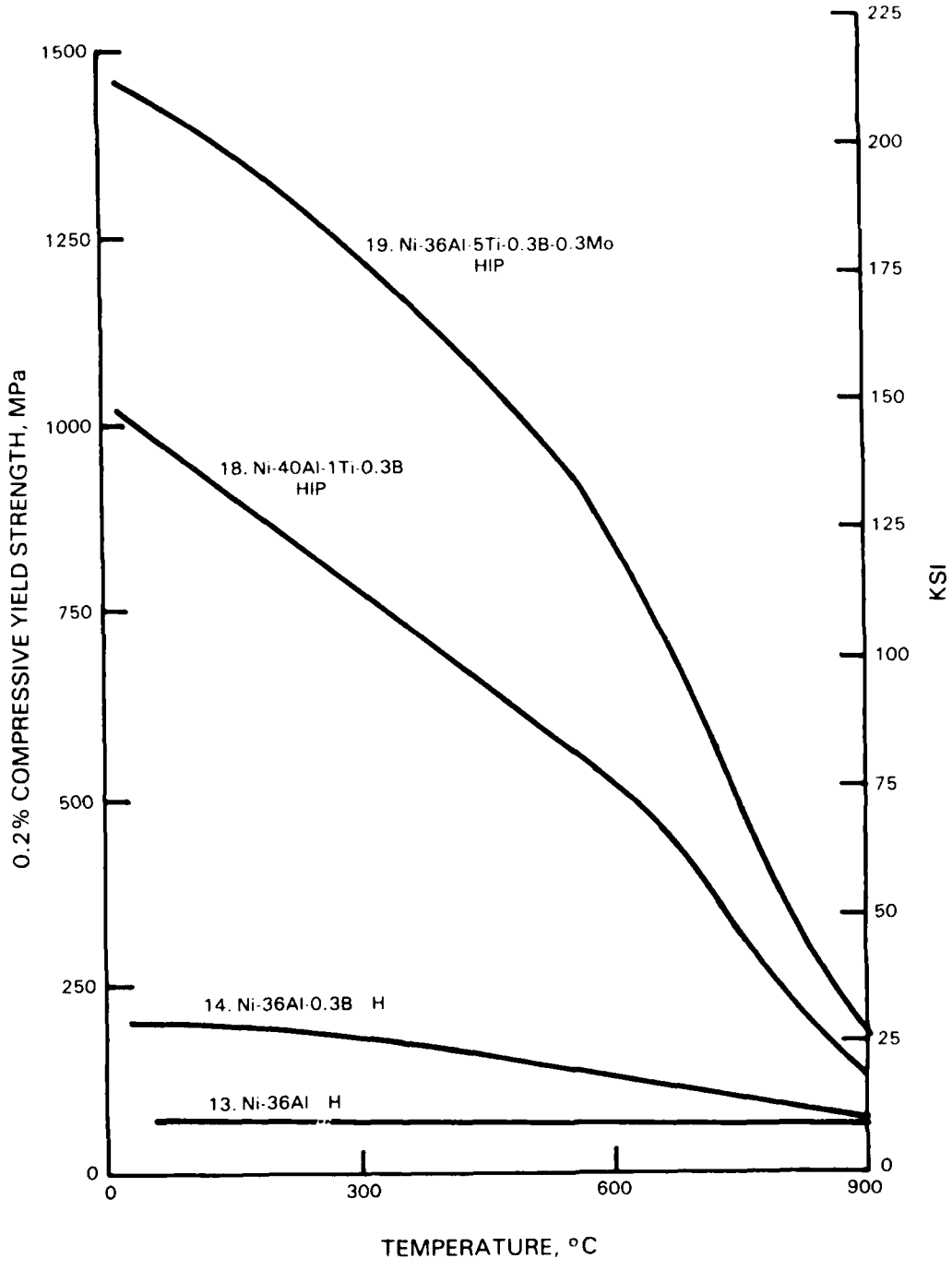

Figure 48 0.2 Percent Compressive Yield Strength vs Temperature Curves for NiAl Alloy Numbers 13, 14, 18, and 19 Illustrating Solute Hardening Effect of Ti and B. Heat Treatment Codes: H: Homogenization at 1260°C (2300°F) for 64 hours, HIP: Hot Isostatic Pressing 1150°C (2100°F)/100MPa/3hrs.

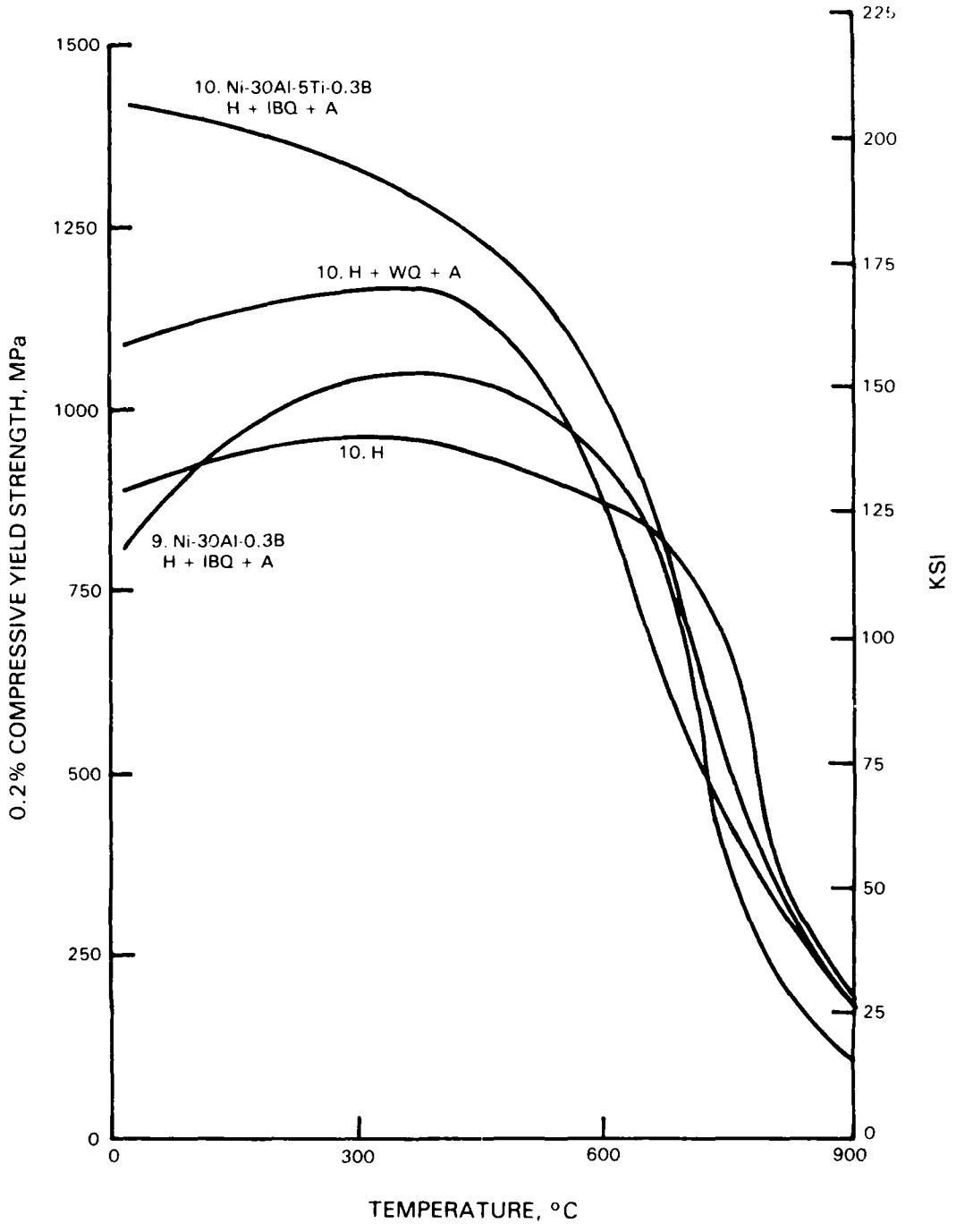

Figure 49 0.2 Percent Compressive Yield Strength vs Temperature Curves for Ni_3Al Particle Hardened NiAl Alloy Numbers 9 and 10 Illustrating the Effect of Heat Treatment on Alloy Number 10. H: Homogenization Heat Treatment at 1260°C (2300°F) for 64 hours, IBQ and WQ: Ice Brine Quench and Water Quench, Respectively, From Solution Heat Treatment at 1150°C (2100°F) for 1 Hour, A: Aging Heat Treatment for 4 Hours at 760°C (1400°F).

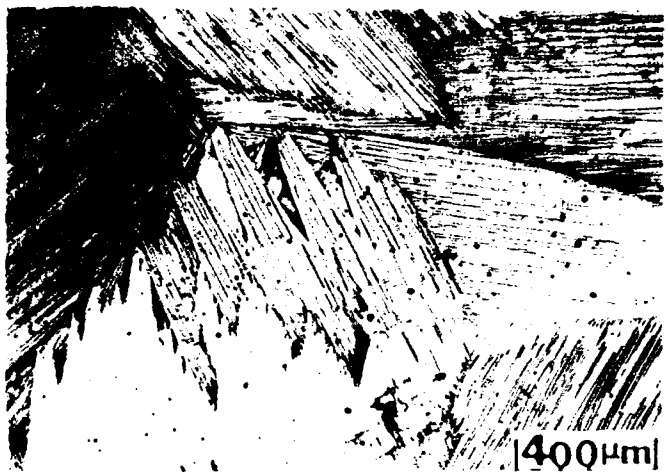

a

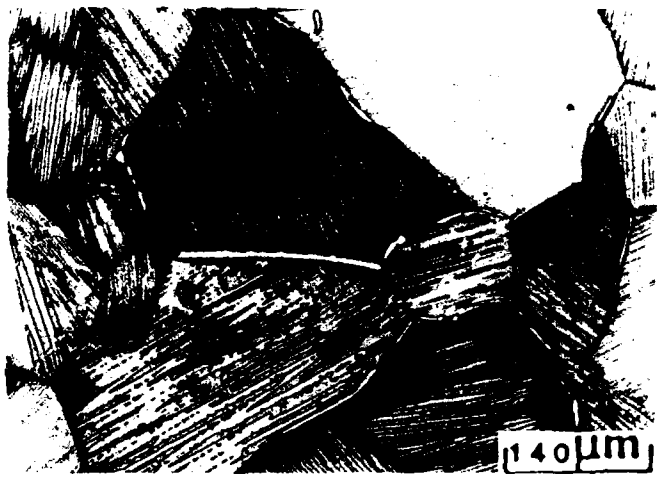

b

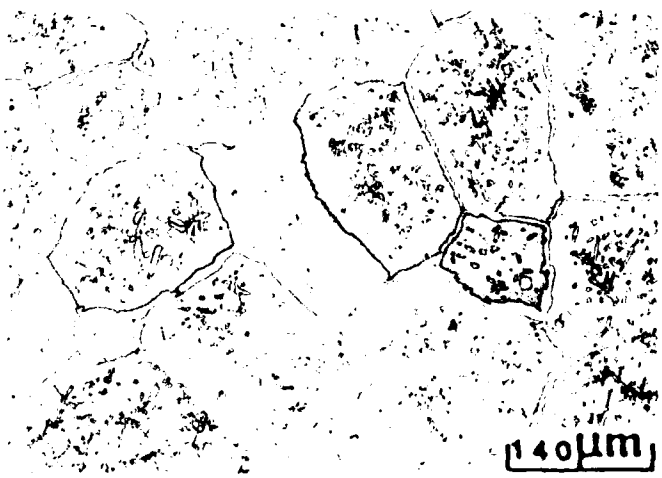

c

Figure 5. Microstructure of Ni-Be-Al Number 10 After Heat Treatment at a. 1000°C, 1 hour, water quench; b. 1000°C, 1 hour, cooled in air cooling and 1 hour, 700°C and furnace cooling;

a

b

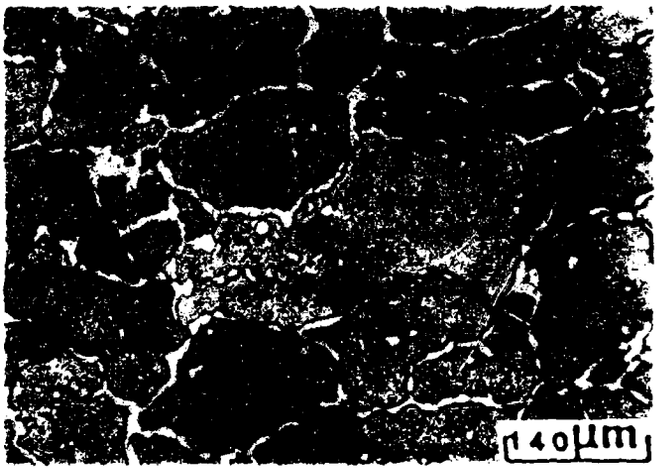

c

Figure 51 Microstructure of [illegible] Treatment at [illegible] (1960°F)/h4 hr/air [illegible] furnace cooling

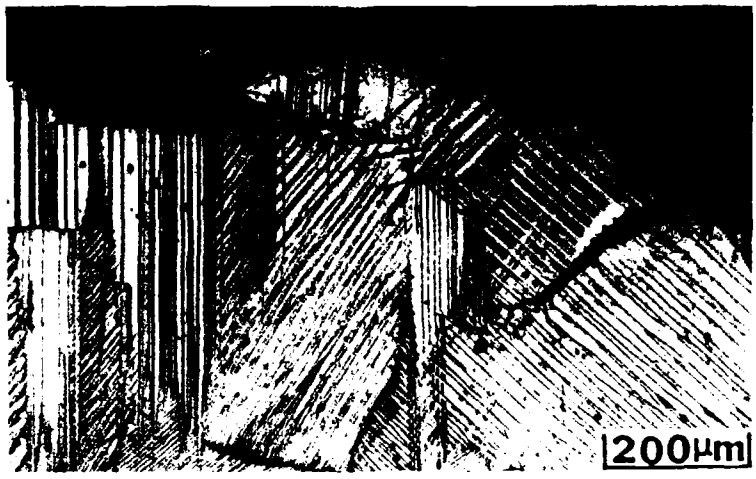

a

b

c

AD-A191 697 RAPIDLY SOLIDIFIED LIGHTWEIGHT DURABLE DISK MATERIAL 2/2
(U) PRATT AND WHITNEY WEST PALM BEACH FL GOVERNMENT
PRODUCTS DIV C C LAW ET AL 15 DEC 87
UNCLASSIFIED PW/GPD-FR-19875 AFWAL-TR-87-4102 F/G 11/6 1 NL

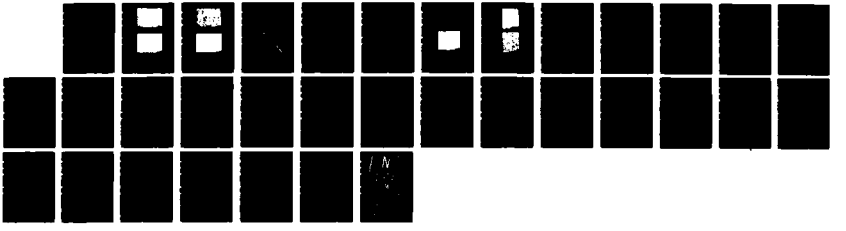

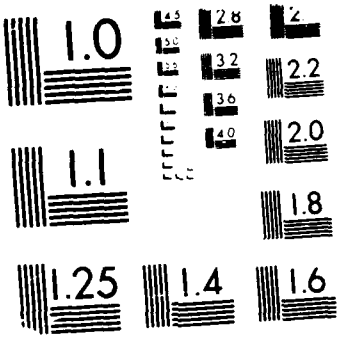

a

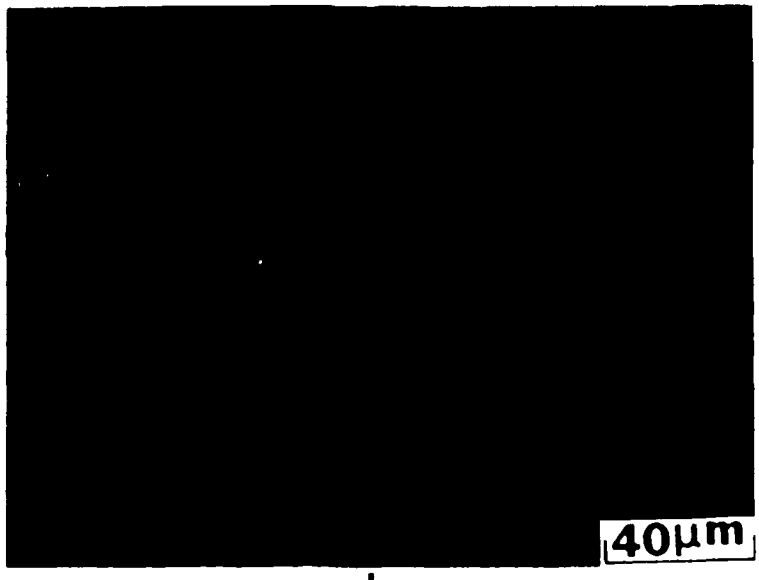

b

Figure 53 Microstructure of Ni-36 a/o Al-0.3 a/o B (Number 9) After Heat Treatment at (a) 1260°C (2300°F)/64 hr/air cooling (homogenization) + 1150°C (2100°F)/1 hr/water quench (solution) + 760°C (1400°F)/4 hr/air cool (age). (b) Higher Magnification of (a).

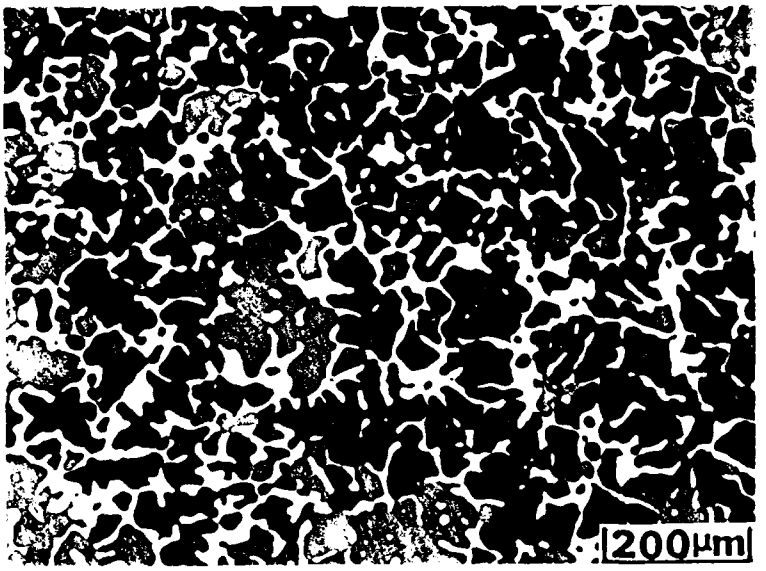

a

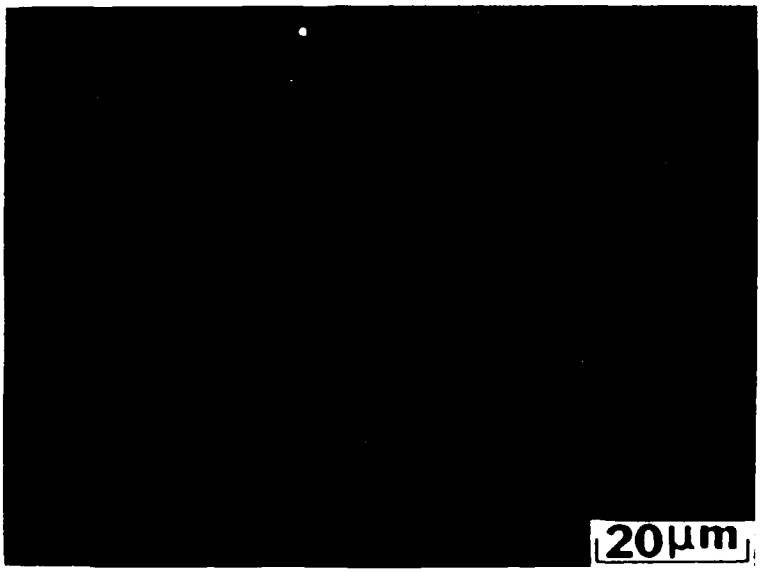

b

Figure 54 Microstructure of Ni-30 a/o Al-5.0 a/o B (Number 10) After Heat Treatment at (a) 1260°C (2300°F)/64 hr/air cooling (homogenization) + 1150°C (2100°F)/1 hr/water quench (solution) + 760°C (1400°F)/4 hr/air cool (age). (b) Higher Magnification of (a).

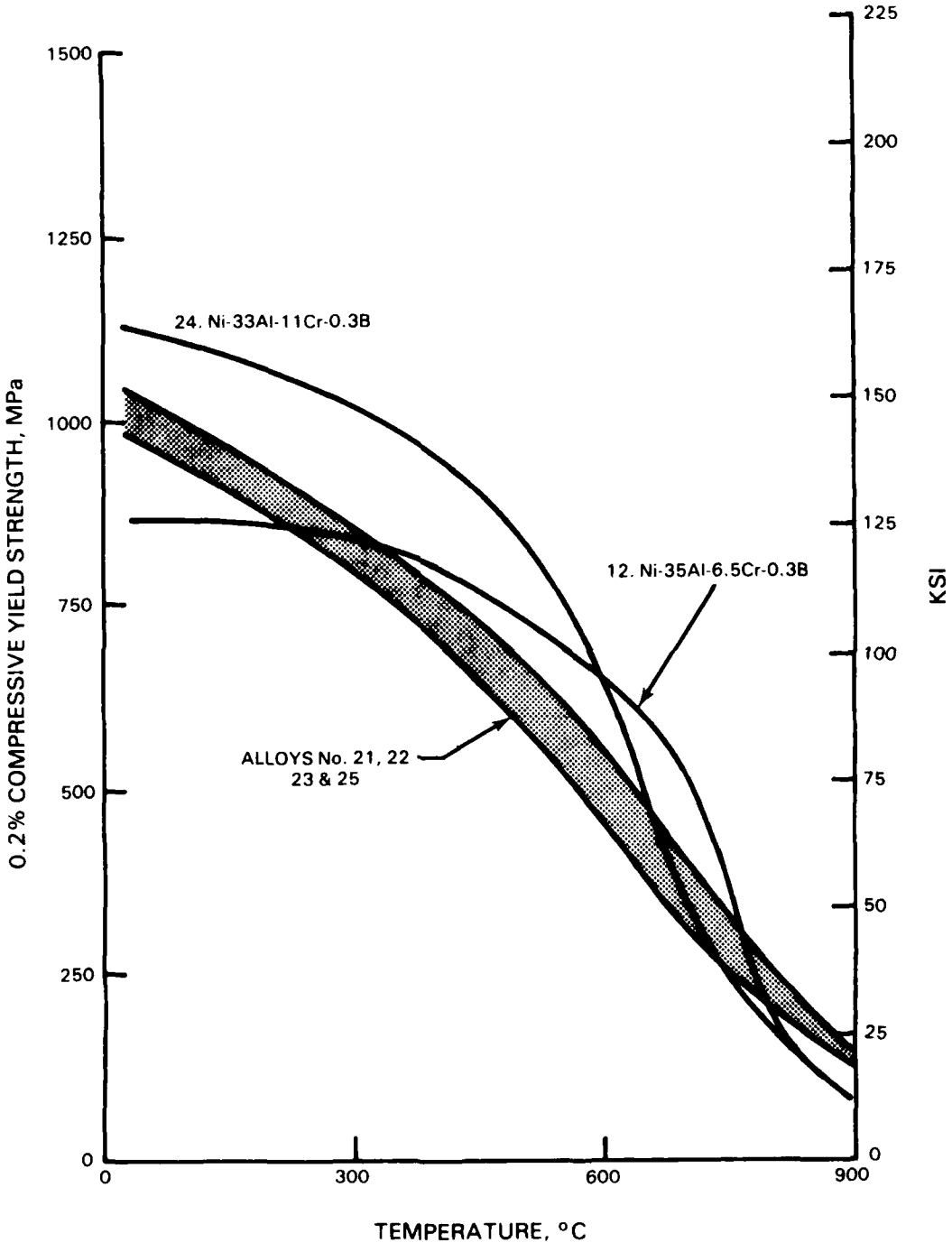

Figure 55 0.2 Percent Compressive Yield Strength vs Temperature Curves for Chromium Modified NiAl Alloys Illustrating the Strength Characteristics Due to Cr Solute, Cr Particle and Ni_2Al Particle Hardening. All Materials in HIP Condition.

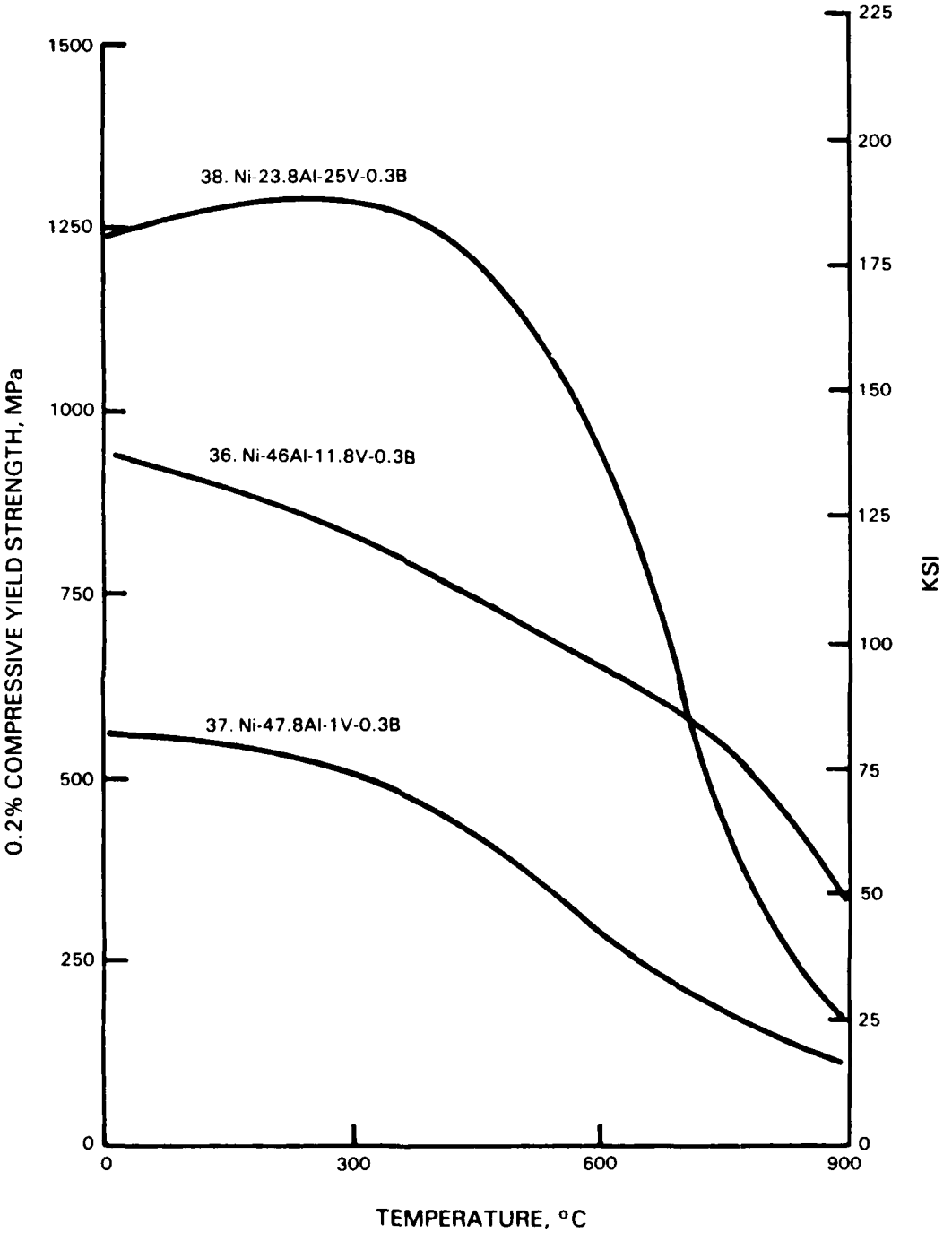

Figure 56 0.2 Percent Compressive Yield Strength vs Temperature Curves for Vanadium Modified NiAl Alloys. All Materials in As-Cast Condition.

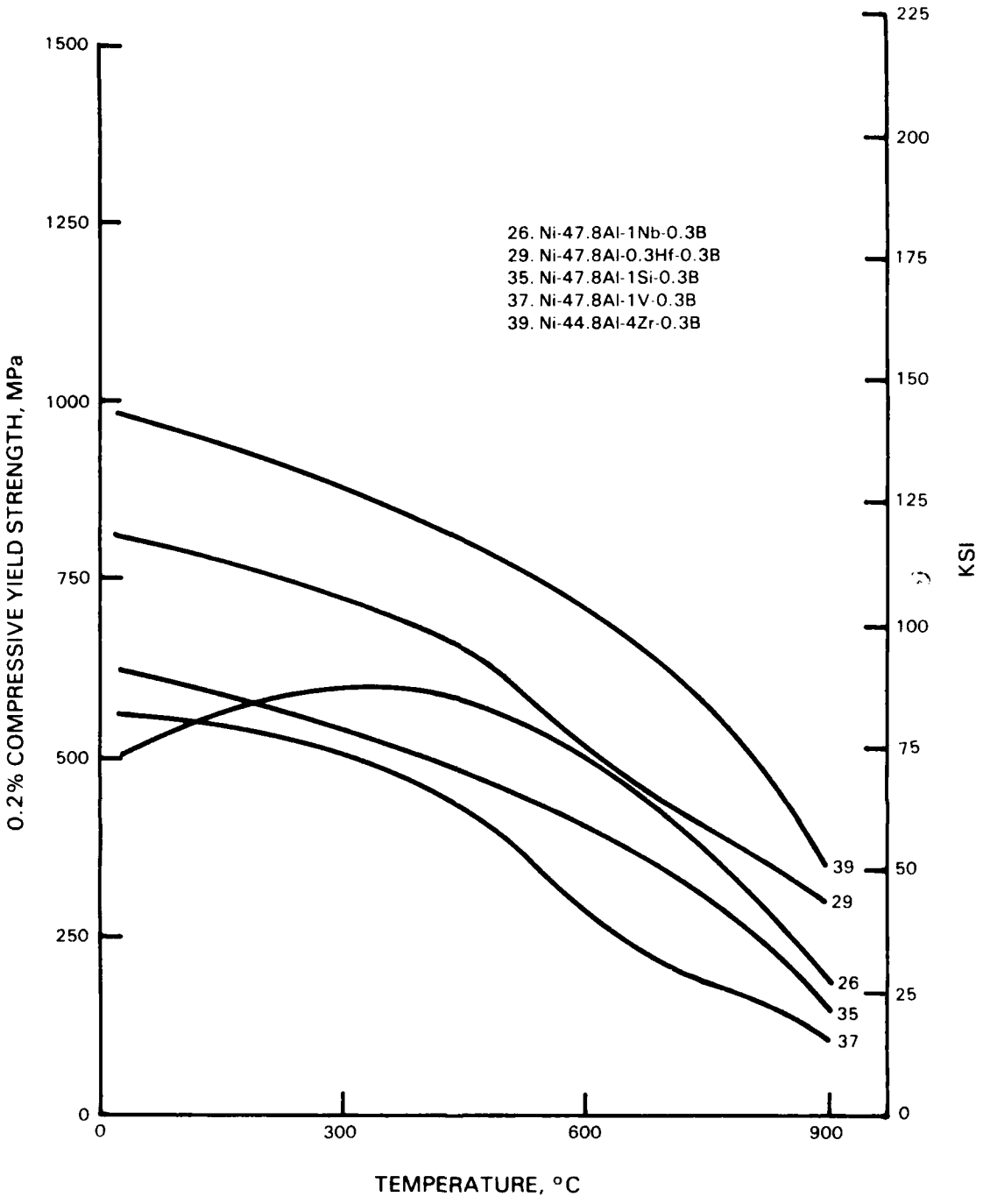

Figure 57 0.2 Percent Compressive Yield Strength vs Temperature Curves for Selected NiAl Alloys in the Ni-Al-X Ternary Systems. X = Nb, Hf, Si, V, and Zr. All Materials in As-Cast Condition.

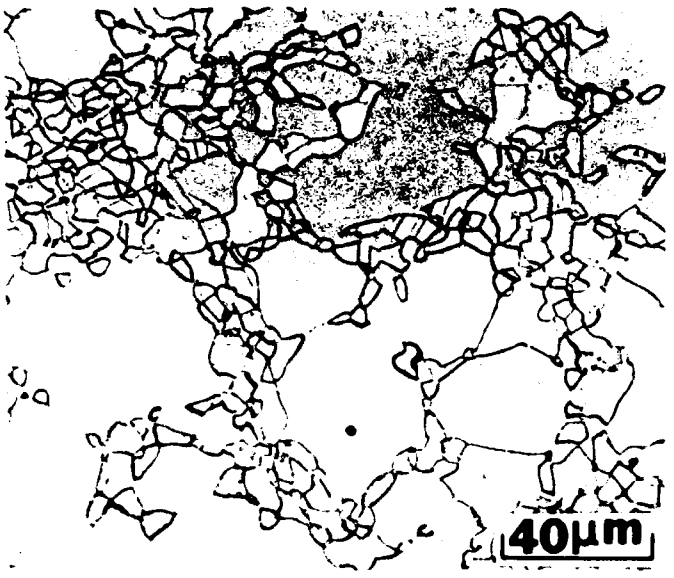

(a)

(b)

Figure 58 General Microstructure Features of the Transverse Section of the Extruded Bars After Heat Treatment for 2 Hours at 1150°C (a) Alloy Number 88 (Ni-22 a/o Al-27 a/o Fe) (b) Alloy Number 89 (Ni-25 a/o Al-25 a/o Co).

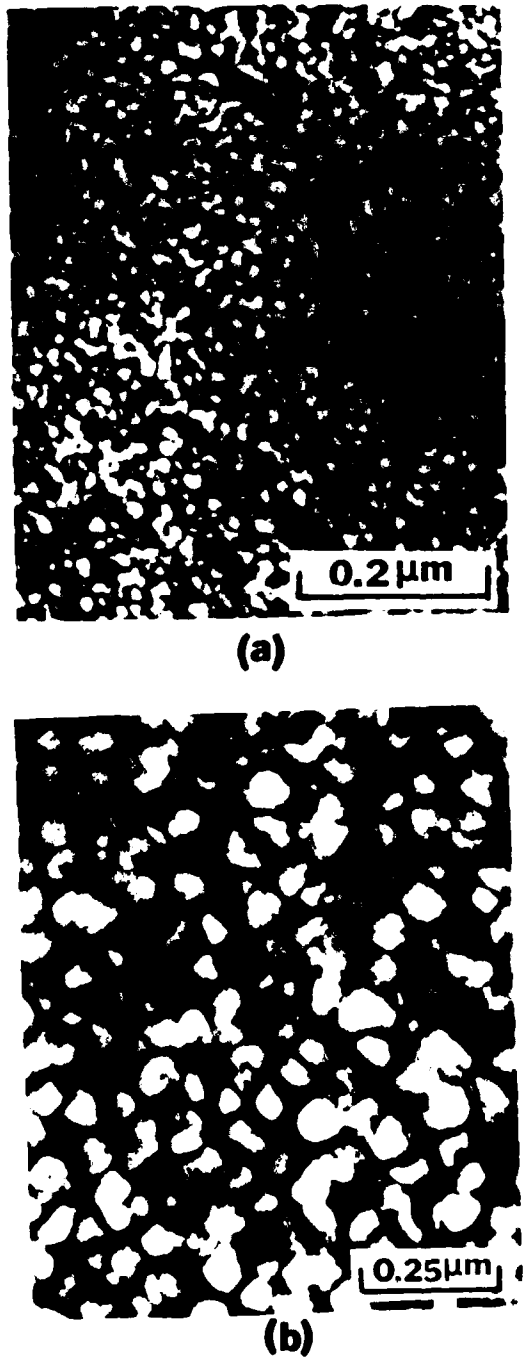

FIGURE 59 Dark Field Electron Micrographs Illustrating the Precipitation of Coherent Fine $L1_2$-Type Particles in Al Phase of Alloys (a) Number 88 (b) Number 89.

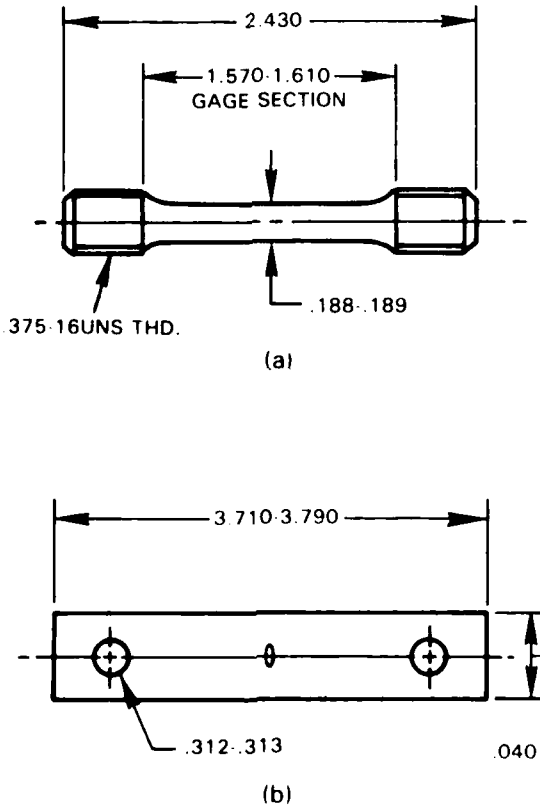

Figure 60 Mechanical Test Specimens (a) Standard Cylindrical Specimen for Tensile and Creep Tests. (b) Center Cracked Panel Specimen for Fatigue Crack Growth Measurements. Dimensions in Inches.

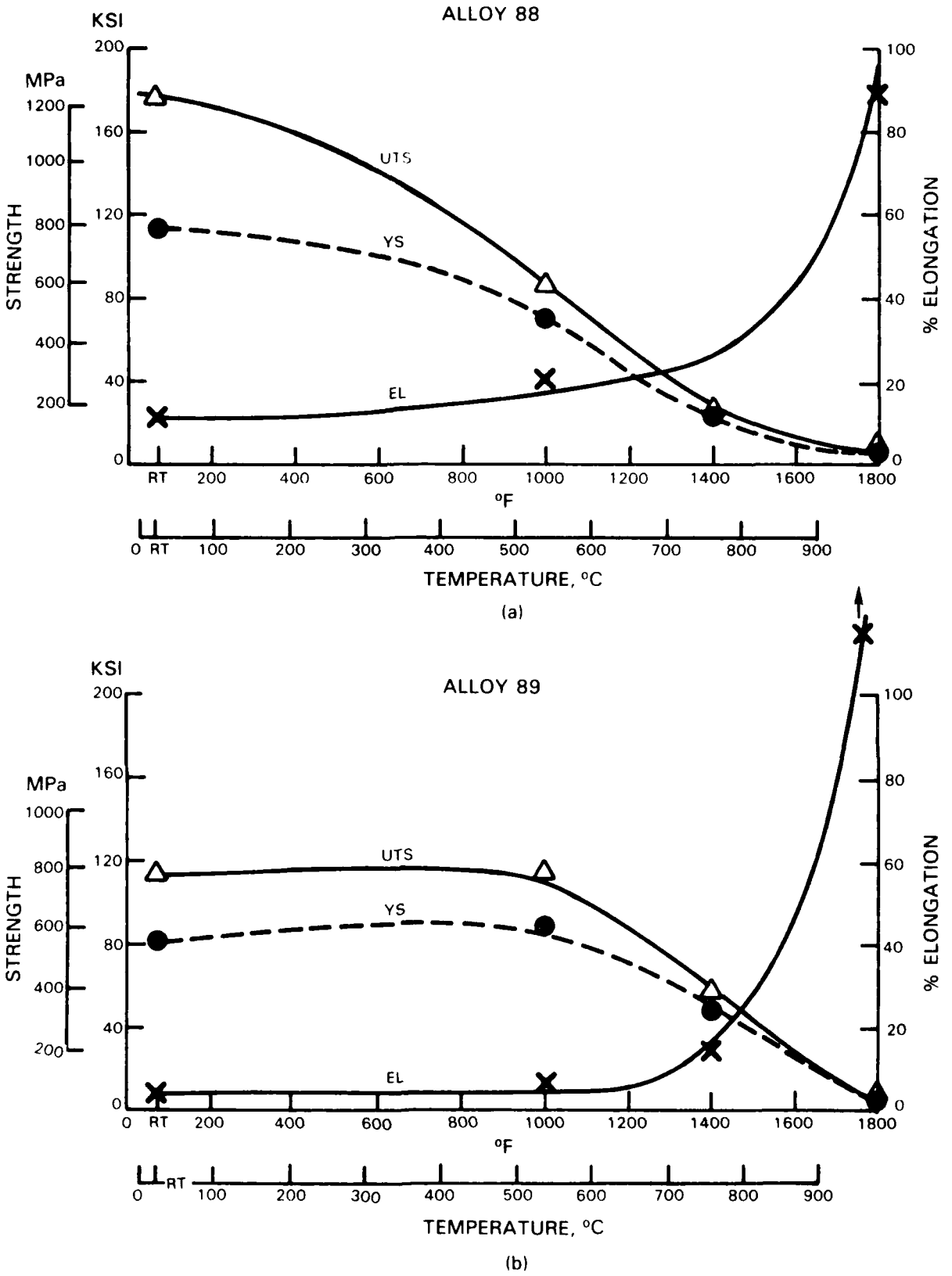

Figure 61 Tensile Properties of Phase III Alloys After Extrusion and Heat Treatment for 2 Hours at 1150°C (a) Alloy Number 88 (Ni-22 a/o Al-27 a/o Fe) (b) Alloy Number 89 (Ni-25 a/o Al-25 a/o Co).

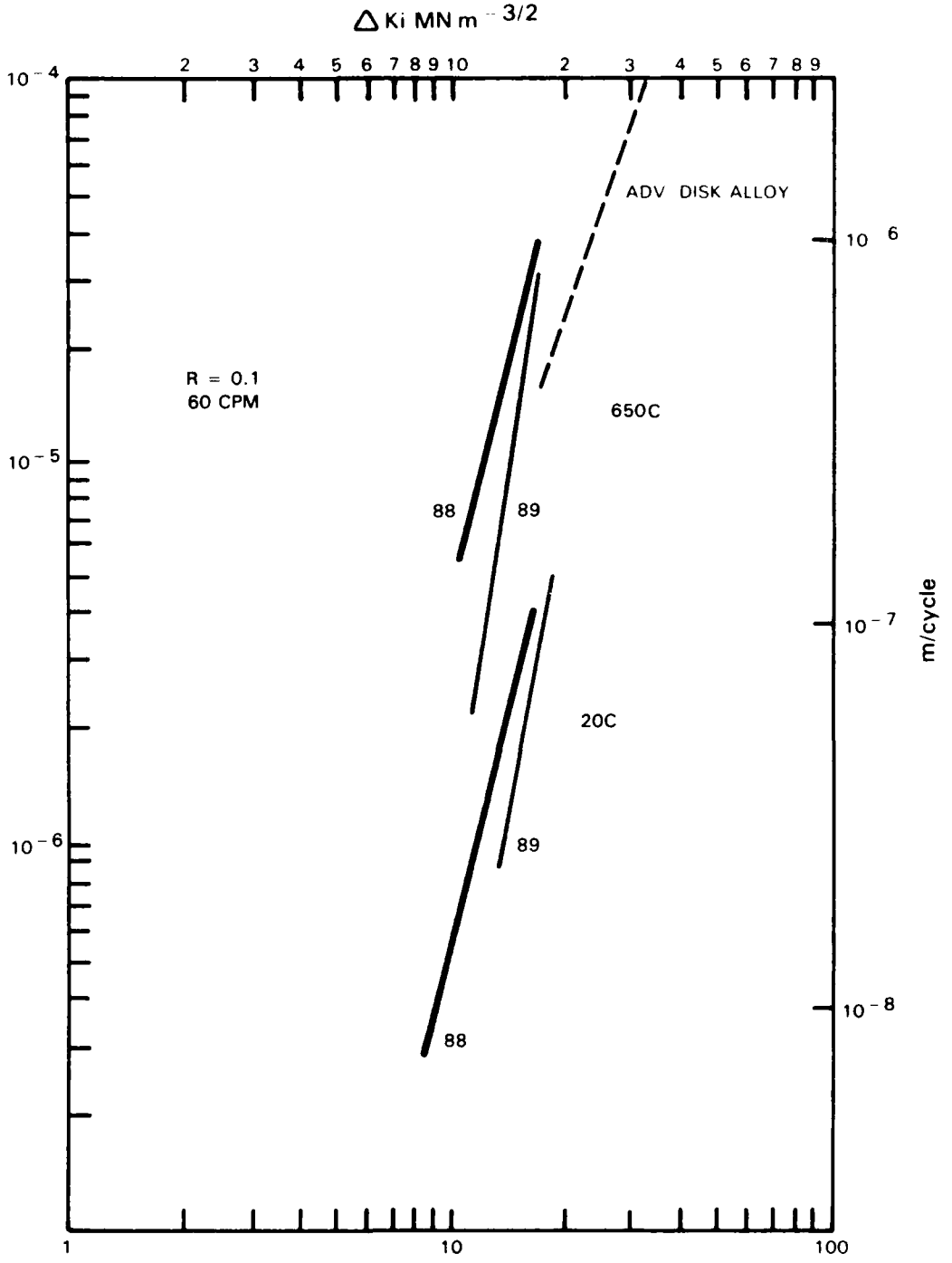

Figure 62 Fatigue Crack Growth Behavior of Phase III Alloys Number 88 and Number 89 at Room Temperature and 650°C.

TABLE 1

HEATS OF FORMATION OF SOME B2 PHASES

A B	$-\Delta H_f$ Cal/g-atom		R_A/R_B	a_o(Å)	T_M(°C)
MnAl	5,800 at 1273K	5,100 at 600K	0.910	-	
FeAl	6,600 at 1173K	6,000 at 600K	0.890	2.902	1,250
CoAl	13,000 at 1273K	13,200 at 600K	0.875	2.870	1,645
NiAl	14,800 at 1273K	14,100 at 600K	0.841	2.887	1,638
NiBe	-	-	1.104	2.621	-
NiSc	-	-	0.760	3.171	-
NiTi	-	-	0.853	3.015	-
NiZn	-	-	0.894	2.914	-
NiGa	11,300 at 1108K	11,300 at 1023K	0.883	2.936	-
NiIn	-	-	0.750	3.099	-

TABLE 2

CANDIDATE A2 COHERENT STRENGTHENERS IN NiAl

	Lattice Parameter(Å)	Possible Formation in NiAl	Lattice Misfit % Ni-35 a/o Al a_o = 2.894A	Lattice Misfit % Ni-50 a/o Al a_o = 2.909A
V	3.039	Yes (Ref. 25)	5.01	4.47
Cr	2.8845	Yes (Ref. 26)	-0.33	-0.84
Mo	3.1466	Yes (Ref. 27)	8.73	8.17
W	3.1648	Yes (Ref. 28)	9.36	8.79

TABLE 3

CANDIDATE L2$_1$ COHERENT STRENGTHENERS IN NiAl

	Lattice Parameter(Å)	Possible Formation in NiAl	Lattice Misfit % Ni-35 a/o Al	Lattice Misfit % Ni-50 a/o Al
Ni_2TiAl	5.872 (Ref. 36)	Yes (Ref. 24)	1.45	0.93
Ni_2ZrAl	6.123 (Ref. 37)	?	5.79	5.24
Ni_2HfAl	6.081 (Ref. 37)	Yes (Ref. 29)	5.06	4.52
Ni_2VAl	- (Ref. 38)	* (Ref. 25)	-	-
Ni_2NbAl	5.974 (Ref. 37)	Yes (Ref. 30)	3.21	2.68
Ni_2TaAl	5.949 (Ref. 37)	Yes (Ref. 31)	2.78	2.25

? No Ni-Al-Zr ternary phase diagram available for assessment.

* Ni_2VAl phase was not shown in the referenced Ni-Al-V ternary phase diagram, probably due to oversight.

TABLE 4

SELECTED PHASE I NiAl BASE-LINE ALLOYS *

Alloy Designation	Atom % Al	Atom % B	Weight % Al	Weight % B	Comments	
NiAl 1	54.0	0.25	35.14	0.065	YS Peak	Stoichiometry Effect
NiAl 2	51.5	0.25	32.89	0.064		
NiAl 3	50.0	-	31.49	-	Boron Effect	
NiAl 4	50.0	0.25	31.57	0.063		
NiAl 5	48.5	0.25	30.29	0.063		
NiAl 6	43.0	0.25	25.81	0.060	Boron Effect	
NiAl 7	43.0	-	25.74	-	YS Peak	

* Nickel balance.

TABLE 5

PHASE II - TASK I SUBSTITUTIONAL ALLOYS FOR DUCTILITY EVALUATION

Alloy	Atom (%) (Balance Ni)	Comments
I	**Ni Substitutional Alloy Series**	**Atom % Ni Substituted**
40	48.5 Al - 5.2 Cr	10% } Hypostoichiometric
41	48.5 Al - 10.3 Cr	20% } Hypostoichiometric
42	48.5 Al - 20.6 Cr	40% } Hypostoichiometric
60	51.5 Al - 9.7 Cr	20% - Hyperstoichiometric
43	48.5 Al - 5.2 Mn	10% } Hypostoichiometric
44	48.5 Al - 10.3 Mn	20% } Hypostoichiometric
45	48.5 Al - 20.6 Mn	40% } Hypostoichiometric
61	51.5 Al - 9.7 Mn	20% - Hyperstoichiometric
46	48.5 Al - 10.3 Fe	20% } Hypostoichiometric
47	48.5 Al - 20.6 Fe	40% } Hypostoichiometric
48	48.5 Al - 30.9 Fe	60% } Hypostoichiometric
62	51.5 Al - 19.4 Fe	40% - Hyperstoichiometric
49	48.5 Al - 10.3 Co	20% } Hypostoichiometric
50	48.5 Al - 20.6 Co	40% } Hypostoichiometric
51	48.5 Al - 30.9 Co	60% } Hypostoichiometric
63	51.5 Al - 19.4 Co	40% - Hyperstoichiometric
II	**Al Substitutional Alloy Series**	**Atom % Al Substituted**
52	43.7 Al - 4.9 Mn	10% } Hypostoichiometric
53	38.8 Al - 9.7 Mn	20% } Hypostoichiometric
54	29.1 Al - 19.4 Mn	40% } Hypostoichiometric
64	41.2 Al - 10.3 Mn	20% - Hyperstoichiometric
55	48.0 Al - 0.5 Ga	1% } Hypostoichiometric
56	46.1 Al - 2.4 Ga	5% } Hypostoichiometric
57	41.2 Al - 7.3 Ga	15% } Hypostoichiometric
65	48.9 Al - 2.6 Ga	5% - Hyperstoichiometric

TABLE 5 (Continued)

Alloy	Atomic % (Balance Ni)	COMMENTS
Al Substitutional Alloy Series - Continued		Atom % Al Substituted
59	46.1 Al - 2.4 Be	Baseline Ni 48.5 Al
76	40.8 Al - 2.2 Be	Baseline Ni 43.0 Al
77	46.1 Al - 2.4 Be - 5.0 Cu	
78	40.8 Al - 2.2 Be - 5.0 Cu	
Ni and Al Substitutional Alloy Series		Atom % Ni and Al Substituted
67	46.4 Al - 10.0 Mn	10% Ni and 10% Al - Hypostoichiometric
68	43.6 Al - 10.0 Mn	10% Ni and 10% Al - Hypostoichiometric

TABLE 6

PHASE II - TASK I MULTIPHASE ALLOYS FOR DUCTILITY IMPROVEMENT

Alloy	Atom (%) (Balance Ni)
79	29.3 Al
80	32.3 Al
81	35.2 Al
82	38.0 Al
84	20 Al - 27.5 Fe
85	22 Al - 30.0 Co
86	30 Al - 5.0 Mn
87	30 Al - 5.0 Cr

TABLE 7

ALLOYS SELECTED FOR PHASE II - TASK II, STRENGTH EVALUATION

Alloy	Atom (%) (Balance Ni)	Constituents According to Phase Diagram
	Ni-Al-Ti System	
13	36Al	B2(NiAl)
14	36Al-0.3B	
19	36Al-0.3B-0.3Mo-5Ti	
18	40Al-0.3B-1Ti	
20	43Al-0.3B-5Ti	
15	36Al-0.3B-12Ti	B2(NiAl),$L2_1$(Ni_2AlTi)
16	30Al-0.3B-12Ti	
17	30Al-0.3B-17Ti	
9	30Al-0.3B	B2(NiAl),$L1_2$(Ni_3Al)
10	30Al-0.3B-5Ti	
11	27Al-0.3B-0.3Mo-12Ti	B2(NiAl),$L1_2$(Ni_3Al),$L2_1$(Ni_2AlTi)
	Ni-Al-Cr System	
12	35Al-0.3B-6.5Cr	B2(NiAl),$L1_2$(Ni_3Al)
21	35Al-0.3B-15Cr	B2(NiAl),A2(Cr)
22	35Al-0.3B-13Cr	
23	35Al-0.3B-0.3Mo-13Cr	
24	33Al-0.3B-11Cr	B2(NiAl),A2(Cr),$L1_2$(Ni_3Al)
25	37.8Al-0.3B-11Cr	B2(NiAl)
	Ni-Al-Nb System	
26	47.8Al-0.3B-1Nb	B2(NiAl)
27	44.8Al-0.3B-4Nb	
28	37Al-0.3B-8Nb	B2(NiAl),$L2_1$(Ni_2AlTi)

TABLE 7 (Continued)

Alloy	Atom (%) (Balance Ni)	Constituents According to Phase Diagram
	Ni-Al-Hf System	
29	47.8Al-0.3B-0.3Hf	B2(NiAl)
30	47.8Al-0.3Mo-0.3Hf	
31	44.8Al-0.3B-4Hf	B2(NiAl),$L2_1$(Ni_2AlHf)
	Ni-Al-Ta System	
32	41.8Al-0.3B-2Ta	B2(NiAl)
33	32.8Al-0.3B-9Ta	B2(NiAl),$L2_1$(Ni_2AlTa)
	Ni-Al-Si System	
34	44.8Al-0.3B-4Si	B2(NiAl)
35	47.8Al-0.3B-1Si	
	Ni-Al-V System	
36	46Al-0.3B-11.8V	B2(NiAl),A2(V)
37	47.8Al-0.3B-1V	B2(NiAl)
38	23.8Al-0.3B-25V	B2(NiAl),$L2_1$(Ni_2AlV)?
	Ni-Al-Zr System	
39	44.8Al-0.3B-4Zr	B2(NiAl)

TABLE 8

BRITTLE-DUCTILE TRANSITION TEMPERATURES OF PHASE I ALLOYS

	Nominal Composition, a/o		Brittle-Ductile Transition Temperature (°C)	
Alloy	Al	B	VIM Alloys	P/M Alloys
1	54.0	0.25	*	*
2	51.5	0.25	675	600
3	50.0	-	500	375
4	50.0	0.25	675	700
5	48.5	0.25	675	725
6	43.0	0.25	675	675
7a	43.0	-	-	625
7b	47.9*	-	500	-

*Material fractured during specimen machining, no test conducted.

*The target chemistry for this alloy was 43 a/o. Use of incorrect formulation was not detected until later in the study.

TABLE 9

PHASE II - TASK I SUBSTITUTIONAL ALLOYS
DUCTILITY OBSERVATIONS ON ARC MELTED DROP CAST INGOTS

Alloy	Atom (%) (Balance Ni)	No. of Ingot Cracks	Cracked During Machining	Fracture Mode
Ni Substitutional Alloy Series				
40	48.5 Al - 5.2 Cr	3	N	(1)
41	48.5 Al - 10.3 Cr	10	Y	(1)
42	48.5 Al - 20.6 Cr	>20	Y	(1)
60	51.5 Al - 9.7 Cr	>30	Y	(1)
43	48.5 Al - 5.2 Mn	1	Y	Mixed
44	48.5 Al - 10.3 Mn	1	Y	Mostly T
45	48.5 Al - 20.6 Mn	>30	Y	T
61	51.5 Al - 9.7 Mn	10	Y	T
46	48.5 Al - 10.3 Fe	2	Y	T
47	48.5 Al - 20.6 Fe	2	Y	T
48	48.5 Al - 30.9 Fe	2	Y	T
62	51.5 Al - 19.4 Fe	3	Y	T
49	48.5 Al - 10.3 Co	2	Y	T
50	48.5 Al - 20.6 Co	1	Y	T
51	48.5 Al - 30.9 Co	3	Y	T
63	51.5 Al - 19.4 Co	0	Y	T
Al Substitutional Alloy Series				
52	43.7 Al - 4.9 Mn	0	N	Mostly T
53	38.3 Al - 9.7 Mn	0	N	T
54	29.1 Al - 19.4 Mn	1	Y	T
64	41.2 Al - 10.3 Mn	0	Y	Mixed
55	48.0 Al - 0.5 Ga	0	N	T
56	46.1 Al - 2.4 Ga	0	N	T
57	41.2 Al - 7.3 Ga	0	N	Mostly T
65	48.9 Al - 2.6 Ga	2	Y	Mixed

TABLE 9 (Cont'd)

PHASE II - TASK I SUBSTITUTIONAL ALLOYS
DUCTILITY OBSERVATIONS ON ARC MELTED DROP CAST INGOTS

Alloy	Atomic % (Balance Ni)	No. of Ingot Cracks	Cracked During Machining	Fracture Mode
Ni Substitutional Alloy Series				
Ni and Al Substitutional Alloy Series				
67	46.4 Al - 10.0 Mn	0	Y	Mixed
68	43.6 Al - 10.0 Mn	0	Y	T
Base-line Alloys				
69	Ni - 48.5 Al	0	N	T
74	Co - 48.5 Al	3	Y	Mostly T
75	Fe - 48.5 Al	0	Y	Mostly T

(1)=Casting very porous, grain boundaries not discernible from other features.

T = Transgranular Cleavage

Mixed = Both transgranular cleavage and intergranular fracture.

N = No
Y = yes

TABLE 10

BRITTLE-DUCTILE TRANSITION TEMPERATURES
OF SOME PHASE II - TASK I SINGLE PHASE ALLOYS

	Nominal Composition*		Avg. Grain Size	Transition Temp.
Alloy	Atom	%	mm	C
52	43.7Al	4.9Mn	0.13	725
53	38.8Al	9.7Mn	0.20	775
55	48.0Al	0.5Ga	0.10	625
56	46.1Al	2.4Ga	0.10	625
57	41.2Al	7.3Ga	0.09	575
69	48.5Al	-	0.15	500

*Nickel Balance

TABLE 11

BURGERS VECTOR ANALYSIS FOR ALLOY NUMBER 69 (Ni-48.5 a/o Al)
PREDICTED AND OBSERVED DISLOCATION VISIBILITY AT VARIOUS g VECTORS

$\vec{b}$ \ $\vec{g}$	$g_1 = 01\bar{1}$	$g_2 = 10\bar{1}$	$g_3 = 1\bar{1}0$	$g_4 = 200$
		[100] type $\vec{b}$		
100	o	x	x	x
010	x	o	x	o
001*	x	x	o	o
		[111] type $\vec{b}$		
111	o	o	o	x
$\bar{1}11$	o	x	x	x
$1\bar{1}1$	x	o	x	x
$11\bar{1}$	x	x	o	x
		[110] type $\vec{b}$		
110	x	x	o	x
$\bar{1}10$	x	x	x	x
101	x	o	x	x
$10\bar{1}$	x	x	x	x
011	o	x	x	o
$0\bar{1}1$	x	x	x	o
Observed	x	x	o	o

*Burgers vector which yields g.b predictions matching the observations.

TABLE 12

BURGERS VECTOR ANALYSIS FOR ALLOY NUMBER 40 (Ni-48.5 a/o Al-5.2 a/o Cr)
PREDICTED AND OBSERVED DISLOCATION VISIBILITY AT VARIOUS
g VECTORS ROOM TEMPERATURE COMPRESSIVE DEFORMATION

$\vec{b}$ \ $\vec{g}$	$g_1 = \bar{1}10$	$g_2 = 110$	$g_3 = \bar{2}00$	$g_4 = 020$	$g_5 = 101$
			[100] type $\vec{b}$		
100	x	x	x	o	x
010	x	x	o	x	o
001	o	o	o	o	x
			[111] type $\vec{b}$		
111	o	x	x	x	x
$\bar{1}11$*	x	o	x	x	o
$1\bar{1}1$	x	o	x	x	x
$11\bar{1}$	o	x	x	x	o
			[110] type $\vec{b}$		
110	o	x	x	x	x
$1\bar{1}0$	x	o	x	x	x
101	x	x	x	o	x
$10\bar{1}$	x	x	x	o	o
011	x	x	o	x	x
$01\bar{1}$	x	x	o	x	x
Observed	x	o	x	x	o

*Burgers vector which yields g.b predictions matching the observations.

TABLE 13

BURGERS VECTOR ANALYSIS FOR ALLOY NUMBER 40 (Ni-48.5 a/o Al-5.2 a/o Cr)
PREDICTED AND OBSERVED DISLOCATION VISIBILITY AT VARIOUS g VECTORS
775°C COMPRESSIVE DEFORMATION

$\vec{b}$ \ $\vec{g}$	$g_1 = \bar{1}10$	$g_2 = 110$	$g_3 = 0\bar{2}0$	$g_4 = \bar{2}00$	$g_5 = 011$	$g_6 = 10\bar{1}$
			[100] type $\vec{b}$			
100	x	x	o	x	o	x
010*	x	x	x	o	x	o
001	o	o	o	o	x	x
			[111] type $\vec{b}$			
111	o	x	x	x	x	o
$\bar{1}11$	x	o	x	x	x	x
$1\bar{1}1$	x	o	x	x	o	o
$11\bar{1}$	o	x	x	x	o	x
			[110] type $\vec{b}$			
110	o	x	x	x	x	x
$1\bar{1}0$	x	o	x	x	x	x
101	x	x	o	x	x	o
$10\bar{1}$	x	x	o	x	x	x
011	x	x	x	o	x	x
$01\bar{1}$	x	x	x	o	o	x
Observed	x	x	x	o	x	o

* Burgers vector which yields g.b predictions matching the observations.

TABLE 14

SUMMARY OF DISLOCATION ANALYSES ON

SELECTED PHASE II - TASK I ALLOYS

No.	Alloy* Al, a/o	Other, a/o	Deformation	Slip Direction	Slip Plane	Dislocations
69	48.5	-	20C Compression	⟨001⟩	{110}	Edge
40	48.5	5.2 Cr	20C Compression	⟨$\bar{1}$11⟩	{1$\bar{1}$2}	Screw
			775C Compression	⟨010⟩	{001}	Edge
52	43.7	4.9 Mn	20C Compression	⟨$\bar{1}$11⟩	{1$\bar{1}$2}	Edge
			775C Compression	⟨010⟩	{101}	Edge
			775C Tension	⟨110⟩	{001}	Edge
			775C Tension	⟨010⟩	{001}	Edge
55	48.0	0.5 Ga	20C Compression	⟨001⟩	{110}	Edge
56	46.1	2.4 Ga	20C Compression	⟨001⟩	{110}	Edge

*Nickel Balance

TABLE 15

ROOM TEMPERATURE BEND DUCTILITY OF NICKEL-RICH
NiAl ALLOYS AT VARIOUS HEAT TREATMENT CONDITIONS

Alloy No.	Ni	Al (Atom %)	Other	Bend Ductility* As-Spun	300°C/2h	1000°C/2h	1200°C/2h
79	Bal.	29.3	-	Some	Some	Some	Some
80	Bal.	32.3	-	No	Slight	Slight	Some
81	Bal.	35.2	-	Some	Slight	Slight	Some
82	Bal.	38.0	-	No	No	No	No
84	Bal.	20.0	27.5 Fe	Ductile	Ductile	Ductile	Ductile
85	Bal.	20.0	30.0 Co	Ductile	Ductile	Ductile	Ductile
86	Bal.	30.0	5.0 Mn	No	No	Slight	Some
87	Bal.	30.0	5.0 Cr	No	No	slight	Some

*Ductile: Ribbon can be folded (180°bend)
Some: Ribbon can be bent plastically 90° to 180° with a radius of curvature of 2mm at the bend.
Slight: Ribbon can be bent plastically 10° to 90° with a radius of curvature of 4mm at the bend.
No: Ribbon fractures without noticeable plastic deformation.

TABLE 16

THE EFFECT OF ALLOY COMPOSITION AND PRODUCT FORM ON TENSILE ELONGATION

Alloy No.	(Atomic %) Ni	Al	Other	RSP Ribbon RT Bend Ductility As-Spun	1200C/2h	Arc Melted Casting Tensile Elogation (%) As-Cast RT	As-Cast 600C	1200C/2h RT	1200C/2h 600C
79	Bal.	29.3	-	Some	Some	3.6	2.5	2.2	0
80	Bal.	32.3	-	No	Some	0	0	0	0
81	Bal.	35.2	-	Some	Some	0	0	0	0
82	Bal.	38.0	-	No	No	0	0	-	-
84	Bal.	20.0	27.5 Fe	Ductile	Ductile	11.6	2.2	12.5	4.2
85	Bal.	20.0	30.0 Co	Ductile	Ductile	5.0	5.3	1.35	1.25
86	Bal.	30.0	5.0 Mn	No	Some	0	0	0	0
87	Bal.	30.0	5.0 Cr	No	Some	0	0	0	2.7
83	Bal.	20.0	-	Ductile	Ductile	6.0	0	8.3	0

TABLE 17

TENSILE FRACTURE STRENGTH OF CAST NICKEL-RICH NiAl ALLOYS

Alloy No.	As Cast				Ht: 1200C/2h			
	RT		600C		RT		600C	
	MPA	Ksi	MPa	Ksi	MPA	Ksi	MPa	Ksi
79	524	76	789	113	372	54	496	76
80	489	71	789	113	338	49	593	86
81	276	40	379	55	152	22	565	82
82	152	22	303	44	-	-	-	-
84	1047	152	372	54	1068	155	407	59
85	517	75	496	72	455	66	462	67
86	365	53	531	77	489	71	517	75
87	682	99	696	101	620	90	889	129
83	289	42	269	39	365	53	338	49

TABLE 18

ROOM TEMPERATURE TENSILE FRACTURE MODES IN CAST NICKEL-RICH NiAl ALLOYS

Alloy No.	Ni	(Atom %) Al	Other	As-Cast	1200C/2h
79	Bal.	29.3	-	DMI*	DMI*
80	Bal.	32.3	-	GB and TG	TG
81	Bal.	35.2	-	GB and TG	TG
82	Bal.	38.0	-	TG	-
84	Bal.	20.0	27.5 Fe	TG	TG
85	Bal.	20.0	30.0 Co	TG	TG
86	Bal.	30.0	5.0 Mn	GB and TG	GB and TG
87	Bal.	30.0	5.0 Cr	ID	TG

DMI: Dendrite Matrix Interface, GB: Grain Boundaries, TG: Transgranular
ID: Intradendritic

TABLE 19

PHASE II - TASK II ALLOYS
DUCTILITY OBSERVATIONS ON ARC MELTED DROP CAST INGOTS

Alloy	Atom % (Balance Ni)	No. of Ingot Cracks	Cracked During Machining
	Ni-Al-Ti System		
13	36Al	0	No
14	36Al-0.3 B	0	No
19	36Al-0.3B-0.3Mo-5Ti	1	No
18	40Al-0.3B-1Ti	2	No
20	43Al-0.3B-5Ti	2	Yes
15	36Al-0.3B-12Ti	3	Yes
16	36Al-0.3B-12Ti	4	Yes
17	36Al-0.3B-17Ti	10	Yes
9	30Al-0.3B	0	No
10	30Al-0.3B-5Ti	0	No
11	27Al-0.3B-0.3Mo-12Ti	2	Yes
	Ni-Al-Cr System		
12	35Al-0.3B-6.5Cr	0	No
21	35Al-0.3B-15Cr	2	No
22	35Al-0.3B-13Cr	2	No
23	35Al-0.3B-0.3Mo-13Cr	4	No
24	33Al-0.3B-11Cr	0	No
25	37.8Al-0.3B-11Cr	1	No
	Ni-Al-Nb System		
26	47.8Al-0.3B-1Nb	1	No
27	47.8Al-0.3B-4Nb	6	Yes
28	37Al-0.3B-8nb	10	Yes
	Ni-Al-Hf System		
29	47.8Al-0.3B-0.3Hf	1	No
30	47.8Al-0.3Mo-0.3Hf	1	Yes
31	44.8Al-0.3B-4Hf	3	Yes
	Ni-Al-Ta System		
32	41.8Al-0.3B-2Ta	4	Yes
33	32.8Al-0.3B-9Ta	10	Yes

TABLE 19 (Continued)

Alloy	Atom % (Balance Ni)	No. of Ingot Cracks	Cracked During Machining
	Ni-Al-Si System		
34	44.8Al-0.3B-4Si	1	No
35	47.8Al-0.3B-1Si	1	No
	Ni-Al-V System		
36	46Al-0.3B-11.8V	0	No
37	47.8Al-0.3B-1.8V	0	No
38	23.8Al-0.3B-25V	1	No
	Ni-Al-Zr System		
39	44.8Al-0.3B-4Zr	1	No

TABLE 20 - NiAl ALLOYS FOR PHASE III STUDIES

Alloy	Atom Percent Ni	Al	Other
88	51	22	27Fe
89	50	25	25Co

TABLE 21 - ALLOY 88 PHASE COMPOSITIONS, ATOM PERCENT

	Ni	Fe	Al	Phase Structure
Bulk Composition:				
Nominal	51.0	27.0	22.0	
Chemical Analysis	51.6	26.5	21.9	
Microprobe (Elemental Standards)	50.1	27.3	22.6	
Microprobe Phase Analysis:				
Matrix	50.9	22.3	26.8	Ni(Al,Fe),B2
Grain Boundary Phase	38.5	49.1	12.4	$(Ni,Fe)_3(Al,Fe),L1_2$ (Fe,Ni) ,Al

TABLE 22 - ALLOY 89 PHASE COMPOSITIONS, ATOM PERCENT

	Ni	Co	Al	Phase Structure
Bulk:				
Nominal	50.0	25.0	25.0	
Chemical Analysis	49.9	25.5	24.6	
Microprobe (Elemental Standards)	50.5	24.5	25.0	
Microprobe Phase Analysis:				
Martensitic Grains	50.0	20.9	29.1	Ni(Co,Al)*
Matrix	49.7	32.9	17.4	$(Ni,Co)_3(Al,Co),L1_2$ (Ni,Co) ,Al

* Crystal structure with low symmetry not identified.

U.S.Government Printing Office: 1988 548-054/80664

END

DATE

FILMED

5-88

DTIC